Use of CRISPR-CAS9 in Psammomys obesus to examine the increased vulnerability of cones to Abca4 gene mutations implicated in Stargardt's disease

Fabiana Sassone

Université de Strasbourg

UNIVERSITÉ DE STRASBOURG

École Doctorale des Sciences de la Vie et de la Santé STRASBOURG

ÉCOLE DOCTORALE des Sciences de la Vie et de la Santé

Institut des Neurosciences Cellulaires et Intégratives CNRS UPR3212

THÈSE

Présentée par :

Fabiana SASSONE

Soutenue le : **6 juillet 2023**

Pour obtenir le grade de :

Docteur de l'Université de Strasbourg

Discipline : **Neuroscience**

Utilisation de CRISPR-Cas9 chez *Psammomys obesus* pour examiner la vulnérabilité des cônes aux mutations du gène *Abca4* impliqué dans la maladie de Stargardt

---

THÈSE dirigée par :
M. HICKS David Directeur de recherche INSERM

RAPPORTEURS :
M. ROZET Jean-Michel Directeur de recherche CNRS
Mme. KALATZIS Vasiliki Directeur de recherche Inserm

EXAMINATEUR :
Mme. DOLLFUS Hélène Professeur, Université de Strasbourg

Table of contents

“E a causa della somiglianza il tutto diventa ugualmente sensibile, e se tocca qualcosa o da qualcosa viene toccato, propagando i movimenti di queste impressioni per tutto il corpo fino all'anima, procura quella sensazione che noi chiamiamo vista.”

(Platone, Timeo, 45e - 46a)

Abbreviations

11-cis Ral= 11-cis retinal

A2E= Bis-retinoid N-retinyl-N-retinylidene ethanolamine

A2-PE= Phosphatidylpyridinium bisretinoid

Aap= Assembly-activating protein gene

AAV= Adeno associated virus

AMD= Age-related macular degeneration

ATP = Adenosine triphosphate

atRal= All-trans retinal

atRal-dimers= All trans retinal dimers

CAG= Chicken β-actin

Cap= Capsid gene

Cas9= CRISPR-associated protein 9

CBA= Hybrid CMV enhancer/chicken β-actin

cGMP= Nucleotide cyclic guanosine monophosphate

cjCas9= *Campylobacter jeujuni* Cas9

CMV= Cytomegalovirus

COS= Cone outer segment

crRNA= CRISPR RNA

CRE= Cyclization recombinase

CRD= Cone-rod dystrophy

CRISPR= Clustered Regularly Interspaced Short Palindromic Repeats

DAPI= 4′,6-diamidino-2-phenylindole

DHA= Docosahexaenoic acid

DNA= Deoxyribonucleic acid

ECD= Extracellular domain

eGFP= Enhanced green fluorescent protein

ER= endoplasmic reticulum

ERG= Electroretinography

FACS= Fluorescence activated cell sorting

FAF= Fundus auto fluorescence

GAPDH= Glyceraldehyde-3-phosphate dehydrogenase

GDP= Guanosine diphosphate

GFAP= Glial fibrillary acidic protein

GFP = Green Fluorescent Protein

GRK1= Rhodopsin kinase 1

GTP= Guanosine-5'-triphosphate

HA= Human influenza hemagglutinin

HDR= Homology directed repair

Hz= Hertz

ICSI= Intracytoplasmic sperm injection

INL=Inner nuclear layer

IPL= Inner plexiform layer

IRBP= Inter photoreceptors retinoid binding protein

IS= Inner segment

ITR= Inverted terminal repeats

KO= Knock out

LoxP= Locus of x-over, P1

LW= Long wavelength cones

MNU= N-methyl-N-nitrosourea

mRNA= Acid ribonucleic messenger

MW= Medium wavelength cones

NBD= Nucleotide binding domain

NHEJ= Non-homologous end joining

NLS= Nuclear localization signal

NRL= Neural retina leucine zipper

NRPE = N-retinylidene-phosphatidylethanolamine

OCT= Optical coherence tomography

ONL= Outer nuclear layer

OPL= Outer plexiform layer

OPN1MW= Opsin M protein

OS= Outer segment

PAM= Protospacer adjacent motif

PBS= Phosphate-buffered saline

PCR= Chain reaction polymerase

PDE= Enzyme phosphodiesterase

PE = Phosphatidylethanolamine

PFA= Paraformaldehyde

PFU PCR= *Pyrococcus furiosus* DNA polymerase PCR.

PKCα= Protein kinase C alpha

PM= Plasma membrane

PNA= Peanut agglutinin lectin

PRs= Photoreceptors

qPCR= Quantitative polymerase chain reaction

RDH5= Retinal dehydrogenase 5

RDH8= Retinal dehydrogenase 8

Rep= Replication gene

RGCL= Ganglion cell layer

RHO= Rhodopsin protein

RNA= Ribonucleic acid

RP= Retinitis pigmentosa

RPCs= Retinal progenitors cells

RPE= Retinal pigment epithelium

RPLP0= Ribosomal protein lateral stalk subunit P0

saCas9= *Staphylococcus aureus* Cas9

sgRNA= Single guide RNA

spCas9= *Streptococcus pyogenes* Cas9

STGD1= Stargardt Disease type 1

STGD3= Stargardt Disease type 3

STGD4= Stargardt Disease type 4

SW= Short wavelength cones

TAL= Transcription activator like

TMD= Transmembrane domain

tracrRNA= Trans-activating CRISPR RNA

UPLC= Ultra-performance liquid chromatography

WT= Wild type

ZFN= Zinc finger nuclease

Remerciements

Je voudrais tout d'abord exprimer mes remerciements à l'ensemble des membres du jury qui ont accepté de juger mon travail de thèse.

Un merci particulier à mon chef, David Hicks. Merci de m'avoir accueilli au sein du laboratoire depuis le stage de Master 2 et de m'avoir toujours fait confiance. Je sais que ça n'a pas été facile lorsque j'ai commencé mon doctorat, néanmoins tu as cru en moi et j'espère ne pas t'avoir déçu. Ce projet de recherche a été comme un enfant qui, petit à petit, a grandi, et je sais qu'il a beaucoup compté pour toi aussi. Nous avons connue des hauts et des bas, ainsi que de nombreuses difficultés, que nous avons réussi à surmonter. Merci d'avoir été toujours là pour moi et de me guider, tout en me laissant mon indépendance et la possibilité de suivre mes idées, en me guidant mais jamais en m'entravant. Cette thèse aura été une expérience inoubliable et je te remercie de m'avoir donné cette opportunité. C'est la fin d'un chapitre important et je suis rassuré de savoir que ce n'est peut-être pas la fin de notre travail ensemble. Merci énormément David, pour tout.

Merci à Marie-Paule Felder-Schmittbuhl. Merci d'avoir été si présent et d'avoir été toujours là pendant tout mon parcours de thèse. Bien que n'étant pas directement impliqué dans le projet, t'as toujours été de soutien scientifique et de réconfort personnel. Merci d'avoir été toujours là pour moi. Merci à Frank Pfrieger pour nos échanges scientifiques, son soutien apporté à la rédaction de l'article et ses conseils très élogieux.

Un merci spécial à Cristina avec qui je partage maintenant le bureau depuis 2017. Quand je suis arrivée, j'étais si petite et elle a toujours été là. Merci de m'avoir aidée toujours, de m'avoir écoutée pendant mes moments de stress et de m'avoir appris autant au laboratoire. T'as été indispensable pour moi, merci.

Je remercie toute l'équipe « Retina », pour votre disponibilité, votre gentillesse, pour l'environnement sain, confortable et stimulant dans lequel je me suis retrouvée. Chacun de vous a contribué à une petite partie de ma formation. Merci à tous les membres de l'équipe. Merci Amandine pour son aide à l'électroporation *in utero* et merci aussi à Naima pour avoir mis beaucoup d'efforts dans le projet depuis son arrivée.

Merci à tous les doctorants NBR pour tous les moments partagés au laboratoire et pour nous petits moments en dehors du laboratoire. Ces moments font partis de la vie d'un doctorant et je ne les oublierai jamais. Merci.

Merci à Dominique Ciocca et Sophie Reibel-Foisset pour le soutien apporté avec les expériences animales et un merci tout particulier à Nicolas Léthenet, Bruno Wolfrom et Olivier Arnaud pour m'avoir toujours aidé avec les animaux, pour avoir été si présents et patients.

Je veux ainsi remercier chaque personne de l'INCI, merci à la plateforme de microscopie électronique et surtout Cathy Royer pour son aide à la préparation des tissus, merci beaucoup pour tout le travail.

Merci à mes piccoli Bérengère, Michael, Jason, Emma et Rosanna. Le laboratoire n'aurait pas été le même sans vous. Lors de ma dernière année à l'INCI, nous avons partagé des moments incroyables. Merci de m'avoir toujours écoutée et soutenu. Merci Berouj et Emma d'avoir toujours étés d'un immense réconfort, Michael pour toute l'énergie positive que tu m'as donné, Jason d'avoir été là, tu m'as aidée plus que tu puisses penser, je ne l'oublierai jamais.

Grazie à vous tous, je garderai toujours tous nos moments dans mon cœur,

Un grazie speciale a Nadia che mi ha spezzato il cuore quando ha lasciato il laboratorio. Grazie perchè sei sempre stata un punto di riferimento per me e sei diventata per me come una sorella maggiore. Grazie per avermi insegnato tanto e per essere stata sempre di conforto per me. Ti voglio bene.

Merci à la petite Marion, si loin mais toujours dans mon cœur. Merci pour tous les moments que nous avons partagés pendant nos thèses, le confinement, même si difficile et triste représente un des plus beau souvenir que j'ai, pour tout le moment qu'on a partagé. Notre amitié traverse toutes les distances. Merci pour tout.

Un grazie speciale va a tutta la mia “famiglia italiana” qui a Strasburgo, quella che non mi ha mai fatta sentire lonata da casa. Margherita, Martina, Rosanna, Filippo e Alessia che da quando sono arrivata rappresentano un punto di riferimento per me, una costante. Abbiamo condiviso momenti intensi e carichi di emozioni che porterò con me per sempre . Strasurgo lascia andare e accoglie sempre e nel corso del mio percorso ho incontrato persone meravigliose, il dottorato è stato anche questo. Grazie Chiara per avermi aiutata a ritrovare una nuova me, sei stata il mio capolinea e il mio nuovo punto di partenza, grazie per essere così presente. Un grazie particolare ad Alessia per il tuo supporto e la tua dolcezza infinita, grazie a Miriam, Marianna, Lucrezia, Mattia, Onofrio, Luca, Stefano, Richi, Fausto, Stefan, Sara per tutti i momenti che abbiamo trascorso insieme e che porterò con me sempre. Spero sia solo l’inizio di una collezione di momenti che condivideremo ancora.

Un grazie parlicolare a Filippo per essere stato costante del mio percorso qui. Da quel colpo di fulmine al Wacken, non ci siamo più lasciati. Abbiamo condiviso momenti fortissimi che rivedo nella mia mente uno ad uno, impossibile dimenticare. Sei sempre stata quella nota di leggerezza che tante volte mi faceva bene al cuore e nonostante non sono mancate litigate e malintesi, questo ci ha resi più autentici. Grazie per aver fatto parte di questo mio percorso di dottorato e sono certa non sarà la fine del nostro insieme. Ti voglio bene.

Grazie a Martina, perchè non potrei immaginare una Strasburgo senza te. Grazie perchè ti sei insinuata a piccoli passi nella mia vita dal 2017 e da li non sei uscita più.Il destino ci ha legate in Erasmus per un puro caso e ancora ci ha riunite per il dottorato. Questo percorso è stato molto duro per entrambe, ma eravamo insieme, l’una a sostegno dell’altra sempre. Grazie per il tuo supporto, per la forza e il sorriso che non mi hai mai fatto mancare, perchè mi giro e tu ci sei sempre, sei sempre accanto a me. Vorrei fermare il tempo e credere che resteremo sempre così, ma tanto so che se anche così non fosse, ovunque nel mondo noi esisteremo per sempre. Grazie Pitti, ti voglio bene.

Grazie alla mia Margherita, grazie perchè senza di te mi sarei persa. Grazie per esserti presa così cura di me come una mamma chioccia e di avermi raccolta quando ero totalmente persa. Grazie perchè non riesco ad immaginare come sarebbe stato questo percorso, talvolta così travagliato, senza di te che mi hai teso la mano, sempre. Grazie perchè nonostante i km che ci separano, il tuo posto è sempre lì accanto a me. Avrei voluto tante volte fermare il tempo a quei momenti solo nostri, mi manca tutto, ma tu resti e resterai per sempre una costante per me. Grazie per non avermi lasciata mai sola. Ti voglio bene.

Grazie Rosanna, come avrei fatto senza la mia Ross ? Grazie per essere un'amica così preziosa per me. Sei stata una guida tante volte, un supporto ed un ascolto nei momenti di sconforto. Grazie per essere stata una collega impeccabile e per i nostri scambi scientifici che ci hanno spesso motivato a vicenda. Grazie per essere un'amica così presente, ti sei insinuata a piccoli passi e sei diventata un punto saldo della mia vita. Non so dove ci ritroveremo un giorno, ma sono sicura che su di te potrò contare sempre. Ti voglio bene.

Grazie Carla perchè ormai non ricordo più nulla in cui non ci sei tu, non c'è nulla che non abbia condiviso con te e questo dottorato, travagliato e complicato come tu sola sai, è uno di quelli. Grazie per essere stata così presente anche se così lontana, per esserci sempre per me e per avermi dato così tanta forza anche quando io stessa credevo di non averne più. E' iniziato tutto tra i banchi di scuola e so che per sempre sarà così tra noi. Grazie per essere semplicemente tu accanto a me sempre.

Grazie Francesco per il supporto che non mi hai mai fatto mancare durante questo percorso, per esserci sempre stato, per avermi dato conforto e coraggio. Grazie per essere per me un punto di riferimento, una costante a cui non potrei rinunciare. Grazie per avermi ascoltata tante volte e per avermi strappato un sorriso nei momenti più bui. Grazie perché mi hai insegnato tanto anche senza saperlo, per avermi incoraggiata sempre nelle mie scelte. Ti voglio bene Franci, sempre sarà cosi.

Infine grazie alla mia famiglia lontana chilometri ma sempre accanto a me. Grazie ai miei genitori senza i quali tutto questo non sarebbe stato possibile. Grazie al vostro amore smisurato e alla vostra forza che mi hanno permesso di credere che ce l'avrei fatta, che sarei arrivata alla fine di questo percorso. Grazie per essere di supporto sempre anche a distanza, una distanza che so bene vi spezza il cuore. Siete il mio raggio di sole quando brancolo nel buio e per sempre sarà così. Grazie a Gaia per essere il mio cuore lontano, quello che mi da coraggio nei momenti di paura profonda. Grazie per il tuo sostegno, per non avermi mai lasciata sola, soprattutto quando ero totalemte persa, tu sempre accanto a me. Resterai la mia piccolina per sempre e a te va il mio abbraccio più grande che ti possa riscaldare e proteggere anche quando non mi vedi.

INTRODUCTION

Introduction

1 Human Retina

1.1 Basic Anatomy of the Retina

Vision, one of the five senses, represents a window on the world, a system of contact with the outside whose importance is already rooted in ancient Greece. When Plato writes of the senses, in fact he describes vision as "divine" in one place. Similarly, Aristotle creates a ranking of senses, putting sight first, followed by hearing, smell, and taste and touch. Vision is always ranked as the highest sense in Western societies throughout the Middle Ages until today (Hutmacher 2019). While all parts of the eye are important, the layer most vital to vision is the retina. The retina is a neuronal tissue that receives stimuli from lights and images from the outside world. We had to wait until 1900 with the Nobel Prize Santiago Ramón y Cajal, to understand the structure and anatomy of the various layers that form the retina.

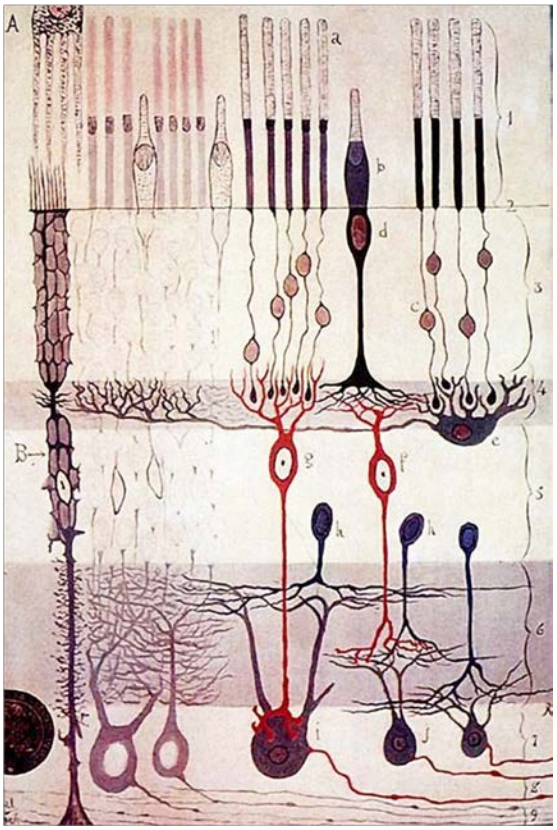

Figure 1 Anatomy of retina by Ramón y Cajal. (2004) Genomic Analysis of Retinal Development in the Mouse. PLoS Biol 2(9): e265.

The retina, the innermost layer of the eye, contains neurons that are sensitive to light and are capable of transmitting visual signals to central targets. There are five principal types of neurons in the retina: PRs, bipolar cells, ganglion cells, horizontal cells, and amacrine cells. PRs, bipolar cells and ganglion cells, vertically organized, provide the most direct route for transmitting visual information to the brain. Horizontal cells and amacrine cells mediate horizontal interactions. The retina is composed of three layers of cell bodies and two layers of synapses. The outer nuclear layer (ONL), located nearest the sclera, contains the cell bodies of the "classical" PRs (PRs), rods and cones. The inner nuclear layer (INL) contains the cell bodies of the bipolar, horizontal and amacrine cells (as well as those of the main macroglial cell type the Muller cells). The most internal nuclear layer, the ganglion cell layer (GCL) contains cell bodies of ganglion cells. Dividing these nerve cell layers are two neuropils where synaptic contacts occur. The first neuropil is the outer plexiform layer (OPL) where there are connections between rod and cones on one side, and bipolar cells and horizontal cells on the other. The second neuropil of the retina, is the inner plexiform layer (IPL), where there are connections between bipolar, amacrine and ganglion cells (Figure 2).

Therefore the light crosses the different retinal layers before reaching the PRs [in direct contact with the Retinal Pigment Epithelium (RPE)] and there, in the photoreceptor outer segment (OS) light energy is transformed into electrical energy, a process called phototransduction .

Before delving into the light transmission mechanism, let's find out better the protagonists, the PRs.

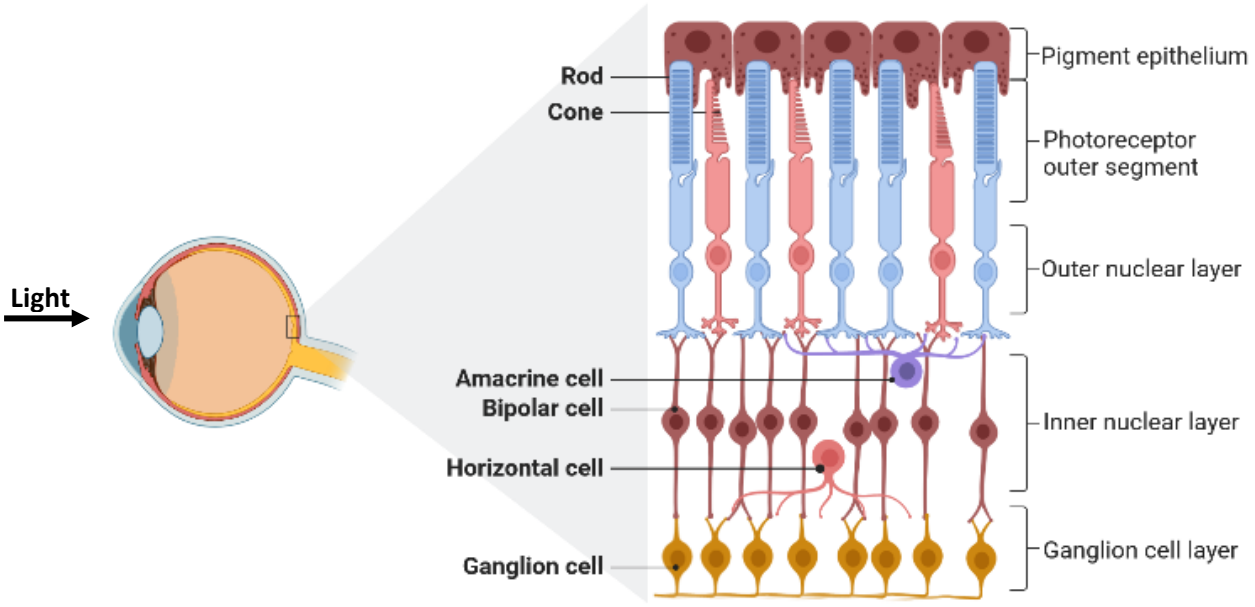

Figure 2 Structure of the human retina. Schematic representation of the human eye in which light passes through the pupil, lens and vitreous before reaching the light-sensitive retina. Section of the human retina, showing its structure, which consists of: the ganglion cell layer, the inner nuclear layer, including bipolar, horizontal and amacrine cells, the outer nuclear layer, which contains the cell bodies and nuclei of PRs (PRs), rods and cones, the outer segments of the PRs , the retinal pigment epithelium (RPE).

1.2 Focus on PRs

The two types of PRs, rods and cones, are distinguished by their shape, with rod OS being slim cylindrical structures while cone OS are shorter conical-shaped structures, and also by the type of photopigment they contain and their distribution across the retina. Both rod and cone PRs are specialized cells with a unique morphology consisting of an elongated OS filled with stacks of membranes containing the visual pigments, an inner segment (IS) containing the apparatus necessary for protein synthesis and ATP formation (mitochondria, Golgi apparatus, ribosomes), a cell body containing the nucleus, and a synaptic terminal (Perkins and Fadool

2010). Even though the general structure is the same in both rod and cone PRs, they have important differences.

1.2.1 Rods

In the metropolitan conditions of the twenty-first century, almost all of our vision is mediated by the cone system, nevertheless the human retina consists of only 5% of cones while the remaining 95% are rods. The reason for this distribution is to be found in the distant past, in fact it is speculated our ancestors lived in near darkness to escape predation. Approximately 400–500 millions of years ago, evolution led to the appearance of rods which supplemented the pre-existing cones.These new PRs provided an advantage to the organism by permitting vision even at very low light levels, at night and in the ocean depths (Lamb 2016). Rods are highly light sensitive and can detect single photons. For this reason, they function in dim light, but not in bright light because of response saturation. Furthermore, the time of a response evoked by a light flash is slow in rods. The rod photoreceptor outer segment OS has been the focus of numerous molecular, cellular, biochemical, and physiological studies due to its unique structure, accessibility, and ease of isolation. The OS of the mammalian rod cell is a cylindrical structure with a typical length of 20–30 μm and a diameter of 1.2–2.0 μm, with a plasma membrane (PM) that encloses an ordered stack of over 1000 disks. The disk membrane is completely independent of the plasma membrane. The disk membrane is packed with the photopigment rhodopsin that initiates phototransduction, with a density of >25,000 rhodopsin molecules/μm 2. Rhodopsin is a member of the G-protein-coupled receptor family with seven transmembrane domains and it consists of the protein opsin covalently coupled with a chromophore ligand, 11-cis-retinal, that isomerized to all-trans-retinal during the visual phototransduction process. In addition to rhodopsin, the disk rim contains two membrane proteins Per2 and Rom1 that generate the highly curved disk rim (Molday and Moritz 2015).

1.2.2 Cones

Cone PRs are responsible for colour discrimination and visual acuity and are of highest importance in human eyesight. In the human retina, cones contain cone opsins, a G-protein-coupled protein with seven transmembrane domains like rhodopsin in rods. In humans and some primates, there are three distinct opsins, each localized to one of three cone types. Each of these

photopigments has a different sensitivity to light of different wavelengths there are three types of cones: so called blue (or “S” for short wavelength)-, green (or “M” for mid-wavelength) and red (or “L” for long wevelength)-sensitive cones, as opposed to a single type of rod. L cones are most sensitive to low frequencies (max~555–565 nm), M cones to middle frequencies (λmax~530–537 nm), and S cones to fast frequencies (λmax~415–430 nm in humans). However the spatial distribution of cones PRs are not the same across the human retina. S cones (only ~5-10% of total cones (Roorda et al. 2001) are far more abundant in the retinal periphery and less in the centre compared to L and M cones that are most concentrated in the fovea, the central region of the macula responsible for high acuity vision. We can discriminate colours only when the light is bright enough to stimulate cones, as they are less sensitive to light and require bright light to function. The OS in mice retina is about 1.2 μm and 13 μm in length for cones and, in contrast to rod OS is formed by serial folding of plasma membrane itself. So cone OS are formed of “open” discs, in reality multiple folds of a single plasma membrane, offering a big surface area for the exchange between the interior and exterior of cells (Figure 3) (Mustafi, Engel, and Palczewski 2009).

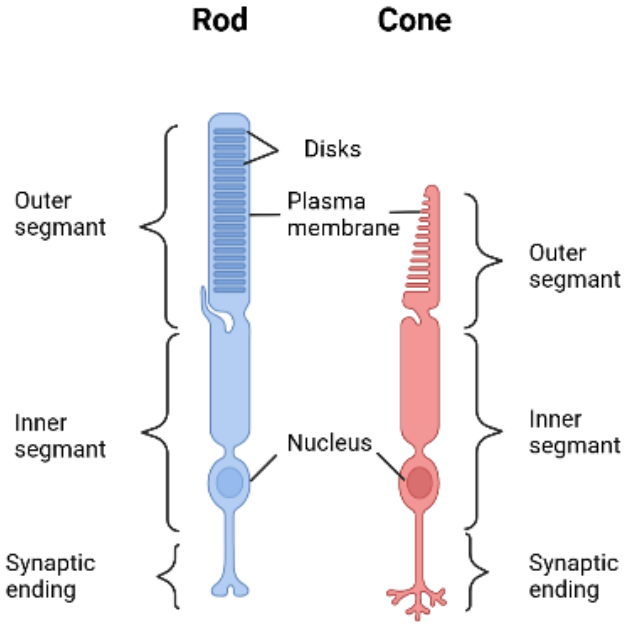

Figure 3 Structure of cones and rods. In both cell types we can distinguish the outer segments linked by a connecting cilia to the inner segments. We can also observe cell nuclei with synaptic terminals.

1.3 Retinal Pigment Epithelium (RPE)

If the PRs are the primary light-sensitive cells of retina, why does light have to go through all the different retinal layers before reaching the PRs which are located at the back of the eye? The reason behind this interesting retinal organisation is tied to the interaction between PR OS and RPE. RPE is formed from a single layer of cells, with the basal side connected to Bruch's membrane and the choroid, and the apical side adjacent to the PR OS. The RPE appears dark, due to the presence of melanosome granules containing melanin which reduces backscattering of light. The apical surface of RPE cells has microvillus structures extending between PR OS forming an extensive interface that allows exchange between these two cell types, such as the phagocytic process. The PR OS disks containing the photosensitive opsins, are completely renewed every 12 days in a phagocytic process called disk shedding. These disks are formed near the inner segment of the PRs and travel to the tip of the OS where they are removed and ingested by the RPE. Furthermore, the RPE contains several enzymes involved in a process called the visual cycle, essential to regenerate photopigment molecules after they have been exposed to light. Finally, the choroid, the vascular layer of the eye that feeds the basal surface of RPE, is the main source of nutrition for PRs. All these considerations probably explain why rods and cones are found in the outermost rather than the innermost layer of the retina. (Yang, Zhou, and Li 2021)

1.4 Light Signal Transmission

Phototransduction, or the conversion of light energy into electrical energy, is performed by PRs (rods and cones). In the dark, the photoreceptor is in a depolarized state (membrane potential of –30 mV), dependent on the open state of cation channels within the plasma membrane that permit Na+ and Ca2+ ions to flow into the cell leading to a continuous release of glutamate neurotransmitter. These cation channels are regulated by the levels of the nucleotide cyclic guanosine monophosphate (cGMP). Thus, in darkness, high levels of cGMP in the OS keep the channels open. In the light, the photoreceptor is in a hyperpolarized state (potential membrane of –70 mV) because cGMP levels decrease and this keeps the channels closed with a consequent decrease of neurotransmitter release. In rod PR, the photo pigment rhodopsin localised on the

descale membrane, is in inactive state and bound covalently with chromophore 11-cis retinal (11-cis Ral). When a photon arrives, the photo absorbent chromophore 11-cis Ral of rhodopsin is isomerized from 11-cis to all-trans retinal (atRal). This change triggers conformational alterations in the protein with a series of modifications that lead to the activation of transducin (a member of the G-protein family), which in turn activates the enzyme phosphodiesterase (PDE) that hydrolyzes cGMP. The hydrolysis by PDE at the disk membrane lowers the number of molecules of cGMP, leading to channel closure and hyperpolarization of membrane. Activated rhodopsin is then inactivated by phosphorylation mediated by rhodopsin kinase (GRK1) followed by binding of arrestin. At the same time, the regeneration of 11-cis Ral is obtain by a process called visual cycle. (Wang and Kefalov 2011).

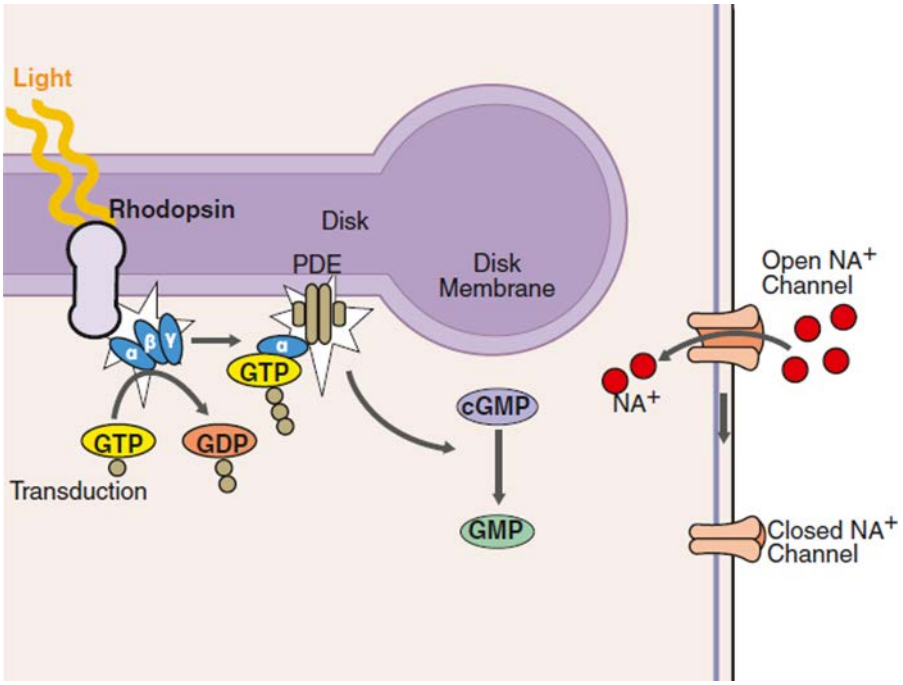

Figure 4 Phototranduction in rod PRs. Light stimulation of rhodopsin in the receptor disks leads to the activation of a G-protein (transducin), which in turn activates a phosphodiesterase (PDE). The PDE hydrolyzes cGMP, reducing its concentration in the outer segment and leading to the closure of sodium channels in the outer segment membrane. From (Konieczka et al. 2012).

1.5 Macula lutea

Rods and cones also differ by their distribution in the retina. The total number of rods in the human retina is ~120 million, whereas the number of cones is around 6 million. Thus, the density of rods is much greater than cones throughout most of the retina. However, this relationship changes dramatically in the *Macula lutea*, a pigmented, elliptically shape area of 5.5 mm in diameter in the centre of retina. The term macula lutea comes from Latin *macula*, "spot", and *lutea*, "yellow". Lutein and zeaxanthin, two types of carotenoids, are in fact responsible for the coloration of the macula which are thought to function as antioxidants and high-energy blue light filters to protect against photo-oxidative damage (Whitehead, Mares, and Danis 2006). The macula is a highly specialized region where the cones constitute over 50% of PRs (while the average proportion of cones across the entire retina is 5% of total PRs) (Curcio, C.A., et al 1990). In the very centre of the macula, we observe the fovea *centralis*, a depression of inner retinal tissue specialized for high acuity vision thanks to the high cone density (200,000 cones/mm^2). In this area (about 1.0-1.5 mm), the retinal layers are displaced laterally from the OPL to the GCL. This displacement of retinal layers, linked with the absence of blood vessels in the fovea, both reduce the light scattering and improve the photon capture efficiency by the OS. A high percentage of Muller cells is also observed, where they seem to play an important role in protecting the fovea from blue light and reducing chromatic aberration. Furthermore, it has been shown that macular Muller glia are important for the maintenance and health of this important region, protecting the neurons from oxidative stress (Zhang et al. 2019). In the foveal centre, the '*foveola*' contains the highest density of cone PRs in the retina. In this region it is remarkable that each cone is in contact with a single bipolar cell, itself connected to a single ganglion cell. This 1/1 connection enables detailed image resolution and reflects the involvement of this region in high acuity vision (Bringmann et al. 2018). So across the retina the mean ratio of rods to cones is 20:1, becoming 1:1 near the centre and 30:1 in the periphery. Towards the periphery, several PRs converge on a single bipolar cell and many bipolar cells converge on a single ganglion cell. The result is that these peripheral ganglion cells are extraordinarily sensitive to light. This region is therefore primarily responsible for low light (scotopic) vision and underlies detection of movement within the peripheral visual field (Hussey, Hadyniak, and Johnston 2022).

2 Retinal degenerations

2.1 Macular dystrophies

The macula is particularly sensitive to degeneration during the course of life. This may be due to high levels of metabolic stress in this area because of high PR density (Hussey, Hadyniak, and Johnston 2022). Sometimes macular degeneration can be due to multifactorial and multi-genetic conditions, like age-related macular degeneration (AMD); or it can be associated with a single gene disruption. Inherited macular dystrophies are rare genetic diseases of the central retina that cause severe central vision loss. They are usually caused by disruption of a single retinal gene. Most of these monogenic diseases are autosomal dominant, but the less frequent autosomal recessive forms result in the worst acuity vision. Macular dystrophies are heterogeneous at the genetic, clinical, and histological levels (Rozet et al. 2005).

A spectrum of diseases is associated with mutations in the *Abca4* gene (see below). In addition to Stargardt's Disease (STGD) which is monogenic, other diseases such as retinitis pigmentosa (RP) and cone-rod dystrophy (CRD) are also associated with *Abca4* gene mutations, although they are heterogenic. Moreover, *Abca4* mutations are present in a subgroup of AMD patients (Klevering et al. 2004; Klevering et al. 2005). With respect to monogenic macular disease, mutations have been found in about 38 genes, and for some of these the phenotype is similar to Abca4-associated-rethinopathy. This group of diseases presents 3 common clinical signs: macular involvement, fundus flecks and peripapillary sparing (Cremers et al. 2020).

2.2 *Abca4* gene

In humans there are 48 genes coding for ATP-binding cassette (ABC) transporters, organized into 7 families ranging from ABCA to ABCG. The ABCA subfamily consists of 12 members with common roles in lipid transport and homeostasis across cell membranes. The ABC transporter can either import from the lumen to the cytoplasm, or export from the cytoplasm to the lumen; ABCA4 functions as an importer (Choi and Ford 2021). The *Abca4* gene is expressed specifically in the PRs (Allikmets et al. 1997), though a recent report shows a small amount is also expressed in the RPE (Lenis et al., 2018). Most of it is located on the rim of the

disc membrane/folds in rod and cone PR OS. However, ABCA4 is also located in the PR inner segments (IS) (Molday et al. 2022). In humans, the gene consists of 50 exons encoding for a protein of 2273 amino acids. Like the other members of subfamily A, two halves each with a transmembrane domain (TMD) and nucleotide-binding domain (NBD) characterize ABCA4 protein structure, with a total of 12 transmembrane segments (6 for each half). In addition, a subfamily A feature is the presence of two extracellular domains (ECDs) containing glycosylation sites and disulphide bridges, important for protein folding and stability (Molday et al. 2022). Furthermore it has been shown that *abca4* mRNA and ABAC4 protein expression levels in cones are relatively higher than rods obtained by comparing values from WT and Nrl−/− mice OS PRs (Verra et al. 2022). The natural ABCA4 substrate is N-retinylidene-phosphatidylethanolamine (NRPE), formed by atRal that reacts with the primary amine of phosphatidylethanolamine (PE) phospholipid in membranes. atRal comes from the isomerization reaction of 11-cis Ral chromophore of rhodopsin in rods, and cone opsin in cones. Regeneration of photosensitive 11-cis Ral following photoexcitation takes place in a process called the visual cycle, in which ABCA4 plays a key role.

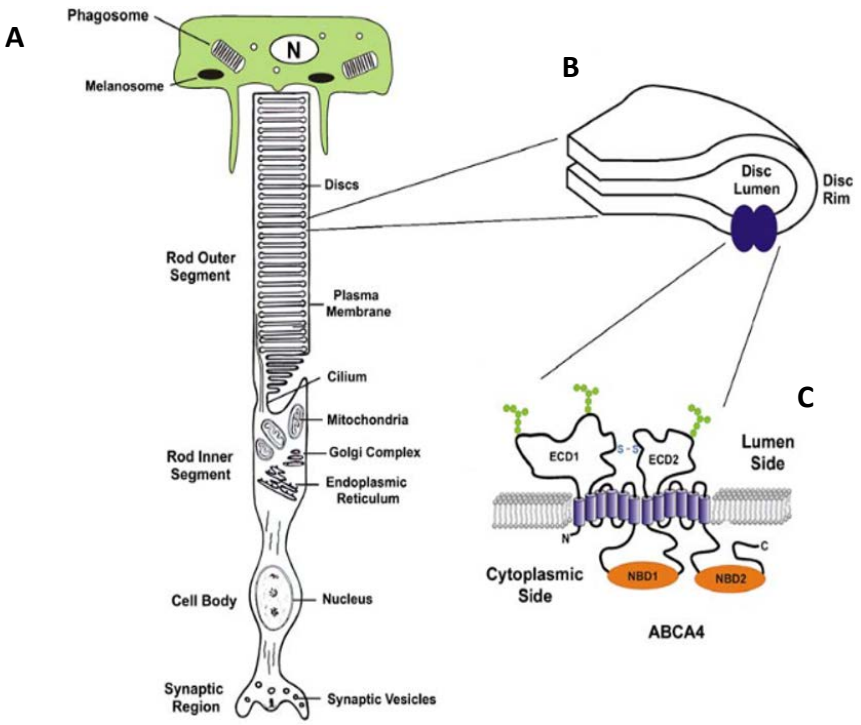

Figure 5 Schematic representation of rod photoreceptor and ABCA4 structure .(A) The rod photoreceptor outer segment with numerous disks surrounded by a separate plasma membrane, an inner segment, cell body and synaptic region. RPE cell with phagosome that contains phagocytises disks. (B) Enlargement of the disc showing the presence of ABCA4 protein on the rim. (C) An ABCA4 protein structure showing the exocytoplasmic domains (ECD), membrane domains and the nucleotide binding domains (NBD). Adapted to (Molday 2007).

2.3 The visual cycle

It has been shown that in the dark, the light-absorbing chromophore 11-cis Ral is conjugated to opsin via a protonated Schiff base. Arrival of a photon converts kinked 11-cis Ral chromophore into conformationally different linear atRal. Thanks to the ABCA4 transporter, it flips from the lumen to the cytoplasmic side, where it is reduced by the enzyme retinol dehydrogenase (RDH8) to all trans retinol (atRol). At this point the atRol binds to inter-photoreceptor retinoid binding protein (IRBP) within the sub-retinal space, and is then transported to the RPE where it will undergo a series of reactions (esterification, hydroxylation, isomerization), which produce dehydrogenated 11-cis retinol then 11-cis Ral from retinol dehydrogenase 5 (RDH5). Once shipped back to the PRs OS by IRBP, it will covalently link to regenerate the visual pigment (rhodopsin or cone opsin). Immediately following photon capture, atRal separates from the opsin backbone but remains in the lipid bilayer where it reacts with PE on the luminal leaflet to form NRPE, which constitutes the actual ABCA4 substrate. Thanks to ABCA4, NRPE passes from the luminal leaflet side to the cytoplasmic leaflet side where it dissociates into atRal and PE, where atRal will be reduced to atRol by RDH8.

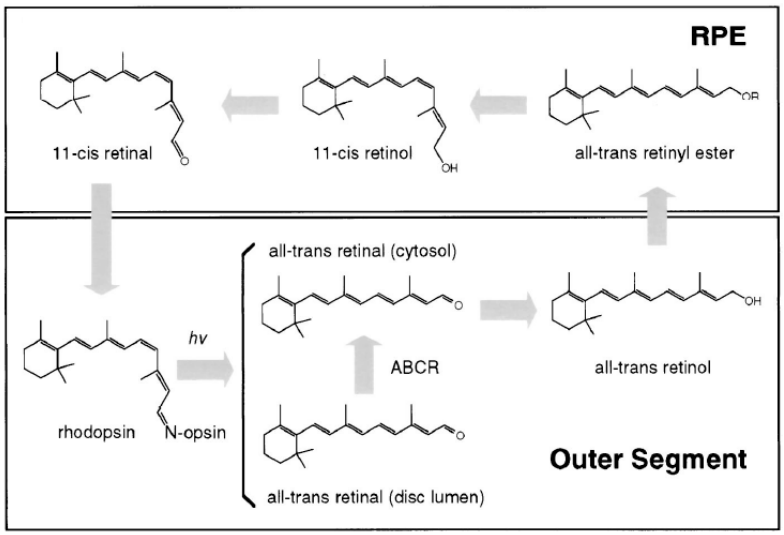

Figure 6 The visual cycle. Photoisomerization of 11-cisRal chromophore into atRal following photon capture, within the disc lipid bilayer. ABCA4 transports atRal joined with PE (NRPE) to the cytosolic side where the enzyme retinol dehydrogenase 8 (RDH8) reduces atRal to atRol. At this IRBP transports atRol to the RPE where it will undergo a series of reactions (esterification, hydroxylation, isomerization) which will regenerate 11-cisRal by retinol dehydrogenase 5 (RDH5) activity. Once returned to the PRs OS by IRBP, it will regenerate photosensitive visual pigment. From (Sun and Nathans 2001).

Mutations in the *Abca4* gene impede or prevent this reduction reaction, causing the accumulation of atRal inside the discs. In this scenario, NRPE reacts with a second atRal molecule to form the dihydropyridinium molecule A2PE, and then within the RPE phosphate hydrolysis produces A2E, the major component of lipofuscin (Sparrow et al. 2012). Lipofuscin is naturally present in the RPE, as a function of aging. It is made up of a mix of bisretinoids that originate in the PRs OS through non-enzymatic reactions of retinyldehyde. Due to the continuous phagocytic mechanism operated by the RPE, these autofluorescent pigments (590-600nm emission) end up in the RPE liposomes. However, compromised ABCA4 function leads to a greater accumulation of these bisretinoids. A2E is the main component and it seems to have a role in retinal disease. It possesses detergent properties, leading to lysosomal dysfunction, as well as exacerbating blue light cytotoxicity and activating the complement system, all of which lead to RPE degeneration and loss of function, which then triggers PRs death by retroaction (Charbel Issa et al. 2013).

2.4 Stargardt's disease

Stargardt's disease (STGD1) is the most common hereditary macular dystrophy in the world, with a prevalence of 1:8000-10 000. The disease description was already documented in the 19th century; however, it was not until 1909 with Karl Bruno Stargardt, that a detailed clinical description of STGD1 was made. According to Karl Stargardt's clinical description, patients showed initial defects in the cone PR followed by degeneration of the RPE, and subsequently of the choroid. Nowadays, knowledge of the disease and phenotypic descriptions are much greater, although it is impossible to reduce STGD1 to a single phenotype, because of high clinical and genetic heterogeneity (Cremers et al. 2020). STGD1 is caused by mutations in the *Abca4* gene located on chromosome 1p22.1 in human and is inherited in an autosomal recessive manner (Allikmets et al. 1997). Autosomal dominant mutations in ELOVL4 (STGD3) on chromosome 6, and PROM1 mutations on chromosome 4 (STGD4) lead to other forms of the disease. STGD1 is the most common form of juvenile onset macular dystrophy. It is characterized by the loss of central vision, macular atrophy and the presence of yellow flecks in the RPE. There is increasing evidence that onset relates to the severity of the underlying *Abca4* variants, with childhood-onset associated with more deleterious variants compared with adult-onset or later onset STGD1. Indeed, in children the initial prognosis is difficult, often they do not have retinal flecks or increased fundus autofluorescence (FAF), as this develops over

time in association with macular atrophy. However, a closer examination by optical coherence tomography (OCT) may reveal an alteration in the retinal architecture in the center of the macula. In adult onset forms, the phenotype is milder, with visual acuity preserved and normal full-field ERG (Tanna et al. 2017). More than 1200 mutations affect the *Abca4* gene and they can be of all types - missense, nonsense, small deletions/insertions, and splicing variants. This makes phenotype-genotype correlation very challenging. Null allele mutations are associated with more severe phenotypes with early disease onset (Fakin et al. 2016).

These variants can hence be grouped and classified according to the related phenotypes into severe, moderate, mild, and hypomorphic. However, the distinction is not always so clear: sometimes missense alleles have been shown to be deleterious, in others deleterious mutations do not lead to loss of function (Cremers et al. 2020). Lois *et al*., (2001) established a classification of three phenotypic STGD1 subtypes based on electrophysiological attributes. Group 1 is classified as a severe pattern ERG abnormality (macular dysfunction) with normal full field ERGs; Group 2 shows generalized pan-retinal loss of cone function with preserved normal rod function; and Group 3 exhibit generalized loss of both cone and rod function. A longitudinal study (Fujinami et al. 2013) has now demonstrated that these groups have prognostic implications and that they do not reflect stages of disease: Group 1 is associated with the best prognosis, Group 3 with the worst, and Group 2 with an intermediate variable prognosis (Tanna et al. 2017).

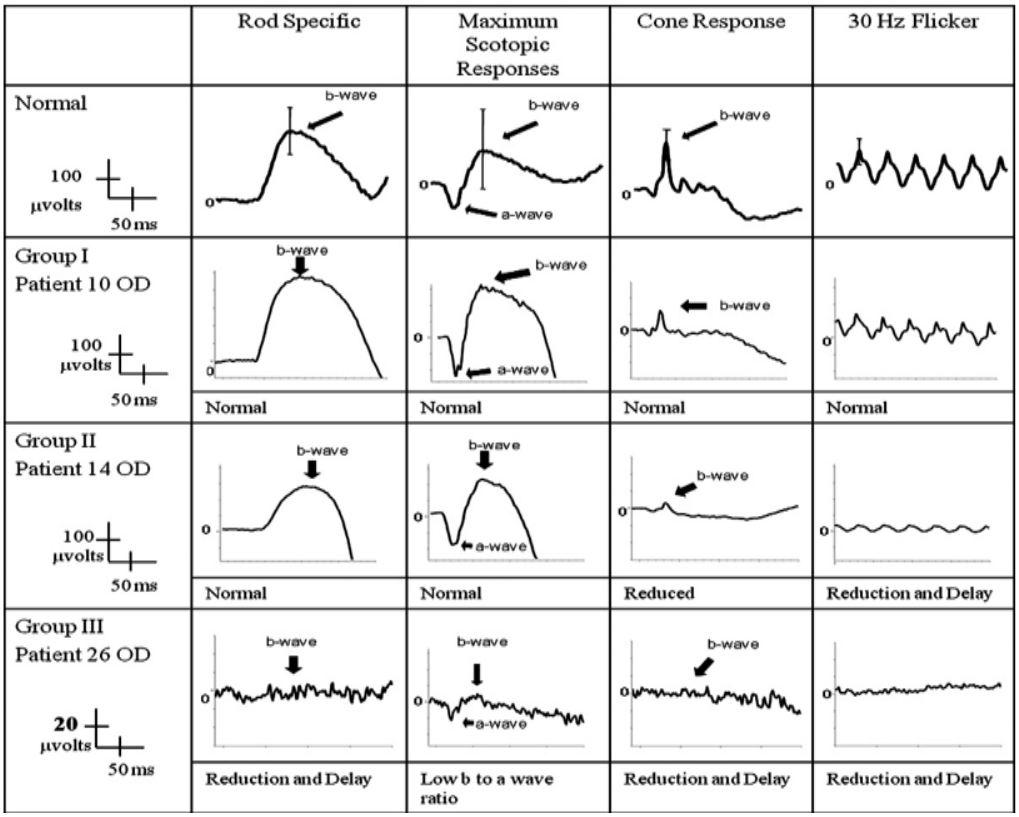

Figure 7 Electrophysiological findings in different groups of STGD1 (Adapted from (Lois et al. 2001)). Group 1 shows normal full-field amplitudes; group 2, shows normal scotopic rod electroretinogram ERG but reduced photopic B wave amplitudes and 30-Hz Flicker; group 3 shows ERG abnormalities involving both rod- and cone-driven responses.

3 Transgenic and knockout animal models of STGD1

A general problem when attempting to study macular dystrophies like ABCA4-associated retinopathy is that mice, the most widely used in vivo model, do not possess many cones and have no macula. In the murine retina, rods constitute ~97% of mouse retinal PRs, with cones accounting for the remainder (Carter-Dawson and LaVail 1979). The human macula region is dense in cones while the peripheral retina is predominantly composed of rod PRs. Several *Abca4* -/- models have been generated to study and better understand STGD1, however none accurately reproduce the disease phenotype. Already in 1999 the *Abca4* -/- mouse model on a bl6 (pigmented) background showed accelerated accumulation of A2E (by 44 weeks), the main component of lipofuscin in the RPE, as well as delayed dark photoresponse in rods; but rod and cone OS structure was normal (Weng et al. 1999). In 2010 *L.Wu* and collegues generated an *Abca4* -/- albino mouse model, which also presents early accumulation of A2E in the RPE (3 months), and starting from 8 months there is moderately reduced thickness of the ONL (loss of the PRs). Thus although the phenotype is more marked on an albino mouse background, it does not show severe retinal atrophy (Wu, Nagasaki, and Sparrow 2010). The double knockout mouse model Nrl -/- *Abca4* -/- allows to better visualize possible differences between cone and rod PRs by comparing them to single *Abca4* -/-. Neural retina leucine zipper (Nrl) is an important transcription factor for rod cell differentiation, and in the Nrl -/- mouse retina, PR precursors fail to produce rods and generate functional cone PRs expressing S-opsin. The study of this animal model showed that in the absence of *Abca4*, cones accumulate more A2E than rods, and atRal clearance is less strong (Conley et al. 2012).

No *Abca4* -/- mouse model exhibits significant PR loss as seen with human disease. This difference may be related to the different anatomy of the human macula and the low number of cones in the mouse retina. Indeed, it seems that in *Abca4*-/- Nrl-/- mouse model, faulty atRal clearance in the cones, which are the most abundant PRs in the macular region, induces toxicity and A2E formation in the degenerating RPE cells (Conley et al. 2012). In fact, it seems that the recycling of the external segments of the PRs operated by the RPE is therefore disturbed and this leads to degeneration of the PRs and death too. It is difficult to reproduce this process in a cone-poor retina such as in the mouse, where the absence of *Abca4* seems to mimic what happens in the periphery of the human retina where rods predominate and only a few cones are in contact with the RPE. *Abca4* Knock-in mouse models have also recently been generated since STGD1 is often caused by missense mutations. The mutant mice showed strong accumulation

of A2E and lipofuscin in their RPE cells but no retinal degeneration up to 12 months. Thus, degradation of this large mutant misfolded protein in the mouse retina caused a very low detectable photoreceptor degeneration (Zhang et al. 2015). Furthermore, in 2018, Molday and colleagues generated a knock-in mouse for the p.Asn965Ser (N965S) mutation in nucleotide domain 1 (NBD1) found in STGD1 patients. ABCA4 partially localizes to the PRs endoplasmic reticulum (ER), lacks ATPase activity and exhibits increased autofluorescence, bisretinoid A2E and lipofuscin in the RPE as in the Abca4 knockout mouse, no obvious signs of PRs degeneration (Molday et al. 2018).

3.1 Diurnal murine model for retinal disease

The rodents usually used in the laboratory (mice and rats) are nocturnal and have few cones. Non-human primates possess the fovea but for obvious ethical reasons and high costs, it is difficult to work with them. There are other species with cone-rich retinas, such as squirrels (90%), chickens (90%) and pigs (15-20%). However, these species exhibit other constraints for experimentation (Saïdi et al. 2011). The search for rodent species that make it easier to work on visual diseases has led to the analysis of the retina of other species such as *Arvicanthis ansorgei* and *Psammomys obesus*.

3.2 Arvicanthis ansorgei

The Sudanian Unstriped Grass Rat *(Arvicanthis ansorgei)* is a wild diurnal rodent that lives in sub-saharan Africa. Individuals were captured in March 1998 in Mali and a colony was established at the Strasbourg Chronobiotron for circadian rhythm analysis (Caldelas et al. 2003);(Mendoza et al. 2012).

The retina of this small diurnal rodent is particularly rich in cones: 33% compared to 2.8% in mice and less than 1% in rats. Furthermore, examination of the topographic distribution of the PRs revealed a relative clustering of the cones in the centre; however we cannot speak of a macular area as such (Bobu et al. 2006). The retina has a high resistance to light damage and toxins such as MNU (Boudard et al. 2011). Furthermore the PR nuclei are organized in distinct

layers in the ONL, which consists of 6 rows (compared to mice and rats with 11-15 rows, typical of nocturnal species: (Verra et al. 2020) of which the outermost two are cones and the next four are rods.

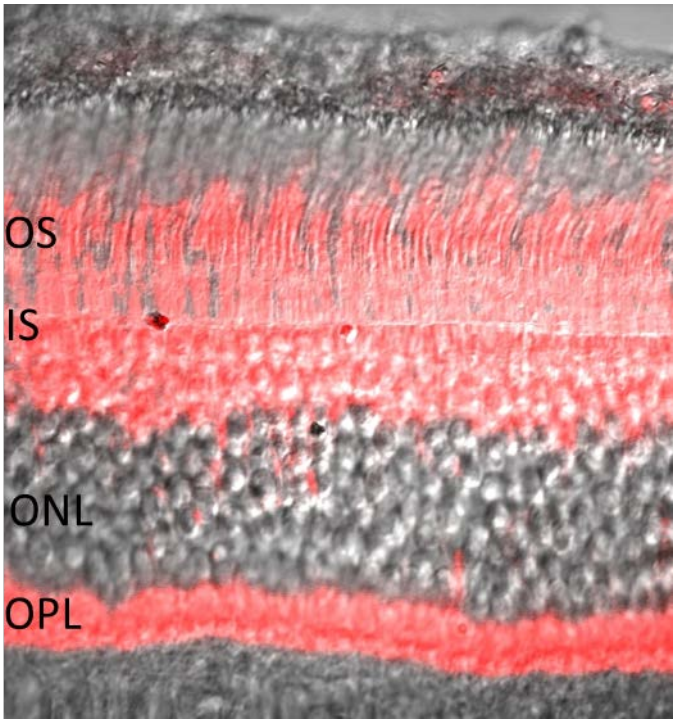

Figure 8 Retina from adult *Arvicanthis ansorgei.* Staining with anti-cone arrestin antibody reveals intense labeling of cone cells, extending from OS down through the cell bodies and is particularly visible in the large synaptic pedicles located in OPL. Modified from (Cheng et al. 2004).

3.1 Psammomys obesus

Fat Sand Rat *Psammomys obesus* belonging to sub-family *Gerbillinae* lives in north Africa in desert areas. It has been shown that when animals are fed on a high energy diet *ad libitum* in the laboratory, they develop type 2 diabetes (Schmidt-Nielsen, Haines, and Hackel 1964). This represents an excellent animal model for studying type 2 diabetes syndromes. In addition to this characteristic, *Psammomys obesus* as a diurnal rodent has a retina characterized by a high percentage of cones, about 40% of the total PRs. Like in *Arvicanthis ansorgei*, also in *Psammomys obesus* the PR nuclei are organized in distinct sub-layers.

Furthermore *Psammomys obesus* has a larger eye diameter than rats (8mm diameter compared to 4-5mm diameter in the rat), potentially increasing its visual capabilities (Saïdi et al. 2011). Concerning ERG measurements, in photopic conditions, where the a-wave amplitude reflects the activity of cones, is very similar to the human response and much higher than in rats (Dellaa et al. 2017). The high percentage of cones and the ratio between the two PR populations makes this species an interesting animal model of central vision disease.

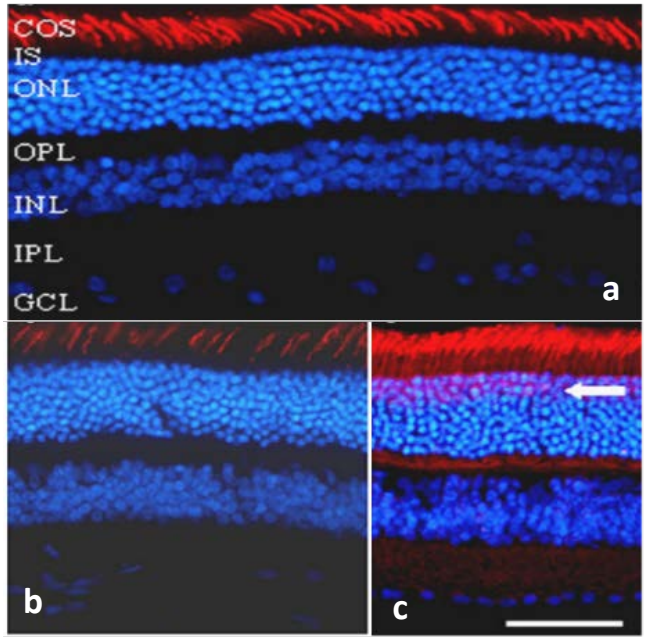

Figure 9 Cone photoreceptor immunohistochemistry in *Psammomys obesus*. (a). Staining of sections with the cone-specific lectin PNA showed label surrounding COS, corresponding to cone matrix (b).Use of short-wavelength cone opsin antibody show specific labelling of lower numbers of COS (c)Staining with anti-cone transducin shows OS, IS and synapsis of cone cells. Modified from (Saïdi et al. 2011).

4 Genome manipulations

The creation of transgenic animal models has made it possible to study human pathologies and to develop new therapeutic approaches. The first genetically modified mouse obtained by inserting a DNA molecule into the embryo dates back to 1974 (Jaenisch and Mintz 1974). The techniques commonly used to generate a transgenic animal involves the insertion of DNA and modification by homologous recombination such as microinjection into the pronucleus of the oocyte, intracytoplasmic sperm injection (ICSI), the use of embryonic stem cells in which exogenous DNA is inserted and then they are injected into the cavity of a blastocyst and transferred into the uterus of a pseudopregnant female where the development of the embryo will continue normally. The transfer of DNA can take place either by electroporation, by means of a microinjection, or by viral vectors.

Over time, however, genetic editing techniques have been increasingly used which allow the animal's genome to be modified directly. In fact, these require the use of enzymatic proteins such as recombinases and nucleases. The CRE-LoxP system is based on a recombination method typical of the P1 bacteriophage. It exploits the ability of the CRE recombinase to recognize and cut at the loxP sites within which the gene of interest will therefore be placed. This method is used to create conditional gene modifications. In fact, by exploiting specific or inducible tissue promoters (i.e. Tamoxifen) it is possible to control the system from a temporal and spatial point of view.

Gene editing can also be performed by nucleases, enzymes that act like molecular scissors capable of making double-stranded cuts in DNA.

The basic principle of the Zinc-Finger Nucleases (ZFN) technology is to use the DNA binding motifs, such as that of the zinc fingers, typical of nuclear proteins, to recognize specific sequences at the level at which the protein can act. Each zinc finger motif, as was well known, contacts 2 or 3 specific adjacent nucleotides on the DNA; So it was interesting to build an artificial protein in which there are several consecutive zinc finger motifs, so that they recognize a precise target sequence fused with a restriction endonuclease that actually mediated the cut on the DNA. For this second and fundamental task, the chosen nuclease was Fok1, which consists of an N-terminal domain responsible for binding to DNA and a carboxy-terminal portion which instead promotes a non-specific cut of the DNA. The domain of interest was precisely the latter, since artificial zinc fingers would be used for the recognition. The choice

of Fok1 also proved to be advantageous because endonuclease cleavage occurs only when the protein is in the form of a dimer. This feature, which may at first glance seem like a limitation, was instead a possibility of doubling the specificity of the technique: by constructing two ZFNs, one of which recognized an upstream sequence and the other a downstream sequence, it would in fact have been possible to guarantee a cut at the level of a unique region of the genome (Carroll 2011).

However, the success of the Zinc-Finger Nucleases technology has been replaced with another interesting competitor in the field of genome editing, a new strategy that was almost contemporary but subsequent to the method just described: the TALENs. A class of proteins produced by some pathogenic organisms of plants, belonging to the genus *Xanthomonas*: these are the TAL proteins (Transcription Activator-Like), responsible for activating the transcription of a series of genes in the infected plant, thus implicated in the bacterial infection. The principle of this technology was to build a chimeric protein which contained, in addition to the NLS nuclear import domain and the nuclease Fok1, both also present in ZFNs, a DNA interaction domain which followed the "code" to recognized the DNA nucleotide sequences. In fact, this domain is composed of repetitions of small peptide sequences, which each expose two amino acids towards the DNA. Each pair of amino acids recognizes a specific nucleotide. Also in this case, Fok1 was generally chosen as the nuclease that was able to guaranteed the specificity of the cutting site in the genome (Mak et al. 2013).

However, both strategies have been largely replaced by CRISPR-Cas9 technology, where recognition of the target sequence is mediated by a guide RNA rather than by protein domains, resulting in a highly specific and efficient binding (Kim and Kim 2014).

4.1 CRISPR-Cas9

The Nobel Prize in Chemistry 2020 went to Jennifer Doudna and Emmanuelle Charpentier for the gene editing technique “Clustered Regularly Interspaced Short Palindromic Repeats”, or CRISPR-Cas9. CRISPR-Cas9 systems are divided into two classes, each further divided into distinct types and subtypes based on different structural characteristics: class 1: CRISPR locus associated with multiple Cas proteins; class 2: CRISPR locus associated with a single Cas protein. An important advance came from the study of the CRISPR-Cas9 system identified in *Streptococcus pyogenes*. This system was initially described as an adaptive immune system in prokaryotes. These short repetitions are exploited by the bacterium to recognize and destroy the genome from viruses similar to those that originated CRISPRs: they therefore constitute a form of acquired immunity of prokaryotes. The CRISPR locus is made by repeats interspersed with short sequences derived from exogenous DNA targets known as spacers. These spacers are transcribed into crRNAs that bind to CRISPR associated proteins (Cas), which target specific complementary sequences. The double-stranded endonuclease activity of Cas9 also requires that a short conserved sequence, (2–5 nts) known as protospacer-associated motif (PAM), follows immediately 3´ of the crRNA complementary sequence. In fact, even fully complementary sequences are ignored by Cas9-RNA in the absence of a PAM sequence. PAM is an essential target that allows distinguishing bacterial self-DNA from non-self DNA. It is in fact absent in bacterial genomes. To achieve site-specific DNA recognition and cleavage, Cas9 must be complexed with both a crRNA and a separate trans-activating crRNA (tracrRNA), that is partially complementary to the crRNA (figure 10).

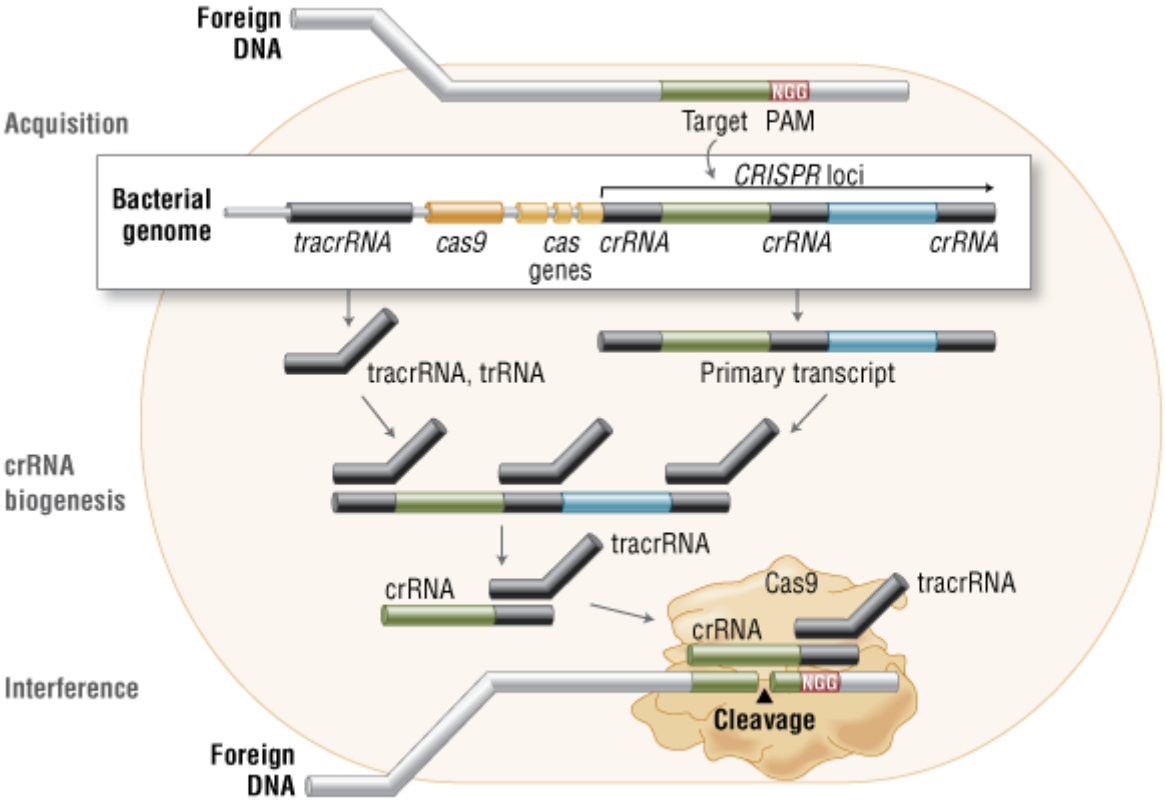

Figure 10 CRISPR-Cas9 in bacteria immune system. Representative scheme shows the foreign DNA incorporated into the bacterial genome at the CRISPR loci. CRISPR loci is transcribed into crRNA. Cas9 endonuclease complexed with a crRNA and separate tracrRNA cleaves foreign DNA containing a 20-nucleotide crRNA complementary sequence adjacent to the PAM sequence. *(CRISPR/Cas9 & Targeted Genome Editing: New Era in Molecular Biology, international.neb.com).*

The simplicity of the system type II CRISPR nuclease, requiring only three components (Cas9, the crRNA and tracrRNA) make this system useable for gene editing. In fact, the mains components crRNA and tracrRNA are engineered to form a single guide RNA (sgRNA) able to recognize and bind the complementary DNA and activate the Cas9 protein which cut in the double strand of DNA. The guide RNA recognizes a target site approximately 20 bp in length adjacent to an NGG motif, representing a protospacer adjacent motif (PAM) recognized by Cas9. Following DNA breakage, error prone non-homologus end joining (NHEJ) repair processes take place, which in the absence of a template is activated and introduces indels into the damaged site. Then there is another homology-directed repair (HDR) mechanism which is

a pathway activated in the presence of a template that precisely corrects the damage (Figure 11) This system of molecular scissors is exploited to modify the genome and generate knock out or knock in by exploiting these endogenous DNA repair mechanisms.

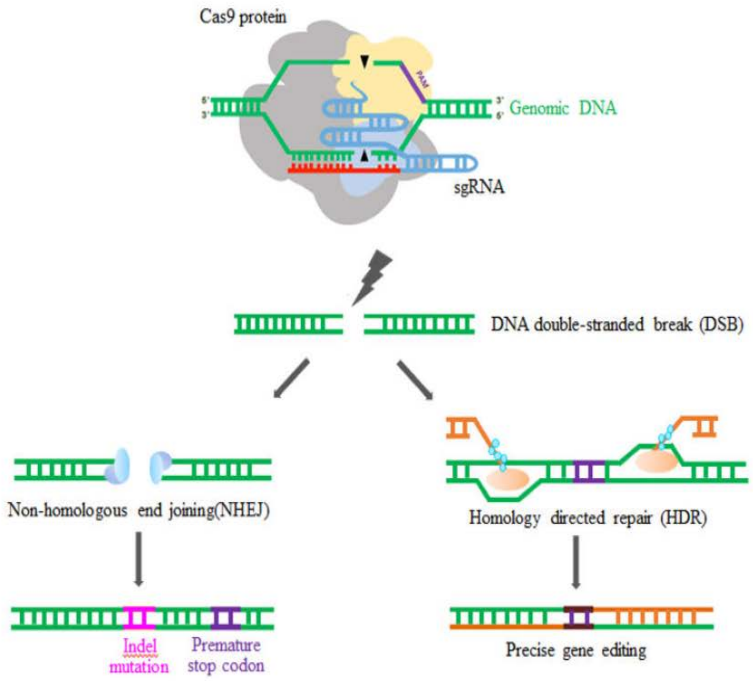

Figure 11 CRISPR-Cas9 mechanism. The Cas9 enzyme is activated by first binding to a guide RNA and then binding to the corresponding genomic sequence that immediately precedes the 3 nucleotides sequence called PAM. The Cas9 enzyme then creates a double-strand break, and the NHEJ or HDR pathway is used to repair the DNA, resulting in an altered genetic sequence Modified from (Liu *et al.*;2017).

4.2 Delivery strategies for CRISPR-Cas9

The CRISPR-Cas9 system is now widely used for gene therapy, including the treatment of eye diseases. The strategy that involves the use of Cas9 endonuclease and sgRNA capable of "guiding" the CAS9 protein to the target site, can be delivered with different strategies. Such strategies are numerous, providing for viral and non-viral delivery CRISPR-Cas9 systems.

CRISPR-Cas9 delivery methods involve the choice of delivery vehicles and the CARGO that it's Cas9 nuclease and guide RNA. There are three categories of CRISPR delivery vehicles: viral, non-viral and physical. The CARGO, more specifically the Cas9 endonuclease, can be delivered as DNA, mRNA or protein. The CRISPR- CARGO can be a DNA plasmid, with both Cas9 and guide RNA genes under the expression of specific promoter. It is a stable system but needs to be delivered into the nucleus and can produce more off -targets. CRISPR-CARGO can also be in the form of Cas9 mRNA and sgRNA. This leads to less off-target artefacts given the transient expression of Cas9, but it is not very stable compared to the plasmid DNA form.

Furthermore, CRISPR-CARGO can also be in form of Cas9 protein directly bound to the guide (Liu et al. 2017; Yu and Wu 2021).

Concerning the delivery method, physical and non-viral approaches consist of either electroporation, the microinjection of CRISPR-CARGO into embryonic cells, or lipid nanoparticle vectors that exploit the electrostatic interactions between negatively charged DNA and positively charged lipids. It can be used for all three types of CARGO, cell transfection taking place thanks to chemical reagents such as Lipofectamine 2000.

Although viral delivery of the CRISPR-Cas9 system is less safe ccompared to non-viral ones, it is certainly the most efficient. Furthermore, the physical delivery system cannot be used for in vivo applications (Liu et al. 2017). Viral vectors are obtained by replacing the sequence responsible for viral replication and proteins with a gene of interest. Several types of viruses, including retroviruses such as lentivirus, adenoviruses, adeno-associated virus (AAV), and herpes viruses, have been modified in the laboratory for use in gene therapy applications (Robbins and Ghivizzani 1998). Viral vectors are now widely exploited as CRISPR-Cas9 system delivery methods.

4.3 AAVs

Adeno Associated Virus (AAV), are single-stranded DNA viruses of 4.7Kb belonging to the parvovirus family. They are not self-replicating, depending on other viruses such as Adenoviruses for replication. They are not pathogenic to humans. Three genes - Rep, Cap and Aap, characterize the single strand of DNA. Rep codes for proteins necessary for genome replication and packaging. Cap instead encodes for viral capsid proteins. Aap appears to play an important role in the assembly of capsid proteins (Yu and Wu 2021).These genes are flanked by inverted terminal repeats (ITRs) (Naso et al. 2017). Vector AAVs are used extensively for gene therapy, including retinal diseases (Hauswirth 2014). Unlike other viral vectors, they have the advantage of possessing a range of serotype specificity, the capacity to infect both dividing and non-dividing cells, to not show pathogenicity and only very mild immunogenicity. Retroviral vectors such as lentiviruses integrate into the genome of the infected cell and can infect only dividing cells. Adenoviral vectors can infect dividing and non-dividing cells, but often generate an immune reaction (Robbins and Ghivizzani 1998). AAVs are used as vectors for delivering the CRISPR-Cas9 gene editing strategy as well as for gene therapy. The disadvantage of AAVs consists in their small packaging capacity of 4.7Kb, and therefore two AAVs are generally used, one capable of delivering the sequence encoding the *Streptococcus pyogenes* Cas9 (SpCas9, ~4.2kbp) and another for the sequence encoding the guides. Alternatively one can use a dual approach, with each AAV containing a portion of the CAS9 sequence and formation of the full protein following co-infection (Wu, Yang, and Colosi 2010). The use of other types of Cas9 such as *Staphylococcus aureus* Cas9 (SaCas9 ~ 3.16 kbp) (Ran et al. 2015) or *Campylobacter jejuni* CjCas9 (CjCas9 ~ 2.95 kbp) (Kim et al. 2017) has the advantage of using a single AAV, given the small size of Cas9 it is possible to insert everything in a single vector. There are 13 different AAV serotypes that have enormous tropism in the human retina. Serotypes 2-5-7-8-9 have been shown to transduce mouse PRs, while AAV2-6-8-9 target Muller cells and AAV2-6-8 ganglion cells. (Yu and Wu 2021). In addition, the increased efficiency and cellular tropism of hybrid AAV vectors with the AAV2 genome and AAV capsid protein 1 to 9 has been demonstrated (Sharma et al. 2010).

AIMS OF THE THESIS

Aims of the thesis

The objective of this experimental study stems from the awareness of not having an Abca4 KO animal model that mirrors and reflects the characteristics of Stargart's patients. In fact, from the various models previously mentioned, the accumulation of lipofuscin as the main characteristic emerges as a common feature, which manifests itself starting from the 8th month but there is no evidence of structural and functional alterations of the PRs. There is not until now a mouse model that truly reproduced the Stargardt's phenotype. In fact, based on the classification of *Lois et al 2001*, we observe three different phenotypes classified based on different electroretinography responses. In summary, therefore, the first group presents normal full field ERGs; the second group shows generalized loss of cone function with normal rod function; and third group exhibit generalized loss of both cone and rod function. The second group has in fact captured our attention, placing the finger on the cones. In fact, by observing a different behaviour between cones and rods, we wondered if there were any basic intrinsic differences between these two PRs that lead them to behave differently. Indeed a recent published study (Verra et al.; 2022) carried out by the research group in which I performed my thesis work.

They hypothesized that the reason why cones are more susceptible to *Abca4* mutations is due to membrane differences between cones and rods. The first set of experiments showed that cones contain up to three times more *Abca4* mRNA and ABCA4 protein compared to rods, and the second showed that the lipid composition of cone membranes is very different from that of rods, which may confer profound changes in bis-retinoid species. Indeed, the cone OS contained five times more di-all trans-retinal (atR-di) than rods. Together these data suggest that cones are much more vulnerable to compromised *Abca4* activity, leading to their preferential demise in patients with mutant *Abca4*.

The aim of the study is to test the increased vulnerability of cones to *Abca4* gene deletion in vivo, through direct inhibition of *Abca4* transcription following subretinal injection of vectors based on the CRISPR-Cas9 system that was initially delivered by electroporation and then replaced by AAV viral vector. In fact, the feasibility of initial approach is proven by a work published in this field (Bakondi, B. et al., 2016) in which the technique was used to repair retinal degeneration in a rat model of autosomal dominant retinitis pigmentosa. For this purpose it is necessary to have access to retinas expressing large numbers of both rods and cones so their respective responses to *Abca4* inhibition can be compared. Thus the animal model of choice

was the cone-rich (33% compared to <3% in mice) diurnal murid rodent *Arvicanthis ansorgei*, a species in which cone PRs are represented in sufficiently large numbers to perform structural, functional and biochemical measures. For reasons related to the availability of animals, to allow our experimental study the animal model *Arvicanthis ansorgei* was then subsequently replaced by another diurnal rodent *Psammomy obesus* that however has an advantageous high number of cones and a high ratio between the PRs which allows the comparison of two cell populations . In fact, mice are not ideal for such studies given their paucity of cones (Jeon, C.J. et al., 1998).

The first important aim is therefore to successfully perform subretinal injection *in vivo*, in order to correctly inject the CRISPR-Cas9 system between the RPE and the PRs to induce ablation of *Abca4* expression in our animal model.

The second part of the project therefore provide an analysis of *Abca4* expression to validate the deletion. Then analysis related to the expression of *Abca4* as messenger and protein will be performed.

Finally, the structural and functional consequences of *Abca4* knock down in the animal model will be analysed. The phenotype will be observed following deletion and retinal function and PRs will be analysed in order to compare this two population following the absence of *Abca4*.

RESULTS

Results

We present here some additional results not given in the attached paper, which formed earlier parts of the doctoral thesis work. We initially planned to use *Arvicanthis ansorgei* as our diurnal rodent experimental model, and preliminary studies were undertaken on this species prior to later substituting them with *Psammomys obesus.* Presented here in order we performed: 1. immunohistochemical characterization of *A. ansorgei* retina ; 2. electroporation of CRISPR-Cas9 plasmids into newborn *A. ansorgei* pups; and 3. in utero electroporation into E12.5 *Mus musculus* embryos.

1 Immunostaining from *Arvicanthis ansorgei* retina

To obtain an experimental baseline of our animal model *Arvicanthis ansorgei*, we performed immunohistochemistry in normal animals (Male-Female *Arvicanthis Ansorgei*, P30). The following characteristic retinal proteins were analyzed : Rom-1, a retina-specific integral membrane protein localized to the photoreceptor disk rim (Bascom et al. 1992); Rhodopsin a visual pigment found in the rod photoreceptor cells of the retina (Park 2014). Glial fibrillary acidic protein (GFAP), the major protein constituent of glial intermediate filaments in differentiated fibrous and protoplasmic astrocytes of the central nervous system (Eng 1985); S-Cone Opsin and M-Cone Opsin, photopigments respectively present in the cones S (10%) and cones M (90%) (Nadal-Nicolás et al. 2020).PKCα, protein kinase associated with bipolar cells (Osborne et al. 1991); Pan-Arrestin, an important protein for regulating signal transduction at G protein-coupled receptors, presents in both of photoreceptor rods and cones (Gurevich et al. 2011). Immunohistochemical staining showed the widespread expression of the S-Opsin and M-Opsin (respectively expressed in Short wavelength cones (SW) and Medium wavelength cones (MW) clearly shows the abundance of cones in this animal model, M-Opsin is much more expressed than the S-Opsin, as the MW cones represent 90% of the total cones (cones SW 10%). In some rodents, the two cone spectral classes (SW-cones and MW-cones) are distributed in an asymmetrical pattern, with SW-cones predominantly located in the ventral field (Szél et al. 1996). In *Avicanthis ansorgei* we observed a significantly higher number of SW cones in the central field compared to the far periphery, but there was no detectable variation in their number as a function of retinal quadrant. (Bobu et al. 2006). Rhodopsin antibody bound strongly to ROS and rod cell bodies but was completely absent from cones. Pan-Arrestin and ROM1 are expressed in both cones and rods. GFAP expression was detected along the vitreal face of the

retina, corresponding to astrocytes. It is also known to appear in radial Müller glia under conditions of stress, which could occur following the subretinal injection of plasmid CRISPR-Cas9. We observe PKC alpha expressed in bipolar cells (cell body to synaptic button). M-opsin and S-opsin mark the population of cones, with a lower percentage of s cones (10%) and a higher percentage of m cones (90%). We observe cone arrestin (CAR) exclusively in the cones, it marks the whole cell from the outer segment, cell body, to the axons that make contact with the bipolar cells. GalphaT2, cone transducin, also specifically labels the cones, but only the outer segments are labeled by staining.

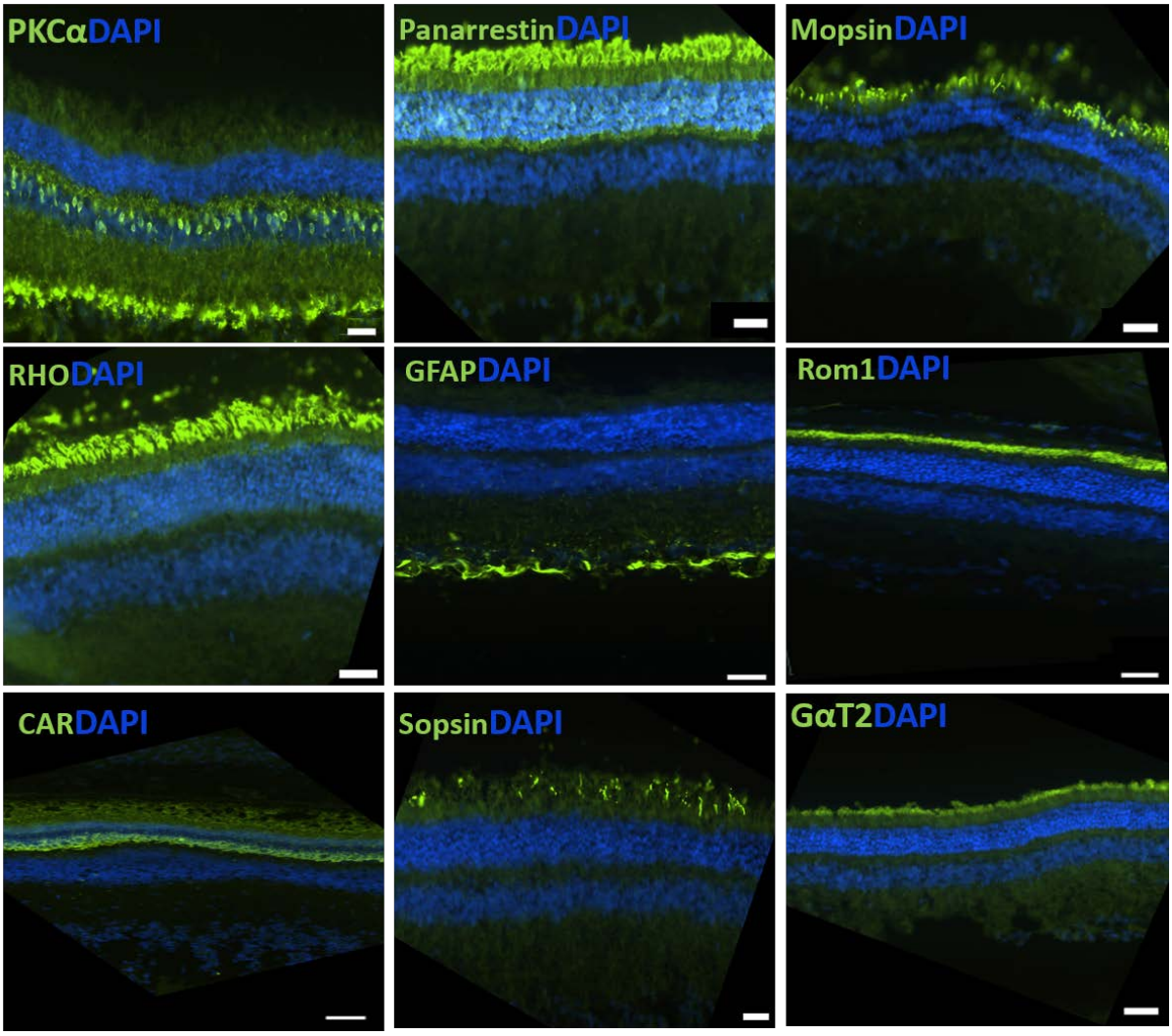

Figure 12 Immunostaining in *Arvicanthis ansorgei* control retinas

Fluorescence microscopy images (Leica EL6000) of Arvicanthis ansorgei (Male-Female, P30) retinal sections (10-12µm) to visualize proteins, use primary antibody Rom-1D5 (anti-Rom1) (mouse, 1:500), PKC-α (rabbit, 1:500), Rho4D2 (anti-rhodopsin) (mouse, 1:500), GFAP (rabbit, 1:500), S-OPSIN (rabbit, 1:500), M-Opsin (rabbit, 1:500), Pan-arrestin (rabbit, 1:500), GαT2 (rabbit, 1:500), CAR (rabbit, 1:200). DAPI, 49,69-diamidino-2-phenylindole.

2 Electroporation in newborn *Arvicanthis ansorgei*

Following the characterization of *Arvicanthis ansorgei* retina and the successful set-up of a subretinal injection protocol, we decided to use an approach developed by (Bakondi et al. 2016) involving the injection of the control plasmid with Cas9 fused to a fluorescence protein

mCherry under the CBh promoter and two irrelevant guide RNAs (gR73 and gR74) under the hU6 promoter.

The control plasmid was used to evaluate, after electroporation of P0 *Arvicanthis ansorgei*, the correct entry of plasmid into PRs. To evaluate the plasmid entry into PRs, the Mcherry fluorescent protein was followed, mCherry absorbs light between 540-590 nm and emits light in the range of 550-650 nm (Shu et al. 2006). When the plasmid entry, the fluorescence was emitted, which corresponds to the expression of Mcherry.

Thus, with Hamilton syringe, 33 gauge blunt end as previously described (Matsuda and Cepko 2008) the plasmid control Rho104, (1µl) containing a dye (Fast green 1%) was injected into the subretinal space of newborn *Arvicanthis ansorgei* (n=5) P0, anesthetized on ice for several minutes. Only the right eye was injected. For *in vivo* transfection of the retina by electroporation, the tweezer-type electrodes were lubricated with SignaGel (to increase the contact between the pup and the electrodes). Then the tweezer-type electrodes were placed around the head of the pup immediately after injection, and slightly squeezed. Five square pulses of 50-ms duration and 100V intensity with one-second intervals between pulses were applied using a pulse generator. The five operated pups were warmed until they recovered, and then returned to the adoptive Albino Wistar rat mother.

Animals were sacrificed at post-natal day 14 (P14). The CBh promoter is frequently used for the expression of Cas9, it is an altered version of the CBA promoter, which provides long-term transgene expression in all cell types seen with the CBA or CMV promoter, at levels matching or exceeding each (Gray et al. 2011). After electroporation of a plasmid pCAG-GFP, the expression of GFP fluorescence protein is visualized after 2 days and it persists at least 50 days (Matsuda and Cepko 2004). For this reason, the expression of mCherry is examined in the same way. However it was able to visualize the expression of mCherry starting from day 14 and not before.

Animals were sacrificed at post-natal day 14 (P14, five injected and electroporated right eyes were rapidly enucleated and prepared for retinal section to assess mCherry distribution (Bakondi, B. et al. 2016).

Looking at mCherry expression at P14 following electroporation of the control plasmid in retinal section of *Arvicanthis ansorgei*, it is possible to observe the presence of the fluorescence

marker in the ONL layer. The marker is present exclusively in the PRs layers and not in other retinal cell types. Thanks to the expression of mCherry, the injection technique and the selected electroporation parameters were positively evaluated.

However, with a closer look it is possible to observe that, among the PRs, only the rods are transfected by mCherry marker and not the cones. It has been shown that the PRs nuclei are organized in distinct layers in the ONL of which the outermost two are cones and the next four are rods. (Verra et al. 2020). Thus it is clear that mCherry expression is exclusively present in rods, marking the rods inner segment and rods cell body. From the co-staining with the DAPI (Fig.13, A), it is possible to visualize the blue cones nuclei, without mCherry superposition. In addition, with a cone arrestin antibody (fig 13, E-F) that exclusively label the cone population, not Mcherry-cone arrestin signal overlap could be found.

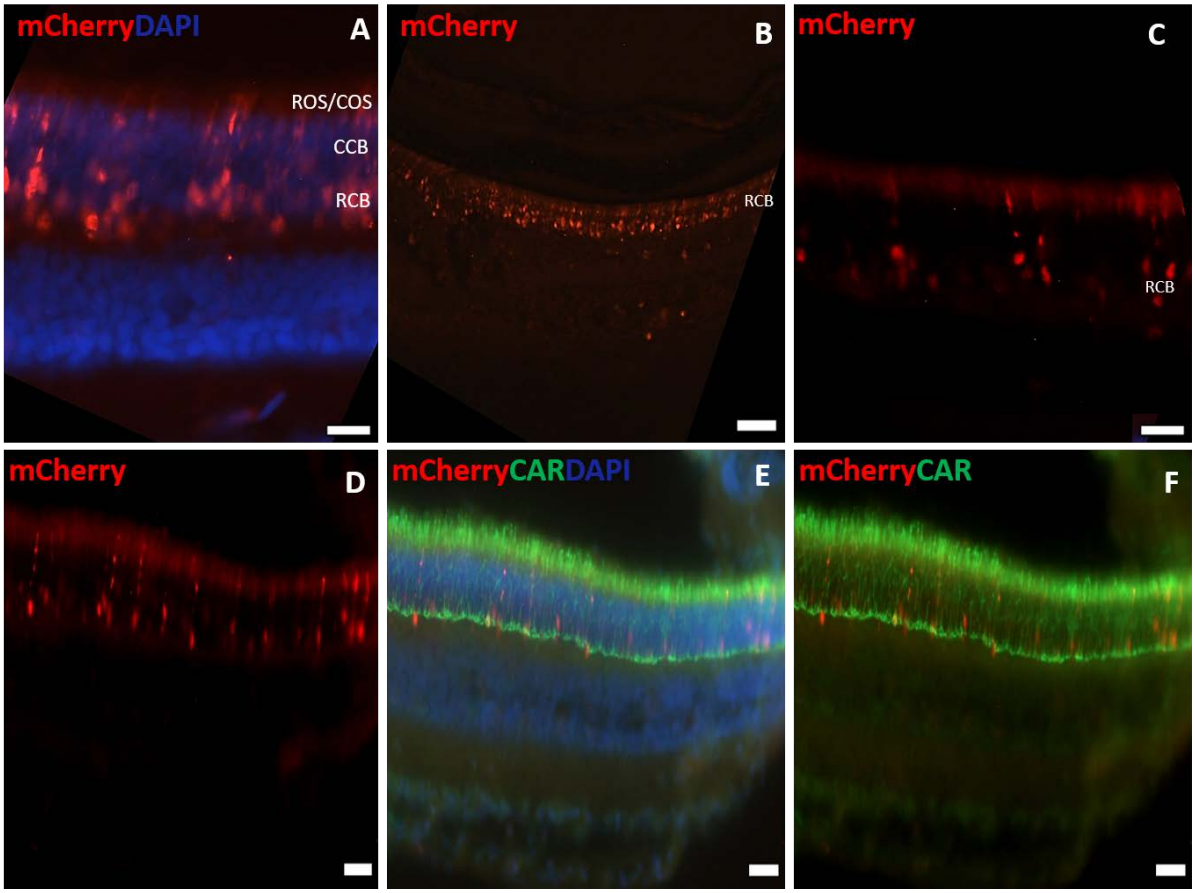

Figure 13 mCherry expression in *Arvicanthis ansorgei* retina (P14)

Fluorescence microscopy images (Leica EL6000) of *Arvicanthis ansorgei* (P14) retinal sections (10-12µm) electroporated by the plasmid control Rho104, (1µl) to visualize mCherry expression (A-B-C-D), use primary antibody cone-arrestin (mouse, 1:500) to visualize cone PRs.(E-F). COS, cones outer segment ; CCB, cone cell body; RCB, rod cell body;DAPI, 49,69-diamidino-2-phenylindole; INL, inner nuclear layer; ONL, outer nuclear layer; Scale bar 100µm.

3 In utero electroporation

Given the difficulty in targeting cones by electroporation of newborn (P0) pups, we decided to inject plasmids followed by electroporation *in utero*, intended to target both PR types efficiently.

The *in utero* electroporation was set up in C57BL/6J mice at embryonic stage E12.5. A CAG-GFP+ Fast Green 0.1% plasmid was used to track target cells following electroporation through GFP expression.

A pregnant C57BL/6J mouse was anesthetized with gas anesthesia and operated by caesarean section to access the uterine horns. The embryos, still in the uterine sac, were injected (in a single eye) with a plasmid with GFP as a reporter and their retina subjected to electroporation. The uterine horns are then reinserted into the womb.

After 48 hours post electroporation, the embryos are collected from the pregnant mouse .With a careful look under the microscope it is possible to detect the presence of green signal emitted by the expression of GFP protein through the lens (Fig 14,a). In transversal sections of the retina (Fig. 14,b) after 48 hours post injection and electroporation *in utero*, it is possible to observe the expression of GFP protein within the progenitor cells of retinal RPCs still in the differentiation phase. The presence of GFP therefore confirms the correct procedure of injection and electroporation in utero.

.

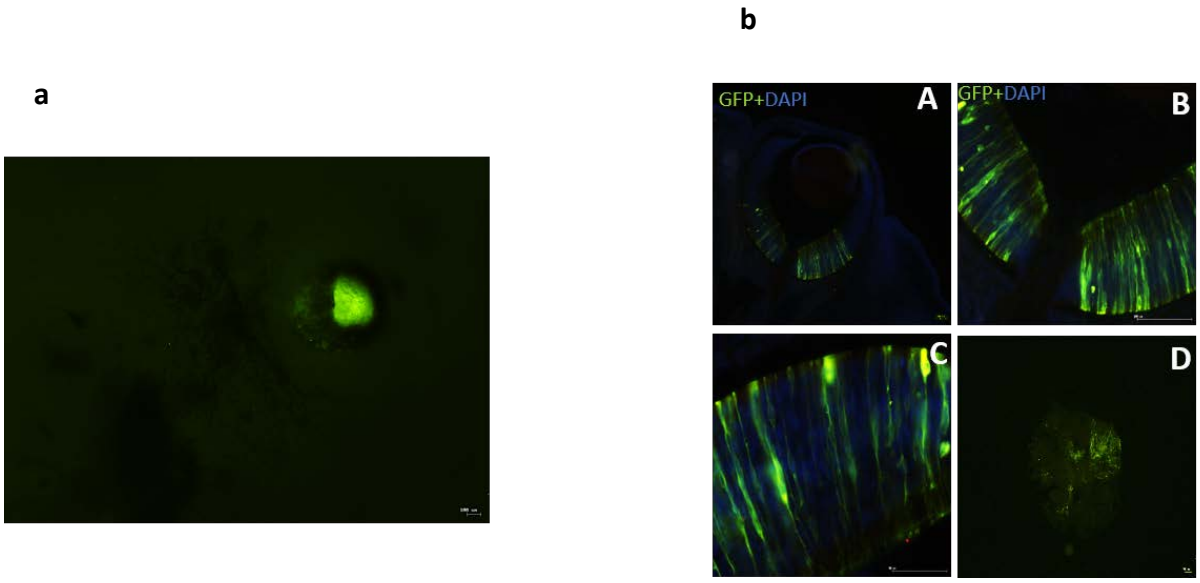

Figure 14 GFP expression in *Mus musculus C57bl/6j* retina (E14.5)

Fluorescence microscopy images (Leica EL6000) to visualize GFP expression of *Mus musculus* (E14.5) eye (Fig.13,a) electroporated by the plasmid CAG-GFP + Fast Green 0.1%, (1µl). GFP+ RPCs in retina sections (10-12µm)(A-B-C) and in retinal flat mount (D) (Fig.13,a).; DAPI, 49,69-diamidino-2-phenylindole; Magnification 40X(A),20X (D-E-F),10X(B-C).

4 Target sequence in *Abca4* gene of *Psammomys obesus*

The search for the *Abca4* gene in *Psammomys obesus* was carried out thanks to the alignment in the Blast database between the *Abca4* gene (end exon 4, intron 4-5, exon 5, beginning intron 5-6) and the whole genome of *Psammomys obesus*.

After ideally identified a part of the *Abca4* gene sequence in *Psammomys obesus*, the design of two pairs of primers (forward 5'-GTTCCTTACCCTTCACTCTCTTG-3', reverse 5'-CACGATTGCTCTGCTTCCT-3'; forward 5'-CTTCTGTAGTTCCTTACCCTTCAC-3', reverse 5'- GGTAGGTTCAGCTTCACGATT-3') were carried out which could amplify a sequence of 707nt (about 300nt upstream and downstream of exon 5 which is the site of interest of the Cas9 cut).

After optimizing the primers and choosing the pair: forward 5'-CTTCTGTAGTTCCTTACCCTTCAC-3', reverse 5'- GGTAGGTTCAGCTTCACGATT-3', the PFU PCR was performed to amplify the region of interest.

The electrophoresis obtained from the PFU PCR products showed the presence of a single band at around 700bp (no band at the negative control).

To confirm the nucleotide sequence, an agarose gel purification was performed in order to sequence the amplification product by Sanger sequencing. From Sanger sequencing we obtained a sequence of 707bp around exon 5 of *Abca4* gene in *Psammomys obesus* corresponding to the predicted one.

A

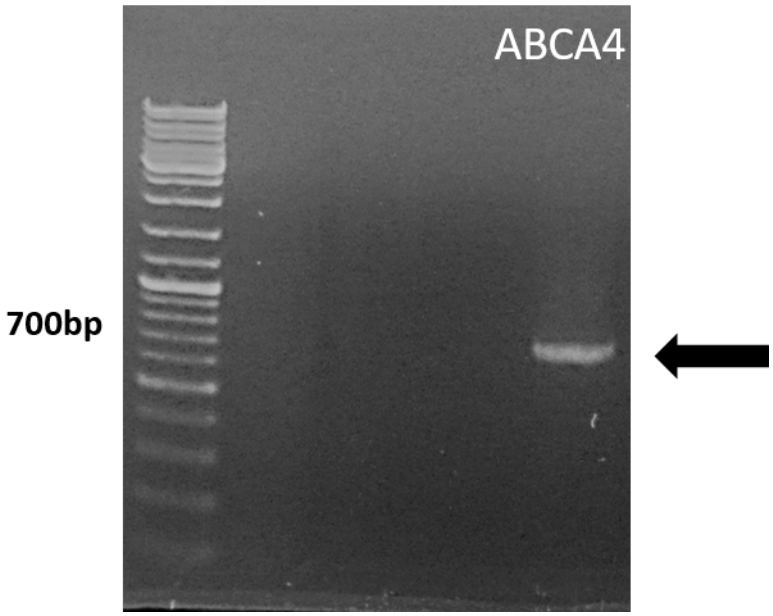

B

```
8072250    AGCCAAAATTCCCCTTCTGTAGTTCCTTACCCTTCACTCTCTTGAAAGCCCCTGTCT  8072306
8072307  TAGTCCAACCCTAAAAAGCACCTGAGATCTCACCCACCCCAGGTTAACATCCCCCACCTT  8072366
8072367  CTATGCCTTTCCACTGTATTGTGCCAGGTTCTTTAGCTGTAAGTGGTATGACTGGATGGG  8072426
8072427  TGGCAGATACTGGCAGCAGCCTTAACCTCCAAGAGTTCCCAAGGAAACCAAGAACACAGC  8072486
8072487  TCTCTTGTAAGAGTCAAGTAGAAATATTTCCAGTCAATTCTAGCTGCTTTTCTTATTTTC  8072546
8072547  GACTCATCTCCCTTCAACATCCTGTTCTTTCTTTCACTCATGTGCAGGAAGAGGATTACA  8072606
8072607  AATCCGAGACATCCTAAGAGATGAAGAGACAATGACTCTATTTCTCAAGAAAAACATTGG  8072666
8072667  CCTGTCTGACTCAGTTGCCCATCTTCTGGTCAGCTCCCAAGTTCGTGTGGAACAGGTAAG  8072726
8072727  TGAGGCCTGTTAAGAGGAGGAAAAAGCACTGAGCCTGAGAGAGACAAGGGTGATTCTGTT  8072786
8072787  TCTTTTCCCTTCTGCGTCTATATTCAGAATCCATGACTCATGCTCCATATTCAGGGACAC  8072846
8072847  ACCTGGGGGTTACTGAGCCAACGAGAACCCCATCACAGCAGTCTGAAGCAGCACTGGCAC  8072906
8072907  TCATAAGACTTCCCAGGTTTTGAAACTTGAAGGAAGCAGAGCAATCGTGAAGCTGAACCT  8072966
8072967  ACCCTGTAGAGTGGGGGAATCTCACCATTCATTTACTAATCAGATCTTCAGGGACAGCTA  8073026
```

Figure 15 *Abca4* gene in *Psammomys obesus*

1.5% agarose gel electrophoresis (Fig 14, A) *Abca4* band at 707bp and no band in the negative control (-). *Abca4* sequence in *Psammomys obesus* (Fig 14,B), correspondence between sequence obtained by Sanger sequencing and sequence predicted by Blast. (blue, primer forward: 5'-CTTCTGTAGTTCCTTACCCTTCAC-3'and primer reverse: 5'-GGTAGGTTCAGCTTCACGATT-3'- green, *Abca4* gene exon 5).

5 Article

Abca4 inhibition in a cone-rich rodent leads to Stargardt Disease type 1-like retinal degeneration

Fabiana Sassone[1], Michel J. Roux[2], Dominique Ciocca[3], Pascale Koebel[2], Marie-Christine Birling[2], Janet R. Sparrow[4] and David Hicks[1*]

1 INCI-UPR3212-CNRS, 8 allée du général Rouvillois, 67000 Strasbourg, France

2 **IGBMC**/Institut Clinique de la Souris - CNRS UMR 7104 Inserm U 1258, 1 rue Laurent Fries, BP 10142, 67404 Illkirch CEDEX France

3 Chronobiotron UPR3415-CNRS, 8 allée du général Rouvillois, 67000 Strasbourg, France

4 Departments of Ophthalmology, and Pathology and Cell Biology, Columbia University Medical Center, New York, NY, USA

Author for all correspondence :

David Hicks, INCI-UPR3212-CNRS, 8 allée du général Rouvillois, 67000 Strasbourg, France

Tel : 33 388456723 ; e-mail : david.hicks@inci-cnrs.unistra.fr

Major Classification : Biological Sciences

Minor Classification : Neuroscience

Keywords : Stargardts Disease; Retina; Visual Function; Cones; Animal Model; Gene Editing

Abstract

Mutations in the gene *ABCA4* coding for photoreceptor-specific ATP-binding cassette subfamily A member 4, are responsible for the most common form of inherited macular degeneration known as Stargardt Disease type 1 (STGD1). STGD1 typically declares early in life and leads to severe visual handicap. *Abca4* gene deletion mouse models of STGD1 accumulate lipofuscin, a hallmark of the disease, but unlike the human disease show no or only moderate structural changes and no functional decline. Reasoning that the low cone complement of mice (<3%) might compromise faithful modelling of human maculopathies, we performed subretinal injections of Crispr-Cas9-Abca4/gRNA Adeno-Associated Virus constructs into young Sand Rats (*Psammomys obesus*), a diurnal rodent containing >30% cones. Compared to control injections of AAV-GFP, treated eyes exhibited extensive and rapid (visible 2 months after injection) retinal degeneration. Non-invasive fundus imaging showed widespread photoreceptor loss, confirmed by optical coherence tomography. Functional recording by single flash and flicker electroretinography showed significant decline in photopic (cone) light responses. Post-mortem real-time PCR, immunohistochemistry and western blotting showed significant decrease of cone-specific (MW cone opsin) but not rod-specific (rhodopsin) markers. Transmission electron microscopy showed large numbers of lipid inclusions in treated but not control retinal pigmented epithelium. Finally, UPLC analysis of whole *P. obesus* eyes showed the presence of all-trans retinal-dimer, not detected in rod-rich rat eyes. In conclusion, this animal model of STGD1 more accurately reflects human STGD1 and should be valuable for characterizing pathogenic pathways and exploring treatment options.

Significance Statement

Stargardts Disease type 1 (STGD1) is the commonest inherited macular disease, patients suffering progressive central vision loss and severe handicap. To date no treatment is available. STGD1 is caused by mutations in *ABCA4*, crucial in photopigment renewal. STGD1 mouse models do not recapitulate the structural and functional decline seen in STGD1. Mice have <3% cones, the major macular cell type. We used CRISPR-Cas9 gene editing to inhibit *Abca4* in *Psammomys obesus*, a diurnal rodent with >30% cones. In contrast to mouse models, *P. obesus* demonstrated early onset, widespread retinal degeneration, predominantly affecting cones. This was confirmed by non-invasive monitoring, visual function recording, and post-mortem cellular and molecular analyses. This improved animal model of STGD1 should facilitate exploration of treatment strategies.

Introduction

Photoreceptor (PR) damage, malfunctioning and death occur in a large number of visual pathologies. Whether the underlying causes are genetic, chemical or environmental, progressive loss of these cells leads to visual handicap and incapacitating blindness. The death of cones is particularly devastating since these cells are responsible for high acuity and chromatic daylight vision [1]. Cones reach maximal density within the fovea, and this region is especially vulnerable in widespread diseases such as age-related macular degeneration and autosomal recessive maculopathy Stargardt Disease type 1 (STGD1). The latter is the most common inherited maculopathy, with carrier frequency of up to 1:50 in the general population. The causal gene has been identified as *ABCA4* encoding the PR-specific flippase ATP-binding cassette subfamily A member 4 [2]. More than 1200 mutations have been identified, the majority of which are compound heterozygous, resulting in retinal degeneration of variable phenotype but in which early foveal damage and severe loss of central vision are commonly observed [3]. Most *ABCA4* mutations lead to a central-peripheral gradient of retinal damage, almost always with macular involvement [4, 5]. A commonly used classification recognizes three sub-types of STGD1: type 1 in which only macular degeneration is seen, with normal full-field rod and cone function; type 2 with macular degeneration and also pan-retinal cone malfunction, but mostly preserved rod function; and type 3 in which both cone and rod loss are widespread [5, 6]. The most severe forms are linked to null mutations, resulting in cone-rod dystrophy that appears early in life and evolves rapidly towards severe visual handicap. Abca4 is expressed by both rods and cones [7], and based on seminal studies using genetically modified mouse strains [8, 9], biochemical analyses of retinal and pigmented epithelium (RPE) preparations [10] and rigorous *in vitro* experiments [11], a pathogenic mechanism has been proposed: truncated or absent ABCA4 impairs the visual cycle, with slowed clearance of all-trans retinal (atRal) leading to formation of toxic bisretinoids within PR outer segments (OS). Daily phagocytic removal of PROS membrane debris by the adjacent RPE leads to accumulation and modification of these bisretinoids within the RPE, resulting in accelerated build-up of lipofuscin, a hallmark feature of STGD1 in humans and mouse models [3, 4, 8]. Lipofuscin exhibits noxious properties such as initiation of inflammatory cascades, photo-sensitization and lysosomal breakdown [12], and eventually toxicity reaches a threshold level at which RPE cells start to die; since RPE is critical for the maintenance of PR, these latter cells also die in their turn, forming a vicious pathogenic circle.

However, this hypothetical mechanism does not account for the cone-dominant phenotype in STGD1. In addition to macular involvement, type 2 STGD1 patients exhibit pan-retinal loss of cone function while rod function remains relatively normal [5, 6]. Furthermore, although the original *Abca4* null mice display accumulation of lipofuscin, there are no or little structural or functional defects even in aged mice [8, 13] or in knock-in mutant *Abca4* transgenic mice [14, 15]. Another *Abca4* null deletion raised on an albino mouse background does show moderate late-onset PR loss, but no functional data have been reported [8]. Finally, in severe forms of human STGD1 it has been reported that retinal abnormalities appear prior to visible changes in the RPE [16].

One potential drawback of relying on transgenic mouse models for maculopathies is the low numbers of cones in such nocturnal rodents: <1% in rats [17], <3% in mice [18]. We reasoned that animals containing high numbers of cones, more closely resembling the PR composition of human macula, would possibly constitute superior models for such diseases. Diurnal rodents possess between 30-40% cone PR, and rod and cone cell bodies are separated into distinct sublayers in the outer nuclear layer (ONL), facilitating their analysis [19,20]. Furthermore their visual response characteristics are more similar to those of humans compared to rats or mice [21, 22]. We show here that contrary to the mouse models, inhibiting *Abca4* transcription in a cone-rich rodent led to massive and rapid degeneration of the retina with prominent functional decline in cones, closely echoing the STGD1 phenotype.

Results

Verification of viral inhibition of *Abca4* transcription in rod and cone PR

We used sub-retinal injection of adeno-associated virus (AAV2/8) to deliver CRISPR-CAS9 and *Abca4* gRNA in order to inhibit *Abca4* transcription in the retina of the Fat Sand Rat *Psammomys obesus*. We initially characterized Abca4 protein expression in postnatal and adult animals, and observed that expression levels were relatively low, compared to another cone-specific marker cone transducin (GαT2), prior to PN20 (Figure 1A-A’’’, B-B’’’), and in terms of their mRNA and protein expression profiles (Figures 1C, D). This provided a time window of ~5d to block transcription between eye opening (~PN13), and prior to higher levels of endogenous protein. We verified that AAV2/8 serotype efficiently and selectively transfected both rod and cone PR by sub-retinal injection of eGFP-tagged AAV2/8 into PN15 pups. We observed widespread transfection of both rods and cones but no other retinal cells in other cell layers (Figure 1E-E’’). For *Abca4* knockdown, due to the limited cargo capacity of AAV

vectors it was necessary to co-inject two viruses, one containing sgRNA targeted against *Psammomys obesus Abca4* and eGFP, and the second containing CAS9 and HA tag, into the sub-retinal space of young (PN14-17) animals (Figure 1F, G).

Next, in order to confirm CRISPR-CAS9 gene editing, retinas were collected 4 weeks post-injection and sorted by FACS to isolate eGFP-tagged control (gRNA only) and test CRISPR-CAS9 PR (Figure 2A). We estimated ~25% total PR were transfected by counting GFP+ve cells in FACS-treated retina (Figure 2A). Agarose gel analysis showed presence of a ~500bp band shift in the test cells only (Figure 2B), and Singer sequence analysis of this band confirmed inhibition of *Abca4* transcription (Figure 2C). In further tests of the efficiency of *Abca4* knockdown, immunohistochemical staining of retinas at 2 months post-injection showed that compared to sham-injected eyes, those receiving CRISPR-CAS9 AAV exhibited qualitatively reduced Abca4 label (Figure 2D-D'', E-E''); CAS9 immunostaining was restricted to transfected PR in animals injected with active viral probe (Supp Figure 1). Finally, qPCR of *Abca4* mRNA expression levels in control and treated eyes showed significant decreases only in test eyes (Figure 2F); and western blots against Abca4 showed reduced band intensity in treated but not control retinas (Figure 2G).

Abca4 inhibition leads to decline in cone but not rod visual responses

Scotopic single flash ERG recordings of CRISPR-CAS9 treated and GFP only virus-injected (control) eyes 2 months post-injection (~PN75) showed typical stimulus intensity/response amplitude relationships. Weak flashes (pure rod responses) produced linear stable "a" wave traces, increasing at higher flash intensities (mixed rod/cone responses) (Figure 3A). There was a significant decline in "a" wave amplitudes at higher stimulus intensities in CRISPR-CAS9 treated but not control-injected controls (Figure 3A). There was a similar decline in scotopic "b" wave amplitudes, particularly at higher intensities (Figure 3B). Photopic (pure cone) responses also showed significant decreases in amplitude, for both "a" and "b" waves (Figures 3C, D). Representative single scotopic and photopic traces are shown in Supp. Figure 2. No significant differences were observed when comparing sham-injected and non-operated eyes (Supp. Figure 3). We also performed photopic flicker ERG recordings, and there too, we saw significant reductions in peak amplitudes only in CRISPR-CAS9-treated animals (Figure 3E). Similar data were obtained for animals after 3 and 7 months post-injection, and showed that cone but not rod ERG amplitudes continued to decrease over time (Supp. Figure 4).

Abca4 inhibition causes widespread photoreceptor degeneration

Fundus imaging of animals at 2 months after injection with control viral probe (sgRNA/eGFP only) showed a very small lesion corresponding to highly localized damage at the site of injection (arrow, Figure 3F). Otherwise the retinal aspect was uniform and normal, with major blood vessels faintly visible (Figure 3F). On the other hand, animals injected with active CRISPR-CAS9 probes showed widespread degeneration after 2 months, with extended depigmented lesion areas and blood vessels appearing under the damaged tissue (Figure 3G). Patches of fluorescence were visible at the lesion borders, indicating continued viral eGFP expression. OCT sections of control-injected animals showed the normal laminated structure of retina, with clearly visible cellular and synaptic layers (Figure 3H); however, CRISPR-CAS9-treated animals displayed severely disrupted tissue, the neural retina either missing entirely or just residual inner retina lacking the outer nuclear layer (ONL) (Figure 3I). Additional examples of fundus and OCT imaging of CRISPR-CAS9-injected eyes are shown in Supp. Figures 5 and 6. Longitudinal follow-up of animals 15, 30 and 60d after subretinal injection showed that eyes receiving control virus exhibited a small lesion due to the injection injury, which did not evolve over time; on the other hand, eyes receiving CRISPR-CAS9 AAV showed progression of retinal changes between 30 and 60d (Supp. Figure 7).

Immunohistochemical staining using a rod-specific antibody marker (rhodopsin, RHO) of 2 month post-injection control-injected and CRISPR-CAS9-injected retinas (the latter at areas close to the lesion borders, with continued eGFP expression in some cells) showed that rhodopsin label intensity was approximately equal in both cases (Figures 4A-A’’’, B-B’’’: compare Figures 4A’’’ and 4B’’’). This similarity was confirmed by quantitative PCR analysis of RHO mRNA in control and test retinas (Figure 4C). In contrast, use of a cone-specific antibody marker (mid wavelength-sensitive cone opsin, OPN1MW) to label 2 month post-injection control-injected and CRISPR-CAS9-injected retinas (Figures 4D-D’’’, E-E’’’) showed reduced OPN1MW signal in CRISPR-CAS9 compared to control eyes (compare Figures 4D’’’ and E’’’). This decrease was confirmed by quantitative PCR analysis of OPN1MW mRNA in control and test retinas (Figure 4F). Ultrastructural observation of the OS/RPE interface by transmission electron microscopy showed that control (unoperated) and sham-injected animals displayed conventional subcellular organization, with well-aligned rod and cone OS abutting the RPE (Figures 4G-I). RPE contained numerous oblong melanosomes, together with occasional phagosomes (ingested OS membranes), along their apical surface (Figures 4G, H). The subcellular aspect of the different cell regions, RPE, OS and inner segments (IS) showed good integrity and well-preserved organelles (Figures 4G-I). On the

contrary, examination of CRISPR-CAS9 treated eyes areas close to lesion borders revealed RPE congested with numerous circular lipid inclusions (Figure 4J, K). Furthermore, many IS and OS displayed disrupted cytoplasm and loss of cellular integrity (red arrows, Figures 4J, L). Additional ultrastructural images of the RPE/OS interface in control and CRISPR-CAS9-treated eyes are shown in Supp. Figure 8.

Ultrahigh performance liquid chromatography (UPLC) of extracts prepared from whole albino rat eyes, or control- or CRISPR-CAS9-injected *Psammomys* eyes, showed large differences in two key bisretinoids: A2E and all-trans retinal-dimer (atRal-dimer). Although there was no difference between control and test *Psammomys* eyes (2 month post-injection, ~75d old animals), both having ~41 pmoles/eye A2E, they contained significantly more A2E than either young (~40d, ~11 pmoles) or old (~200d, ~32 pmoles) rat eyes (Figure 4M). And while both groups of *Psammomys* eyes contained high amounts of atRal-dimer, this bisretinoid was below detection limits in both groups of rat eyes (Figure 4N).

Discussion

STGD1 is a devastating inherited blinding disease, the more severe forms declaring in early childhood and progressing rapidly to extreme visual handicap. Although knockout mouse models have existed for many years [8, 9] (and more recently knockin mutant *Abca4* transgenic mice: 14, 15), and exhibit some features of the disease (notably lipofuscin accumulation in the RPE), they do not recapitulate the degenerative phenotype and functional losses seen in patients. In the present study, inhibition of *Abca4* transcription in the cone-rich rodent *Psammomys obesus* led to rapid and profound degenerative changes in the PR and RPE, and preferentially affected cone function and survival. This is despite the transfection of only ~25% total PR as opposed to complete germline ablation in the mouse studies. A major difference between these two types of models is the percentage of cones, <3% in mice [18] compared to ~33% in *Psammomys* [20]. We speculate that in such diurnal rodents the retina basically constitutes one whole macula-like tissue, at least in terms of cone density. This could provide an enormous advantage for better understanding the detailed etiology of macular diseases, not limited to STGD1 but possibly also relevant for pathologies like age-related macular degeneration.

Based on the knockout mouse models and extensive biochemical analyses, a hypothetical scenario for PR death in STGD1 has been proposed: under normal conditions, following light activation of rhodopsin, lipophilic atRal separates from the opsin protein and

remains within the luminal face of disc membranes. There it reacts with phosphatidyl-ethanolamine (PE) to form N-retinylidene-PE (NRPE), which is rapidly transported into the OS cytosol by the flippase ABCA4 localized in the disc periphery. Once in the PR cytosol, atRal is reduced by retinol dehydrogenase to all-trans-retinol, whereupon it is transported across the sub-retinal space to the adjacent RPE to complete re-isomerization to *11-cis* retinal *via* the visual cycle [23]. In STGD1, mutations in *ABCA4* lead to reduced or absent transport of NRPE; excess atRal remaining within the disc lumen further reacts with PE to form a complex mixture of irreversible bisretinoid adducts. Bisretinoids are toxic bi-products of the visual cycle, including but not limited to A2E, exhibiting both photo-reactive and detergent properties [12]. Since PR undergo continuous membrane turnover involving apical displacement of discs and their internalization by the adjacent RPE [24], this latter cell type accumulates these toxic bisretinoids which cannot be degraded. They incorporate into lipofuscin deposits in RPE, which in normal ageing and STGD1 are visible as conspicuous autofluorescent flecks by ophthalmological examination [25]. Eventually a toxic threshold is reached causing the RPE to die, the metabolic maintenance of PR integrity is lost and the PR then die in turn.

Still, such a mechanism does not account for the preferential cone malfunction and loss seen in type 2 STGD1, and we propose a modified pathogenic sequence to take this into account. We recently demonstrated that cones exhibit several distinct molecular differences compared to rods: cones contain significantly more Abca4 mRNA and protein; they are highly deficient in very long chain fatty acids in general, and the neuroprotective poly-unsaturated fatty acid docosahexaenoic acid (DHA, 22:n:6) in particular; they contain far less PE; and show reduced amounts of A2E and five-fold greater amounts of atRal-dimer [26]. Additionally, phagocytic turnover of cones by the RPE is much slower than rods [19], which would hinder clearance of toxic debris. We hypothesize that these compositional and functional differences render cones more vulnerable to cellular stress such as oxidative damage, and that disease mutations in STGD1 would lead to preferential cone death through direct poisoning, in addition to the indirect route described above. We speculate that because of the compositional differences, Abca4 failure in cones leads to the formation of bisretinoid species - such as atRal-dimer - distinct from those detected in rods. There is evidence both for [27] and against [28] increased toxicity from atRal-dimer, but we suggest they constitute an important component of cone bisretinoids and are more toxic than rod bisretinoids, which would explain the early and heightened vulnerability of the cone-rich macula seen in STGD1. An alternative/parallel pathogenic pathway could come from Abca4-induced perturbations in retinoid recycling

leading to “congested” membranes and reduced ability of 11-cis retinal to reinsert into the PR. Different mouse models in which genes involved in the visual cycle were deleted have shown that reduced availability of 11-cis retinal affects cone survival and function more than rods [29-31]. Tying together the phenotype seen in *Psammomys* (extensive areas of total PR loss, residual areas still containing transfected rods but not cones) and clinical features of type 2 STGD1, we suggest that *Abca4* mutations are highly toxic for cones but less for rods. In regions where the cone:RPE ratio is high (as in the human macula and throughout cone-rich rodent retinas), cone death would likely also poison the overlying RPE leading to generalized cell death. When the cone:RPE ratio is lower, as in human peripheral retina, cones still die by direct poisoning (as seen in type 2 STGD1 patients: 5, 6) whereas there is no RPE loss and rods are unaffected. We further speculate that the degree of cone poisoning is correlated with specific gene mutations, resulting in the diversity of STGD1 phenotypes seen in the three subgroups.

In the present study, the method used (virally-delivered CRISPR-Cas9-mediated transcriptional inhibition) leads to a mosaic of untransfected (normal) and transfected (*Abca4* transcriptional blockade) rod and cone PR. This provides an experimental setting to test the proposed differential effects of *Abca4* inhibition upon rod and cone survival. Even though our estimates show a maximum of ~12% PR are transfected, *Abca4* inhibition results in widespread cell loss, already detectable after two months. The data clearly suggest cones are more impacted than rods, in terms of both structure (reduced expression of cone- but not rod-specific genes) and function (decreased photopic and flicker ERGs). Indeed, even after 9 months post-injection, transfected rods were still clearly present in residual retina, showing that *Abca4* inhibition in these cells has much less impact on their survival. We were unable to find any unequivocally transfected cones 9 months after injection. This aligns with the lack of PR damage in *Abca4* knockdown and knockin mice [8, 14, 15]. In support of our hypothesis, double knockout *Abca4/Nrl* mice with abundant cones exhibit increased damage compared to single *Abca4* knockout mice [29]. We further postulate that such direct cone poisoning has important implications for clinical strategies, since it would suggest that therapies involving stem cell replacement of RPE [30] may help rescue rods but be of only limited value for cones.

In conclusion, cone-rich rodents offer a unique scenario to explore molecular and cellular changes occurring in human maculopathies like STGD1, and should provide a valuable means to further explore genotype-phenotype relations, and to appraise potential therapeutic strategies.

Materials and Methods

Animals: *Psammomys obesus* were originally imported from the laboratory of Dr. Kronfeld-Schor, Tel Aviv, Israel, and have since been maintained as a viable breeding colony in the Chronobiotron CNRS UMR3415, in controlled ambient illumination on a 12 h light/12 h dark cycle, in environmentally enriched cages and with access to low caloric-density food which does not induce diabetes [31] (Altromin International, Germany) and water *ad libitum*. Animal use in the present project was authorized by local ethics committees (CREMEAS and Com'Eth) and the French Ministry of Research (APAFIS 8472-2016121318254073 v10 and 37348-2022051311067405 v5) from the Ministry of Research. Their sanitary status was assayed monthly, the animals were free of known pathogens and parasites. Breeding couples of clean *Psammomys obesus* are available on demand.

Subretinal injection: *Psammomys obesus* were anaesthetized by inhalation of gaseous anesthetic (Isoflurane 2%) administered constantly through a small animal mask connected to a pump. The eyes were anesthetized by local anesthetic (Tetracaine) before surgery. The eyeball was exposed by pulling down the skin. A small incision was made through the *ora serrata* on the temporal side using the tip of a sharp 33-gauge needle. An injection needle (Hamilton syringe, 33 gauge blunt end) was inserted into the eyeball through the incision until slight resistance was felt, and slowly ~2µl of AAV vectors per eye were injected into the subretinal space.

Plasmid construction: The pAAV-CMVep-HA-SpCas9 plasmid was constructed by inserting by SLIC (Sequence and Ligation Independent Cloning) the NLS-SpCas9-NLS sequence, amplified from pLentiCRISPRV1 plasmid [32] with an HA tag at its N-terminal end, in the pAAV-MCS plasmid (Stratagene) downstream of the CMV promoter. In order to reduce the size of the pAAV, the hGHpolyA signal of the pAAV-MCS plasmid was replaced by a small synthetic polyA sequence. For the construction of the pAAV-U6-gR58-U6-gR80-CAG-eGFP, the two guide RNAs R58 (TTTCACTCATGTGCAGGAAG) and R80 (GGTAAGTGAGGCCTGTTAAG) selected with the programme, were separately cloned in the BpiI site of the intermediate plasmid pSL1190-U6-lacZ-trRNA (Molecular Biology and Virus Service, IGBMC, Illkirch, France). The U6-gRNA-trRNA cassettes were amplified and cloned by assembly (NEBuilder, New England Biolabs) in a pAAV already containing a CAG-eGFP cassette.

AAV production: Recombinant adeno-associated virus (AAV) serotype 8 (AAV8) were generated by a triple transfection of HEK293T/17 cell line using Polyethylenimine (PEI) transfection reagent and the 3 following plasmids: pAAV-U6-gR58-U6-gR80-CAG-eGFP or pAAV-CMV-HA-spCas9, pAAV2/8 (Addgene 112864 deposited by Dr Wilson, Penn Vector Core) encoding the AAV serotype 8 capsid and pHelper (Agilent) encoding the AV helper functions. 48 h after transfection AAV8 vectors were harvested from cell lysate and treated with Benzonase (Merck) at 100U/mL. They were further purified by gradient ultra-centrifugation with Iodixanol (OptiprepTM density gradient medium) followed by dialysis and concentration against Dulbecco's Phosphate Buffered Saline (DPBS) using centrifugal filters (Amicon Ultra-15 Centrifugal Filter Devices 100K, Millipore). Viral titres were quantified by Real-Time PCR using the LightCycler480 SYBR Green I Master (Roche) and primers targeting eGFP (5'-GACGACGGCAACTACAAGA-3', 5'-CATGATATAGACGTTGTGGCT-3') or spCas9 (5'-GCATCCTGCAGACAGTGAAG-3', 5'-TTCTGGGTGGTCTGGTTCTC-3'). Titres are expressed as genome copies (GC) per ml.

Electroretinography (ERG): *Psammomys obesus* were dark-adapted overnight, and the experimental procedures were done under complete darkness using an infra-red camera, as reported previously [21]. Animals were anesthetized with a subcutaneous injection of ketamine (25ng/kg) and medetomidine (7ng/kg). The pupils were dilated using Atropine 1% and the cornea was anesthetized with a drop of 0.5% Tetracaine. The scotopic ERG responses were evoked to stepped flashes of white light of increasing intensity, 0.0003-10.0 cd.s/m2 (rod responses and mix rod-cone response). Following scotopic recordings and after 10 minutes of light-adaptation (30 cd.m-2 background light), photopic (cone-mediated) ERGs were evoked using flashes of white light of 0.01-10.0 cd.s/m2. A 6-10-15-30-Hz photopic flicker response was also obtained using 1.0 cd.s/m2 and background illumination.

Non-invasive Ocular Imaging: *Psammomys obesus* were anaesthetized by inhalation of isoflurane (IsoFlo®, Zoetis, Malakoff, France) administered constantly at 4% through a small animal mask in a 50/50 mix of air and O_2 at 0.8l/min. A single drop of tropicamide 0.5% (Mydriaticum ®, Théa Pharma, Clermont-Ferrand, France) was used for pupil dilation, and the ocular surface was lubricated with either artificial tears (Artelac®, Bausch & Lomb, Montpellier, France) for OCT, or with ophthalmic gel (Ocry-Gel®, TVM, Lempdes, France) for fundus imaging. Retinas were first imaged with an Envisu R2200 SD-OCT (Bioptigen-Leica, Durham, USA), then with a Micron III fundus / fluorescence camera (Phoenix Research Laboratories, Pleasanton, CA, USA), during the same anaesthesia. Short sequences of fundus

images were aligned, averaged and sharpened in Fiji [33, 34] using a macro developed by Mark Krebs (the Jackson Laboratory, Bar Harbor, MA, USA).

Quantification of mRNA: For RT-PCR analysis, retinal RNA was isolated with RNeasy mini kit (Qiagen), following the manufacturer's instructions including DNAse treatment. We modified slightly the first step, as dissociation of tissues was performed using a pestle with 500 µL of TriReagent solution. 100µl chloroform was directly added, and the preparation was transferred to a phase-lock gel tube after 15min incubation at room temperature. The gel tube was centrifuged 15 min at 12,000g and 4°C. To recover RNA, the supernatant was added to an equal volume of 70% ethanol. RT-PCR was performed from 700 ng of RNA with the high capacity RNA-to-cDNA kit. A second negative control was added, consisting of water, enzyme and RT buffer only, to confirm the absence of contamination. QPCR was performed in 96-well plates (Applied Biosystems), following the manufacturer's instructions. Experiments were carried out on a 7300 Real-Time PCR System (Applied Biosystems) with a first step of denaturation for 5 min at 95 °C, followed by a cycle of 40 repetitions of 15s at 95°C, then 1 min at 60°C. After estimation of the sample concentration to use (between 1/10 and 1/100) and validation of primer efficiency (>80%), each sample was processed in duplicate and using a dilution range, for all studied genes:, Abca4, rod-specific (Rho), cone-specific (Opn1mw), and housekeeping genes (Gapdh,Rplp0). See Supplementary Table 1 for primer references. Analysis was performed using the ΔΔCt method.

Western Blotting: Protein from *Psammomys obesus* retina was extracted by sonicating in 100µl of lysis buffer (20 mM Tris-HCl pH7.6, 150 mM NaCl, 1% triton X-100, 1mM EDTA, 0.2% SDS) containing 1µl of proteinase inhibitor,as previously reported [19]. The lysate obtained was centrifuged 30 min at 13 000 rpm and 4°C, and the supernatant protein concentration was estimated by the Bradford method. Samples (20 µg protein/lane) were loaded and separated on SDS-PAGE gels, 90 min at 110V, following by semi-dry transfer to nitrocellulose membranes, 30min at 25V. After protein transfer, membranes were incubated in blocking solution (20mM Tris-HCl pH 7.6, 150mM NaCl, 0.1% Tween 20, 3% Bovine Serum Albumin), 1h at room temperature before overnight incubation at 4°C with the primary antibodies. After extensive washing in buffer, 4 x 5 min, membranes were incubated with secondary antibodies (rabbit anti-mouse IgG-HRP for monoclonal primaries, goat anti-rabbit IgG-HRP for polyclonal primaries), diluted 1:10,000 for 30min at room temperature. After washing again, 4 x 5 min, membranes were developed in the dark with the ECL Western Blotting Detection kit (Pierce), following the manufacturer's instructions. Exposure times for each blot ranged between 5 to 30 seconds to obtain linear densitometric readings.

Immunofluorescence: *Psammomys obesus* eyes were collected after euthanasia. Eyes were cut along the ora serrata to remove the cornea and lens and fixed 2 h at room temperature in 4% paraformaldehyde (PFA) in sucrose/phosphate-buffered saline (PBS). After extensive washing in PBS, dissected eyeballs were cryoprotected overnight and then embedded in OCT and sectioned by cryostat (10-12µm). *Psammomys obesus* retinal sections were permeabilized with 0.1% Triton x-100 for 5 min at room temperature, then incubated for 1h in blocking buffer (3% Bovine Serum Albumin, 0.1% Tween20 in PBS) at room temperature. As published previously [19-21], primary antibodies were diluted in blocking buffer and incubated overnight at 4°C. Sections were washed three times in PBS and incubated with fluorochrome-conjugated secondary antibodies (1:1000) for 2h at room temperature. Secondary antibodies were donkey anti-rabbit or anti-mouse IgG conjugated with Alexa Fluor™ 488 or 647.Sections were washed again and then incubated 2 min with 1 4,6-diamidino-2-phenylindole (DAPI) (1:500). Sections were washed again and mounted with PBS-Glycerol 1:1. Images were captured using an inverted microscope (Zeiss Observer 7) equipped with objectives (63x, N.A. 1.4), a module for optical sectioning by structured illumination (Zeiss ApoTome.2) and a digital camera (Hamamatsu ORCA-Flash 4.0). Primary antibodies used in this study are listed in Supplementary Table 4.

Retinal whole-mounts: To prepare flatmounts of retina, *Psammomys obesus* eyes were enucleated as quickly as possible after euthanasia and immediately placed in 4% paraformaldehyde (PFA) as above. Retinas were gently detached from the eyecup, washed with PBS and mounted in Mowiol® 4-88, with the photoreceptor layer facing up. Imaging was conducted on a NanoZoomer S60 Digital slide scanner.

Electron microscopy: *Psammomys obesus* eyes were fixed in 2.5% glutaraldehyde in 0.1M sodium cacodylate buffer for 24h-48h. Samples were washed with 0.1M sodium cacodylate buffer and post-fixed with osmium tetroxide 0.5% in water, then dehydrated in an ethanol series (25%-50%-70%-90%-100%2X) (15 min each) and propylene oxide 2x15 min and embedded in Epon EMbed 812 resin. For electron microscopy, ultrathin sections (70-80nm) were cut with an Ultracut EM FC7 Leica. Sections were collected on 200 mesh copper grids and stained in 1% uranyl acetate and observed using a Hitachi H 7500 transmission microscope equipped with an AMT Hamamatsu camera (Tokyo Japan).

UPLC-MS analysis of bisretinoids: *Psammomys obesus* eyes derived from either control injected or Crispr-Cas9 injected animals (n=4 each group) were sent for analysis by ultra-high performance liquid chromatography (UPLC) coupled with mass spectrometry (MS). The person performing the analysis was blinded to donor origin. Using previously published methods

(Sparrow et al. 2010)], compound elution was achieved using an Alliance HPLC (Waters Corp Milford, MA, USA) with a Delta Pak[circlecopyrt]R C4 (5 μm, 3.9 × 150 mm; Waters) or an AtlantisR dC18 (3 μm, 4.6 × 150 mm; Waters) column. The mobile phase for the C4 column a gradient of acetonitrile in water with 0.1% trifluoroacetic acid: 0-5 min; 75% acetonitrile, flow rate, 0.8 ml min−1; 5-30 min, 75-100% acetonitrile; flow rate, 0.8 ml min−1; 30-35 min,100% acetonitrile, flow rate, 0.8-1.2 ml min−1; 35-50 min, 100% acetonitrile, flow rate, 1.2ml min−1. With the dC18 column a gradient of acetonitrile in water with 0.1% trifluoroacetic acid was utilized: 75-90% acetonitrile (0-30 min); 90-100% acetonitrile (30-40 min); 100% acetonitrile (40-100 min) with a flow rate of 0.5 ml min−1. Absorbance (Waters 2996 Photodiode Array) and fluorescence (Water 2475 Multi λ Fluorescence Detector; 18 nm bandwidth) were detected at wavelengths indicated. Fluorescence efficiency was estimated as fluorescence peak area (μV s)/absorbance peak area (μV s).

Statistical analyses

For RT-qPCR data, differences among groups were analyzed using one-way analysis of variance (ANOVA I), followed by Post-hoc analyses.

For ERG data, differences between groups were tested using an ANOVA II, with factors “group”, “light intensity”,and their interactions, followed by Post-hoc analyses. For all statistical procedures,the level of significance was set at $p<0.05$. All data are presented as mean±SEM, unless otherwise stated. Sigma Plot (v14) was used for statistical analyses.

Acknowledgements

The authors wish to thank Drs. M.P. Felder-Schmittbuhl and F. Pfrieger for constructive discussions during manuscript preparation; Ms. C. Rouyer for expert technical assistance for transmission electron microscopy; Dr. C. Sandu for valuable help with qPCR analyses; and Ms. N. ElKorti for immunochemical staining. The authors extend their deep gratitude to the funding agencies that made these experiments possible: UNADEV/ITMO Aviesan 2018-2021, Fondation de France (Association Berthe Fouassier) and USIAS (DH); (JRS).

Figure Legends

Figure 1. Abca4 expression in Psammomys obesus retinal development and subretinal injection of AAV-CRISPR-Cas9. (**A-B**) Immunostaining of Abca4 (A-A’’’, green) and cone transducin (GαT2) (B-B’’’, green) in retinal tissues collected from *Psammomys obesus* aged postnatal day P15, P20, P30 and P90. At all ages, whereas GαT2 labelling is already strong, Abca4 is only faintly visible at P15 and 20, becoming more intense by P30. Abbreviations: DAPI, 4′,6-diamidino-2-phenylindole; GCL ganglion cell layer; INL inner nuclear layer; ONL outer nuclear layer; OS outer segments. Scale bar in B’’’ = 40μm for all panels. (**C**) Western blotting of Abca4 in P15-90 *P. obesus* retina. Compared to the housekeeping gene β-actin, Abca4 immunoreactivity increased with postnatal age. (**D**) Quantification of Abca4 immunoreactivity in P15-90 *P. obesus*. Densitometric scanning of Abca4 immunostained bands, normalized to β-actin, showed significant increases in expression levels with increasing age, n of 3 independent experiments. (**E**) Representative retinal whole-mounts (top panel, insert shown as white box at higher magnification in E’) and sections (E’’) of a treated animal 7d post-injection. EGFP expression (green) indicates transcription by the AAV-sgRNA vector in the PR layer. Abbreviations: IS, inner segments; ONL, outer nuclear layer. Scale bars = 100μm for panels E and E’, 40μm for panel E’’. (**F**) Timeline for the Abca4 knockdown experiments. *Psammomys obesus* received subretinal co-delivery of 1.4 x 1^{10} vector genomes (vg) AAV-Cas9 and 1.4 x 1^{10} vg AAV-sgRNAs-EGFP per eye at P14-P17. Same doses of AAV-sgRNAs-EGFP were injected in fellow eyes as controls. (**G**) Schematic representation of the AAV vectors delivering SpCas9 and SgRNAs. Abca4 locus showing the location of the sgRNA targets (gR58, gR80). The targeted genomic site is Exon 5 in black. Protospacer adjacent motif (PAM) sequence is marked in red.

Figure 2. Abca4 knockdown in Psammomys obesus photoreceptors by AAV-CRISPR-Cas9 gene editing. (**A**) Representative FACS plots of dissociated cells from retinas receiving CRISPR-Abac4 vectors. GFP positive population represents 11.8% of total retinal cells. (**B**) Electrophoresis of *Abca4* RNA following PCR amplification (~700bp around exon 5): Bp, base pair ladder; 1, negative control (water only), no amplification; 2, positive control, *P. obesus* whole retina, expected band ~700bp; 3, *P. obesus* retina transfected with AAV gRNA/GFP only, EGFP-FACS-sorted cells show single band ~700bp; 4, *P. obesus* retina transfected with AAV gRNA/GFP and CAS9, EGFP-FACS-sorted cells show two amplicons, one with edited *Abca4* (~500bp) (blue arrow) and the other with wild type *Abca4* (~700bp). (**C**) Two Sanger sequencing chromatograms, top one from forward primer, lower from reverse primer. In each

condition, we observed flattening of peaks and loss of correlation with DNA sequence in EGFP-FACS-sorted cells starting from nucleotide ~200-300 up to nucleotide ~300-400, ie. the exon 5 target region of sgRNAs CRISPR- CAS9, compared to EGFP-ve-FACS-sorted cells with a normal chromatogram profile, shown below. (**D, E**) Immunostaining of ABCA4 in retinal tissues collected from *Psammomys obesus* retina, AAV-sgRNA-EGFP (control) (D-D'''') and AAV-sgRNA-EGFP+AAV-Cas9 (CRISPR treated) (E-E'''), 8 weeks post injection. Panels D, E: merged images of DAPI staining, Abca4 immunostaining and EGFP. Panels D', E', substantial reduction of Abca4 immunostaining was observed in the CRISPR-ABCA4-treated retina compared to control. Panels D'', E'', EGFP signal in transfected PR. Scale bar in E'' = 80µm for all panels. Abbreviations: INL inner nuclear layer; ONL outer nuclear layer. (**F**) Quantitative real-time RT–PCR analysis of *Abca4* mRNA expression in *Psammomys obesus* retinas 8 weeks post-injection AAV-sgRNA-EGFP+AAV-Cas9 (CRISPR treated) (n=3), AAV-sgRNA-EGFP control retinas (n=4), and unoperated retinas (n=3). The mRNA expression values were determined after normalization to internal control GAPDH and RPLP0 mRNA levels. Treated CRISPR vs. control p=0.024, treated CRISPR vs. WT p=0.011, one way ANOVA. Data represented as mean ± SEM. *P < 0.05. (**G**) Representative immunoblot of ABCA4 (260kDa) in *Psammomys obesus* AAV-sgRNA-EGFP+AAV-Cas9 (CRISPR treated) retinal lysate, and unoperated retinal lysate at 270 days post injection. α tubulin (50kDa) as loading standard.

Figure 3- Morphological and functional changes of Psammomys obesus retina following Abca4 knockdown. (**A-D)** Mean ERG amplitudes recorded across a range of light flashes under scotopic or photopic conditions. Statistically significant lower amplitudes of scotopic a- and b-wave (**A, B**) (n=6), and photopic a- and b- wave (**C, D**) (n=3) were obtained in response to increasing intensities of flash stimuli. Values from CRISPR-CAS9-treated eyes (left eye, red trace) were compared to AAV-sgRNAs-EGFP control eyes (right eye, black trace). There were significant differences between the treated and control eyes at light flash intensities of ~0.5-1 Log.cd .s/m^2 for scotopic conditions, intensities at which a mixed rod-cone response is present. Significant differences between treated and control eyes in photopic conditions were seen for light flash intensities 0.5-1 Log.cd .s/m^2. Data represented as mean ± SEM. *P < 0.05; **P < 0.01; ***P < 0.001. Significance values between CRISPR-CAS9-treated eyes and control sgRNAs eyes was calculated using two way ANOVA. (**E**) Photopic light-adapted flicker recordings were made from 5 to 30 Hz, and also showed reduced signals in CRISPR-CAS9-treated eyes. Statistical analysis performed as for single flash experiments. (**F-I**) Fundus imaging of CRISPR-CAS9-treated and sgRNAs-EGFP control eyes at 8 weeks post-injection.

Control eyes showed a small lesion corresponding to the injection site (**F**, white arrow), but otherwise showed smooth uniform bluish retina with blood vessels emanating from the optic nerve head (ONH); **G**, Optical Coherence Tomography (OCT) imaging of control retinas showed the normal laminated retinal structure, with a brightly reflective retinal pigmented epithelium (RPE) and dark cell layers (INL, inner nuclear layer; and ONL, outer nuclear layer) with the GCL (ganglion cell layer) separated by a wide plexiform layer; **H**, fundus imaging of CRISPR-CAS9-treated eyes showed extensive loss of retina with pigmented patches and visible blood vessels; (**I**) OCT imaging of CRISPR-CAS9-treated eyes showed a complete disappearance of the ONL, while vestigial inner retina was still present.

Figure 4. Rod, cone and RPE changes following Abca4 knockdown in Psammomys obesus. (**A, B**) Immunostaining of rhodopsin (RHO) in retinal tissues collected from *Psammomys obesus*, AAV-sgRNA-EGFP (control) (A-A’’’) and AAV-sgRNA-EGFP+AAV-Cas9 (CRISPR treated) (B-B’’’) at 8 weeks post injection. Sections were made close to lesion edges, where residual retina was still present. A, B: merged images of DAPI staining (blue), EGFP expression (green) and RHO immunostaining (red). DAPI (A’, B’), EGFP (A44, B’’) and RHO (A444, B’’’) alone do not show major differences between control and treated tissue. Scale bars = 40µm. (**C**) Quantitative real-time PCR analysis of *rho* mRNA expression in *Psammomys obesus* retinas 8 weeks post-injection. AAV-sgRNA-EGFP+AAV-Cas9 (CRISPR treated) (n=4), AAV-sgRNA-EGFP control retinas (n=4), wild type retinas (n=3). The mRNA expression values were determined after normalization to internal control GAPDH and RPLP0 mRNA levels. There is no statistically significant difference between CRISPR-treated and either EGFP control retina or wild type retina (P = 0.915). One way ANOVA. (**D, E**) Immunostaining of OPN1MW in retinal tissues collected from *Psammomys obesus*, AAV-sgRNA-EGFP (control) (D-D’’’) and AAV-sgRNA-EGFP+AAV-Cas9 (CRISPR treated) (E-E’’’) at 8 weeks post injection. D, E: merged images of DAPI staining (blue), EGFP expression (green) and OPN1MW immunostaining (red); whereas DAPI (D’, E’) and EGFP (D’’-E’’) alone do not differ between the two samples, there is a large decline in OPN1MW immunostaining in treated compared to control retinas (D’’’, E’’’). Scale bars = 40µm. (**F**) Quantitative real-time PCR analysis of *opn1mw* mRNA expression in *Psammomys obesus* retinas 8 weeks post-injection. AAV-sgRNA-EGFP+AAV-Cas9 (CRISPR treated) (n=4), AAV-sgRNA-EGFP control retinas (n=4), wild type retinas (n=3). The mRNA expression values were determined after normalization to internal control GAPDH and RPLP0 mRNA levels. CRISPR-treated vs. control p=0.036, CRISPR-treated vs. WT p=0.027. One way ANOVA. Data represented as

mean ± SEM. *P < 0.05. (**G-L**) Transmission electron microscopy of the RPE/PR interface in EGFP control (**G-I**) and CRISPR-treated eyes (**J-L**) at 27 weeks post-injection. **G**, low magnification images of the entire area showed normal ultrastructural features: RPE contained elongated melanosomes closely adjacent to PR OS, the rod OS appearing cylindrical, more darkly staining and closer to the RPE surface, whereas cone OS were more deeply embedded and lighter stained (open arrow). The inner segments (IS) were demarcated from the underlying cell bodies in the ONL by the outer limiting membrane (arrow). **H**, higher power image of RPE/OS interface, again showing numerous elongated melanosomes within the RPE, as well as occasional phagosomes. The rod OS show normal stacked discs. **I**, higher power image of OS/IS junction, again the OS are intact and neatly aligned, the cones OS showing a tapered aspect (*). J, low power images of RPE/PR region in CRISPR-CAS9 treated eyes. The RPE contains numerous circular inclusions packed into the apical cytoplasm, and many holes and damaged cells are seen in the OS layer, particularly at the level of the cone OS (red arrows); K, higher power images of RPE/OS interface, highlighting the abundant small round deposits packing the RPE (red arrows), as well as several phagosomes. These deposits form a dense layer between the deeper RPE containing melanosomes and the abutting OS; L, higher power images of the OS/IS region, showing the scattered free cytoplasm from degenerated cells and spaces between OS. Again, the rod OS appear less damaged than the cone OS, which are no longer recognisable (red arrows). Scale bar = 10µm (G, J), 2µm (H, I, K, L). **(M)** UPLC quantification of the bisretinoid A2E from whole eyes of 2 month post-injection *Psammomys obesus* (n=4) and albino Wistar rats *Rattus norvegicus* at 2 weeks and 5 months old (n=4). Data represented as mean ± SEM. High levels of A2E are detected in *P. obesus* compared to Wistar rats, in both control and CRISPR-CAS9-treated eyes. (**N**) UPLC quantification of all-trans Retinal dimer (atRal-di) from whole eyes of 2 month post-injection *Psammomys obesus* (n=4) and albino Wistar rats *Rattus norvegicus* at 2 weeks and 5 months old (n=4). *P. obesus* contain significant amounts of this molecule, whereas it is undetectable in Wistar rats. Data represented as mean ± SEM

References

1. D.A. Baylor, Photoreceptor signals and vision. *Invest Ophthalmol Vis Sci* **2**, 34-49 (1987).
2. R. Allikmets, A photoreceptor cell-specific ATP-binding transporter gene (ABCR) is mutated in recessive Stargardt macular dystrophy. *Nat Genet* **17**, 122 (1997).
3. F.P.M. Cremers, W. Lee, R.W.J. Collin, R. Allikmets, Clinical spectrum, genetic complexity and therapeutic approaches for retinal disease caused by ABCA4 mutations. Prog Retin Eye Res. **79**, 100861 (2020).
4. Y. Rotenstreich, G.A. Fishman, R.J. Anderson, Visual acuity loss and clinical observations in a large series of patients with Stargardt disease. *Ophthalmology* **110**, 1151–8 (2003).
5. K. Fujinami *et al.,* A longitudinal study of Stargardt Disease: clinical and electrophysiologic assessment, progression, and genotype correlations. *Am J Ophthalmol* **155**,1075-88 (2013).
6. N. Lois, G.E. Holder, C. Bunce, F.W. Fitzke, A.C. Bird, Phenotypic subtypes of Stargardt macular dystrophy-fundus flavimaculatus. Arch Ophthalmol. **119**, 359-69 (2001).
7. L.L. Molday, A.R. Rabin, R.S. Molday, ABCR expression in foveal cone photoreceptors and its role in Stargardt macular dystrophy. *Nat Genet* **25**, 257-8 (2000).
8. J. Weng *et al.,* Insights into the function of Rim protein in photoreceptors and etiology of Stargardt's disease from the phenotype in abcr knockout mice. *Cell* **98**, 13–23 (1999).
9. L. Wu, T. Nagasaki, J.R. Sparrow, Photoreceptor cell degeneration in Abcr (-/-) mice. Adv Exp Med Biol. **664**, 533-9 (2010).
10. J.R. Sparrow *et al.*, The Bisretinoids of Retinal Pigment Epithelium. *Prog Retin Eye Res* **31**, 121– 35 (2012).
11. S. Beharry, M. Zhong, R.S. Molday, N-retinylidene-phosphatidylethanolamine is the preferred retinoid substrate for the photoreceptor-specific ABC transporter ABCA4 (ABCR) *J Biol Chem* **279**, 53972–9 (2004).
12. K. Ueda, H.J. Kim, J. Zhao, J.R. Sparrow Bisretinoid Photodegradation Is Likely Not a Good Thing. Adv Exp Med Biol. **1074**, 395-401 (2018).
13. P. Charbel Issa *et al.,* Fundus autofluorescence in the Abca4(-/-) mouse model of Stargardt disease--correlation with accumulation of A2E, retinal function, and histology. Invest Ophthalmol Vis Sci. **5**, 5602-12 (2013).

14. L.L. Molday, D. Wahl, M.V. Sarunic, R.S. Molday, Localization and functional characterization of the p.Asn965Ser (N965S) ABCA4 variant in mice reveal pathogenic mechanisms underlying Stargardt macular degeneration. Hum Mol Genet. **27**, 295-306 (2018).
15. N. Zhang *N et al.,* Protein misfolding and the pathogenesis of ABCA4-associated retinal degenerations. Hum Mol Genet. **24**, 3220-37 (2015).
16. A. Fakin et al., Phenotype and Progression of Retinal Degeneration Associated With Nullizigosity of ABCA4. *Invest Ophthalmol Vis Sci*. **57**, 4668-78 (2016).
17. A. Szél, P. Röhlich, Two cone types of rat retina detected by anti-visual pigment antibodies. Exp Eye Res. **55**, 47-52 (1992).
18. C.J. Jeon, E. Strettoi, R.H. Masland, The major cell populations of the mouse retina. *J Neurosci* **18**, 8936 – 8946 (1998).
19. C. Bobu, C.M. Craft, M. Masson-Pevet, D. Hicks, Photoreceptor organization and rhythmic phagocytosis in the nile rat Arvicanthis ansorgei: a novel diurnal rodent model for the study of cone pathophysiology. *Invest Ophthalmol Vis Sci* **47**, 3109-18 (2006).
20. T. Saïdi, S. Mbarek, R.B. Chaouacha-Chekir, D. Hicks, Diurnal rodents as animal models of human central vision: characterisation of the retina of the sand rat Psammomys obsesus. Graefes Arch Clin Exp Ophthalmol. **249**, 1029-37 (2011).
21. D.L. Boudard et al., Cone loss is delayed relative to rod loss during induced retinal degeneration in the diurnal cone-rich rodent Arvicanthis ansorgei. Neuroscience. **169**, 1815-30 (2010).
22. A. Dellaa et al., Characterizing the Retinal Function of Psammomys obesus: A Diurnal Rodent Model to Study Human Retinal Function. Curr Eye Res. **42**, 79-87 (2017).
23. R.S. Molday, F.A. Garces, J.F. Scortecci, L.L. Molday, Structure and function of ABCA4 and its role in the visual cycle and Stargardt macular degeneration. Prog Retin Eye Res. **89**, 101036 (2022).
24. R.W. Young, Renewal systems in rods and cones. Ann Ophthalmol. **5**, 843-54 (1973).
25. N.L. Gomes *et al.,* A comparison of fundus autofluorescence and retinal structure in patients with Stargardt disease. *Invest Ophthalmol Vis Sci*. **50**, 3907-14 (2009).
26. D.M. Verra *et al.,* (2022) Intrinsic differences in rod and cone membrane composition: implications for cone degeneration. Graefes Arch Clin Exp Ophthalmol. **260**, 3131-3148.

27. J. Zhao *et al.,* Aberrant Buildup of All-Trans-Retinal Dimer, a Nonpyridinium Bisretinoid Lipofuscin Fluorophore, Contributes to the Degeneration of the Retinal Pigment Epithelium. Invest Ophthalmol Vis Sci. **58**, 1063-1075 (2017).
28. Z. Gao *et al.,* Conversion of all-*trans*-retinal into all-*trans*-retinal dimer reflects an alternative metabolic/antidotal pathway of all-*trans*-retinal in the retina. J Biol Chem. **293**, 14507-14519 (2018).
29. A. Ruiz *et al*., Retinoid content, visual responses, and ocular morphology are compromised in the retinas of mice lacking the retinol-binding protein receptor, STRA6. Invest Ophthalmol Vis Sci. **53**, 3027-39 (2012).
30. S.L. Znoiko, B. Rohrer, K. Lu, H.R. Lohr, R.K. Crouch, J.X. Ma, Downregulation of cone-specific gene expression and degeneration of cone photoreceptors in the Rpe65-/- mouse at early ages. Invest Ophthalmol Vis Sci. **46**, 1473-9 (2005).
31. M. Jin *et al*., The role of interphotoreceptor retinoid-binding protein on the translocation of visual retinoids and function of cone photoreceptors. J Neurosci. **29**, 1486-95 (2009).
32. S.M. Conley et al., Increased cone sensitivity to ABCA4 deficiency provides insight into macular vision loss in Stargardt's dystrophy. *Biochim Biophys Acta*. **1822**, 1169-79 (2012).
33. S.D. Schwartz *et al.,* Human embryonic stem cell-derived retinal pigment epithelium in patients with age-related macular degeneration and Stargardt's macular dystrophy: follow-up of two open-label phase ½ studies. *Lancet* **385**, 509–16 (2015).
34. T. Saïdi, S. Mbarek, S. Omri, F. Behar-Cohen, R.B. Chaouacha-Chekir, D. Hicks D, The sand rat, *Psammomys obesus*, develops type 2 diabetic retinopathy similar to humans. Invest Ophthalmol Vis Sci. **52**, 8993-9004 (2011).
35. O. Shalem *et al.,* Genome-scale CRISPR-Cas9 knockout screening in human cells. *Science* **343**, 84-87 (2014).
36. J. Schindelin *et al.,* Fiji: an open-source platform for biological-image analysis. *Nat Meth*ods **9**, 676–682 (2012).
37. C.A. Schneider, W.S. Rasband, K.W. Eliceiri, NIH Image to ImageJ: 25 years of image analysis. *Nat Methods* **9**, 671–675 (2012).
38. J.R.Sparrow *et al.,* Fundus autofluorescence and the bisretinoids of retina. *Photochem Photobiol Sci* **9**, 1480-1489 (2010).

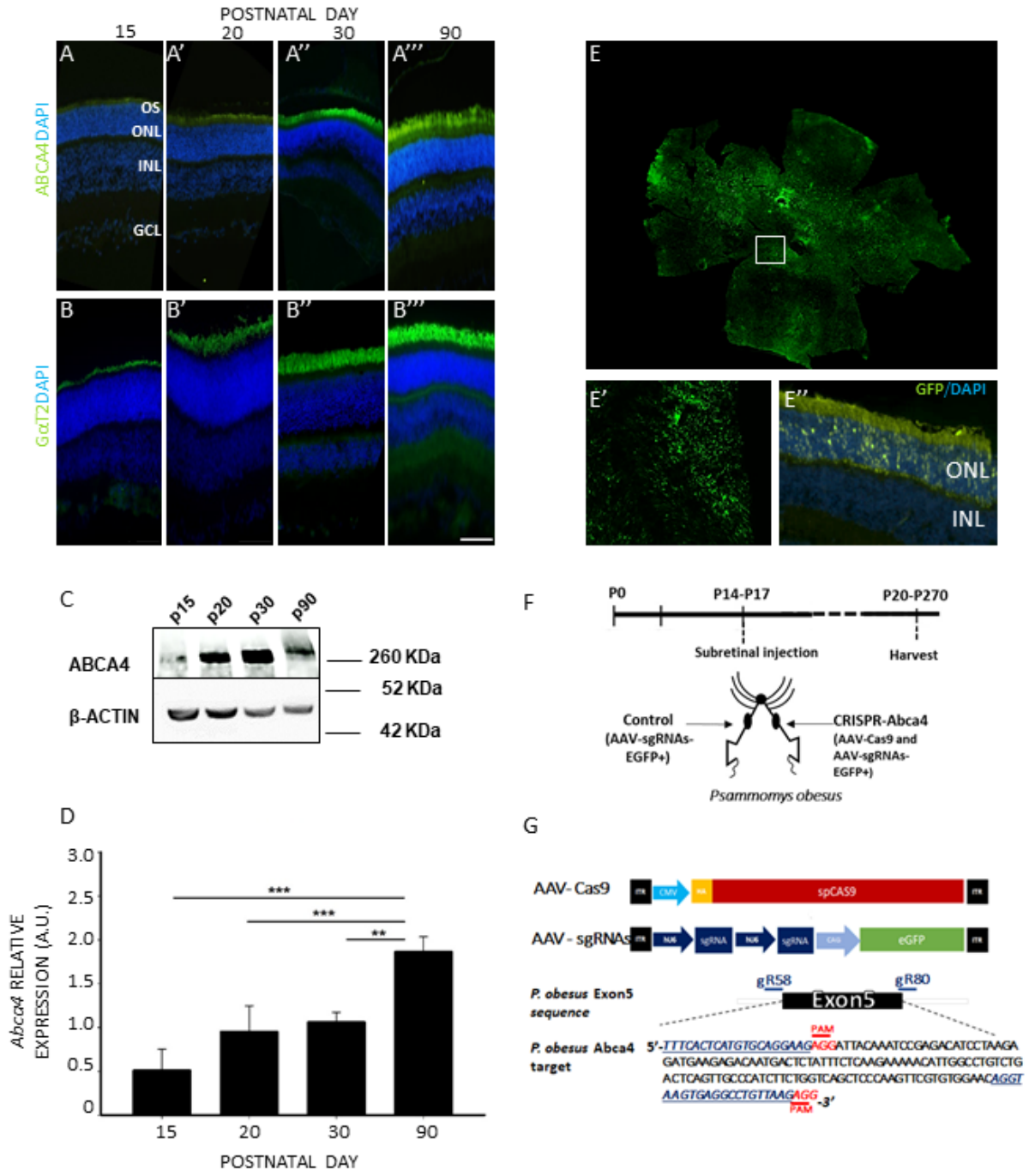
POSTNATAL DAY
15
20
30
90
A
A'
A''
A'''
OS
ONL
INL
GCL
ABCA4 DAPI
B
B'
B''
B'''
GαT2 DAPI
E
E'
E''
GFP/DAPI
ONL
INL
C
p15
p20
p30
p90
ABCA4
β-ACTIN
260 KDa
52 KDa
42 KDa
D
Abca4 RELATIVE EXPRESSION (A.U.)
3.0
2.5
2.0
1.5
1.0
0.5
0
***
***
**
15
20
30
90
POSTNATAL DAY
F
P0
P14-P17
P20-P270
Subretinal injection
Harvest
Control (AAV-sgRNAs-EGFP+)
CRISPR-Abca4 (AAV-Cas9 and AAV-sgRNAs-EGFP+)
Psammomys obesus
G
AAV- Cas9
spCAS9
AAV - sgRNAs
sgRNA
eGFP
gR58
gR80
Exon5
P. obesus Exon5 sequence
P. obesus Abca4 target
PAM
5'-TTTCACTCATGTGCAGGAAGAGGATTACAAATCCGAGACATCCTAAGA
GATGAAGAGACAATGACTCTATTTCTCAAGAAAAACATTGGCCTGTCTG
ACTCAGTTGCCCATCTTCTGGTCAGCTCCCAAGTTCGTGTGGAACAGGT
AAGTGAGGCCTGTTAAGAGG-3'
PAM

Figure 1

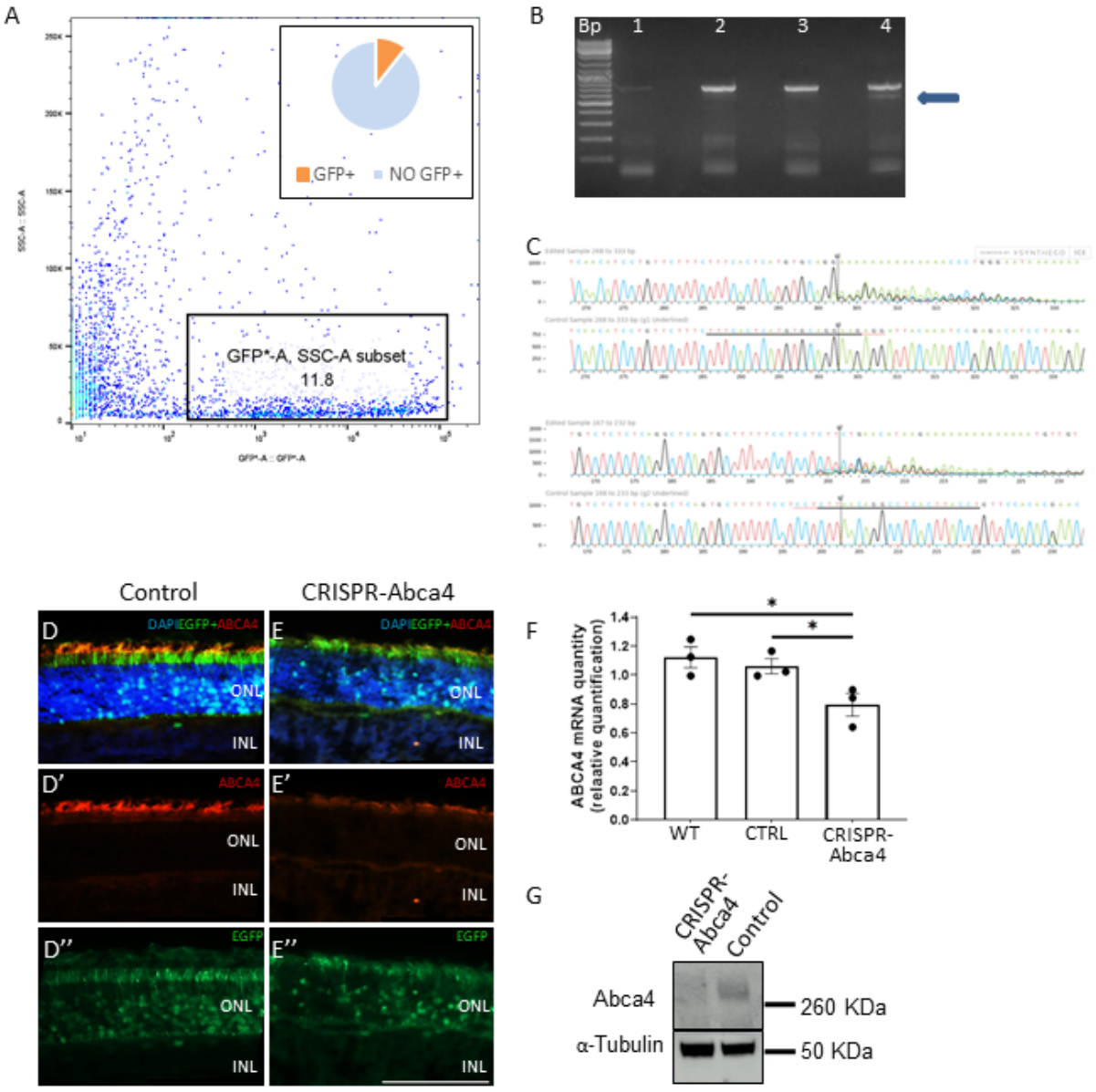
A
GFP+
NO GFP+
GFP*-A, SSC-A subset
11.8
B
Bp
1
2
3
4
C
Control
CRISPR-Abca4
D
DAPIEGFP+ABCA4
ONL
INL
D'
ABCA4
D''
EGFP
E
E'
E''
F
ABCA4 mRNA quantity
(relative quantification)
WT
CTRL
CRISPR-
Abca4
G
CRISPR-
Abca4
Control
Abca4
α-Tubulin
260 KDa
50 KDa

Figure 2

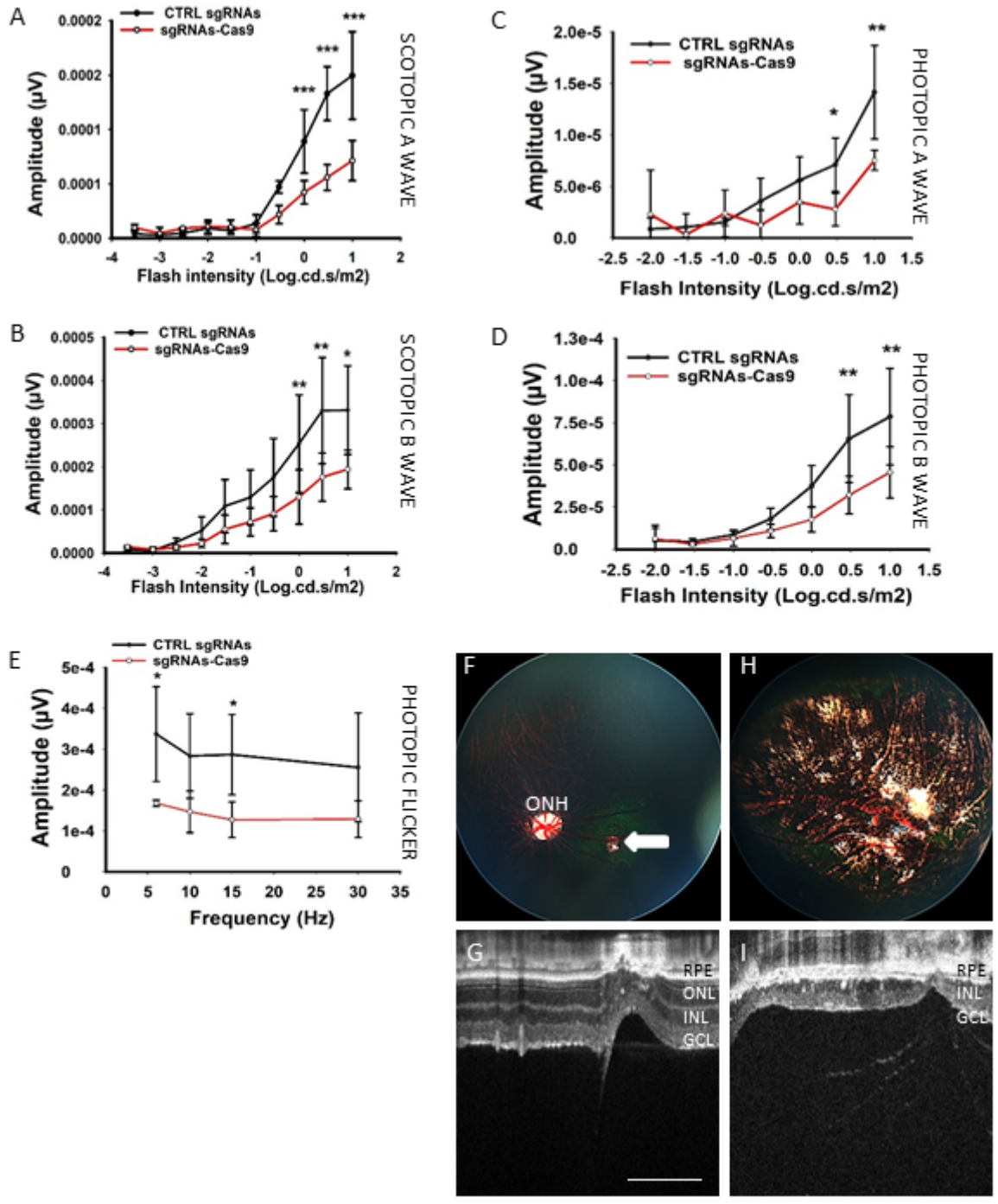
A
CTRL sgRNAs
sgRNAs-Cas9
Amplitude (µV)
Flash intensity (Log.cd.s/m2)
SCOTOPIC A WAVE
B
Flash Intensity (Log.cd.s/m2)
SCOTOPIC B WAVE
C
PHOTOPIC A WAVE
D
PHOTOPIC B WAVE
E
Frequency (Hz)
PHOTOPIC FLICKER
F
ONH
H
G
RPE
ONL
INL
GCL
I
RPE
INL
GCL

Figure 3

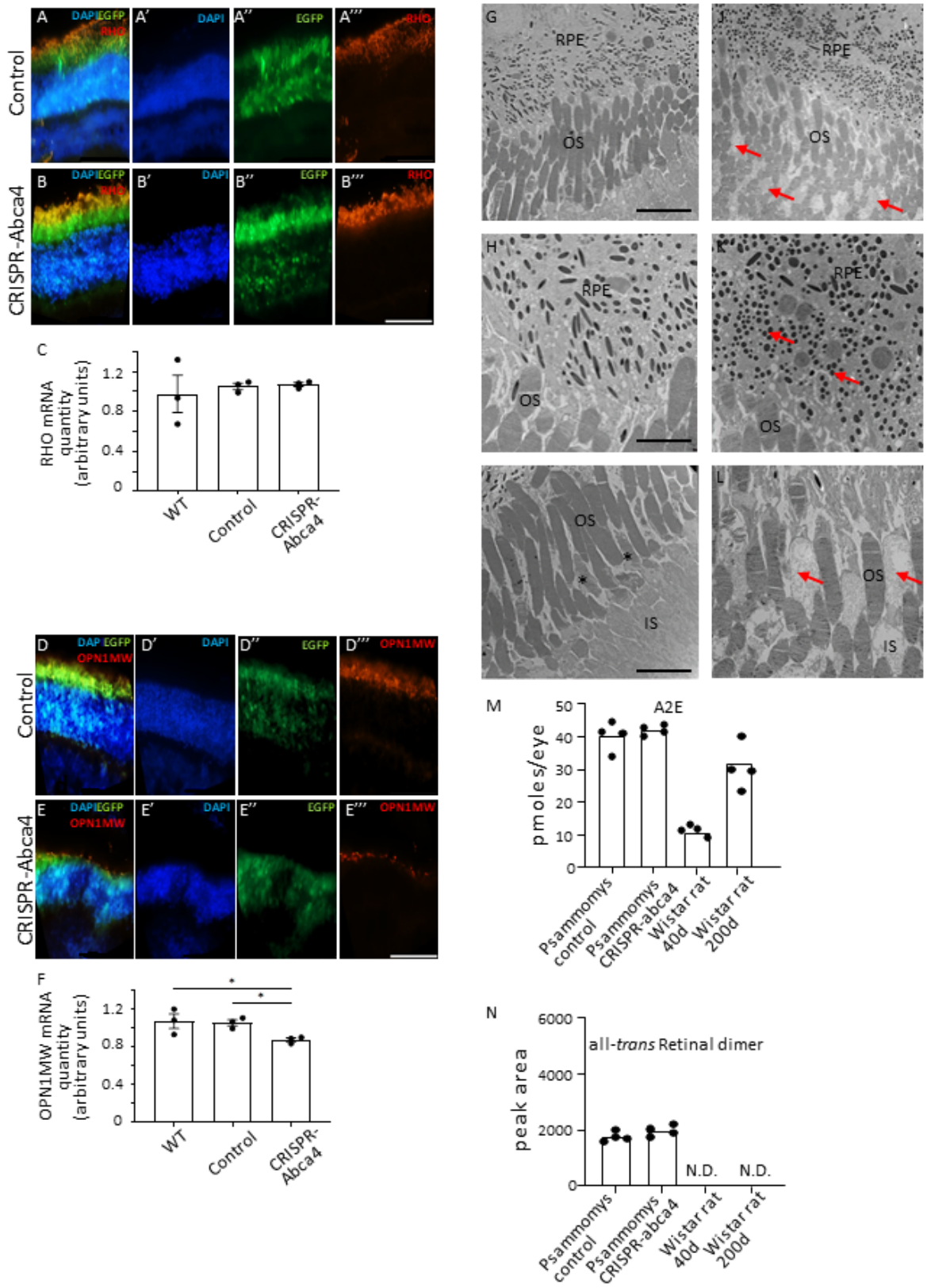
A
DAPI EGFP RHO
A'
DAPI
A''
EGFP
A'''
RHO
Control
B
DAPI EGFP RHO
B'
DAPI
B''
EGFP
B'''
RHO
CRISPR-Abca4
C
RHO mRNA quantity (arbitrary units)
1.2
0.8
0.4
0
WT
Control
CRISPR-Abca4
D
DAP EGFP OPN1MW
D'
DAPI
D''
EGFP
D'''
OPN1MW
Control
E
DAPI EGFP OPN1MW
E'
DAPI
E''
EGFP
E'''
OPN1MW
CRISPR-Abca4
F
OPN1MW mRNA quantity (arbitrary units)
1.2
0.8
0.4
0
*
*
WT
Control
CRISPR-Abca4
G
RPE
OS
J
RPE
OS
H
RPE
OS
K
RPE
OS
I
OS
IS
L
OS
IS
M
A2E
pmoles/eye
50
40
30
20
10
0
Psammomys control
Psammomys CRISPR-abca4
Wistar rat 40d
Wistar rat 200d
N
all-trans Retinal dimer
peak area
6000
4000
2000
0
N.D.
N.D.
Psammomys control
Psammomys CRISPR-abca4
Wistar rat 40d
Wistar rat 200d

Figure 4

DISCUSSION

Discussion

This thesis project aimed to evaluate the preferential vulnerability of cones in an animal model of *Abca4* knockdown, mimicking some forms of STGD1. Our hypothesis was that use of a cone-rich rodent species would faciltate experimental analysis, allowing us to compare the outcome of abca4 inhibition in the two PR populations. Our original plan was to use the diurnal rodent *Arvicanthis ansorgei* as an animal model. The retina of this animal has been characterized extensively by histology, immunohistochemistry and functional recording, confirming the presence of a large population of cones (Bobu et al, 2006) (Bobu et al. 2008; Bobu et al. 2013) (Boudard et al. 2011) (Boudard et al. 2010) (Gianesini et al. 2015) (Verra et al, 2020).

This represented our starting point for the development of a sub retinal injection protocol, between the RPE and the PRs, of a plasmid capable of delivering the genetic editing CRISPR-Cas9 strategy of our choice. The strategy involves the use of two RNA guides sg64 and sg77 capable of targeting exon 5 of the total 50 of the *Abca4* gene. In fact, this deletion involves the generation of a frameshift and a consequent loss of the transcript and therefore of the protein.

A disadvantage of this strategy is that a short protein (208 amino acids) might be expressed after deletion of exon 5 (or indels at the splice donor or splice acceptor sites of exon 5) if RNA decay does not occur. Furthermore, it could occur that, given the size of *Abca4*, a protein of, a most, 2008 amino acids might be expressed if restart occurs at one of the in frame ATG located in exon 7 or further exons (low probability).

Sub retinal injection in *Arvicanthis ansorgei* was performed at postnatal time P0 followed by electroporation based on an approach described for rescuing PR death seen in a rat model of retinitis pigmentosa (Bakondi et al. 2016). The results obtained from the electroporation of the CRISPR-Cas9 plasmid showed clearly that although transfection was successful, the only PR cells transfected at that post-natal moment were the rods. There was no expression of mCherry (the fluorescent marker that allowed us to track the transfected cells) in the cones, which in this species are spatially separated from rod cell bodies in the ONL.

Actually it has been shown that in mouse and rat retina, retinal cell-type specification occurs in a sustained period between embryonic day 9 (E9) and postnatal day 7 (Heavner and Pevny 2012). The seven retinal cell types are generated in an evolutionarily conserved order during

development, although multiple cell types are produced simultaneously at any given developmental stage. The cones are generated early in development, whereas rods are generated during the last two thirds of retinogenesis (Morrow, Belliveau, and Cepko 1998). Thus considering the different cell cycle exit and differentiation times, we speculated that this was the reason why only rods were transfected and not cones, since rods are not yet differentiated cells but are actively dividing.

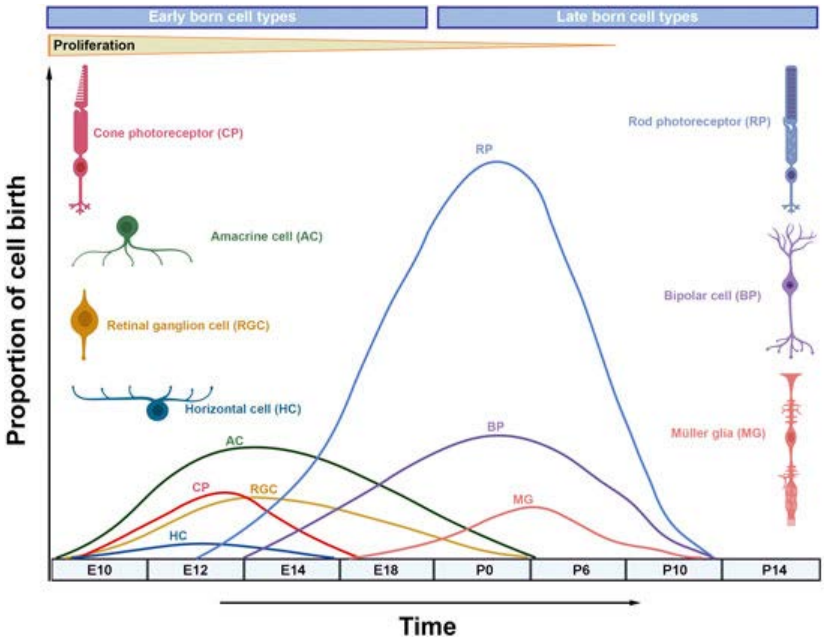

Figure 16 Retinal neurogenesis and organization of the mammalian retina.

Schematic diagram illustrating waves of retinal neurogenesis and approximate timing of retinal cell type birth where rod photoreceptors, bipolar cells and Müller glia are mainly formed postnatally. Modified from (Daghsni and Aldiri 2021).

Electroporation leads to plasma membrane pore formation due to electrical shocks, thereby increasing the permeability of the plasma membrane. It is a non-viral method of transfection, very efficient in dividing cells. This is due to the fact that during mitosis, the nuclear membrane which represents a barrier for the entry of transfected DNA, breaks down and then reforms (Cervia et al. 2018), thereby enabling integration of the electroporated plasmid DNA.

Therefore, considering the impossibility of electroporating cones at the postnatal time P0 as they are already fully post-mitotic and already partly differentiated compared to rods, we speculated that the electroporation of the plasmid containing the CRISPR-Cas9 construct should be performed earlier, in a stage in which neither the cones nor the rods were differentiated.

For this reason, we next attempted *in utero* electroporation, the idea being to perform injection of the CRISPR-Cas9 plasmid into a single eye of an embryo at the E12.5 embryonic stage (when the cones are still actively dividing) in *Arvicanthis ansorgei*. The injection was then followed by electroporation and the embryos placed back into the mother's uterus.

Pilot studies to set up the technique were performed on C57BL/6J mice, and 48h after electroporation it was possible to confirm the efficient transfection of retinal precursor cells (RPCs), thanks to the GFP+ reporter present in the control vector used (CAG-GFP+). Thus the *in utero* electroporation technique was more efficient in targeting all PRs than that at post-natal moment P0.

Unfortunately, there were serious drawbacks in this technique. One disadvantage of *in utero* electroporation is the uncertainty about the duration of transgene expression (Yamashiro, Ikegaya, and Matsumoto 2022). This is because electroporated plasmid vectors are episomal and the number of vectors in each daughter cell is less than that in the mother cell because the total number of vectors (which remain episomal in the mother cell) is constant. Furthermore, the embryonic survival rates were very low; we observed that only the embryos not subjected to electroporation arrived at term, whereas electroporated ones degenerated and were reabsorbed. We speculated that it was probably the electroporation *in utero* which caused high mortality in electroporated embryos. One of the main difficulties is the lack of survival up till birth of electroporated embryos. In most cases the female is no longer pregnant. The most frequent cause is the death/reabsorption of the embryo following electroporation and this may depend on a prolonged procedure, but may also depend on traumatic manipulation during the surgical operation, electroporation parameters, animal stress (Fares Taie 2012).

This would have made it difficult to follow the phenotype of *Arvicanthis ansorgei Abca4* KO following injection and electroporation of the CRISPR-Cas9 plasmid. The difficulties we had in targeting PR via the electroporation technique led us to evaluate another delivery strategy of the CRISPR-Cas9 gene editing technique, namely the use of an Adeno Associated Virus (AAV) viral vector, which is widely used in the retina for gene therapy (Ong et al. 2019). Although its

small size obliged us to use two vectors, it has two fundamental advantages compared to electroporation. Firstly, it is able to target mitotic and also post-mitotic cells, allowing us to bypass the use of embryonic and newborn animals. secondly, it has been shown that several serotypes of AAV are known to specifically target PRs. Both serotype 2/5 and 2/8 target PRs, but we chose 2/8 because it is more efficient than 2/5 in pig retina (Mussolino et al. 2011). Furthermore, the feasibility of AAV delivering CRISPR-Cas9 as a strategy was validated by (Yu et al. 2017), in which the technique was used to repair retinal degeneration in a mouse model of autosomal dominant retinitis pigmentosa, using double AAVs serotype 2/8.

During the thesis project, in addition to the difficulties encountered with the use of the electroporation technique, there were also limitations concerning the animal model we chose, *Arvicanthis ansorgei*.

Limited knowledge regarding the reproductive cycle of the animal has greatly hindered the creation of a transgenic *Abca4* KO model, which would have allowed investigation of PR vulnerability under more controlled conditions. It was previously found to be very difficult to characterize the reproductive cycle of *Arvicanthis ansorgei,* a necessary requiremen for reimplantation of generically modified embryos (Fares Taie 2012). Considering these difficulties already encountered in the past, coupled with the restricted numbers of animals available for experiments (small litter sizes, unpredictable breeding cycle, high mortality of injected pups due to maternal rejection and cannabalism), we completely re-evaluated the genetic editing strategy.

Fortunately our institute possesses a second diurnal rodent species, the Fat Sand Rat *Psammomys obesus*. Although it primarily represents a good model to study type 2 diabetes and diabetic retinopathy as a consequence (Saidi et al, 2011) , this species has the same advantages for our project as *Arvicanthis ansorgei*: a high number of cone PR (~40%) similar to the human macula; background data on retinal structure and function (Saidi et al, 2011a, b; Dellaa et al); ease of handling and animal care. Furthermore, contrary to *Arvicanthis ansorgei*, there were no problems of availability of animals or disturbed maternal behaviour.

All of these advantages led us to use *Psammomys obesus* as a model to study the STGD1 disease phenotype.

However, the choice of *Psammomys obesus* had limitations. The genome of *Psammomys obesus* is known but not annotated, making it more difficult to find genes of interest such as *Abca4 in*

primis and also other genes quantified during the thesis project such as RHO and OPN1MW. It was therefore necessary to amplify and confirm with Sanger sequencing the *Abca4* gene in *Psammomys obesus* to design new guides RNA for the CRISPR-Cas9 strategy. The complete genomic sequences of *Arvicanthis ansorgei* and *Psammomys obesus* are not available in the databases. The closest genomic sequences are those of the rat, hence the search for the rat genome guide. The sequences of *Arvicanthis ansorgei* and *Psammomys obesus* are highly homologous but not identical, leading us to change the guides because they had to physically cut the genomic DNA of the species we were working on. CRISPOR software allows identification of all potential guides (with a PAM-nGG) of a given sequence The software also makes it possible to find any potential off-target sites, which represents one of the most critical points of CRISPR-Cas9 technology. In our case, the genomes of *Arvicanthis ansorgei* and *Psammomys obesus* not being available, it is not absolutely certain that off-target searches were correct. Ideally any sequences predicted by CRISPOR, should be amplified and sequenced to preclude potential off-target effects.

Given the problems associated with performing experiments on very young pups (difficulties to safely induce anesthesia, maternal rejection,…), we considered performing injections on older postnatal individuals, after eye opening when the babies are less fully dependent on the mothers. In order for such an approach to be feasible, we needed to determine *Abca4* expression levels during postnatal growth, since the presence of high endogenous protein levels would compromise de novo *Abca4* inhibition. So the first step after the design of the guides was to quantify *Abca4* expression over time in *Psammomys obesus*, starting from post-natal day P15 up to adult age (11month). The data confirmed that *Abca4* was correctly expressed in the OS of rod and cone PRs and that its expression was very low before P15-20. Therefore, this provided a time window to block the transcription of *Abca4* while endogenous levels were still low; and it should be borne in mind that the STGD1 phenotype is usually seen in juveniles.

The subretinal injection was performed between P14-P17 with two AAV vectors, one containing the two guides and the other containing the gene encoding Cas9. Test injections were alwas made in the left eye, while right eyes were injected only with the vector containing the guides (control). Initially thanks to the expression of the fluorescence marker eGFP and with the use of an antibody against the Cas9 protein it was possible to confirm that the two AAVs transduced both PRs correctly and not other retinal cells.

It was crucial to validate *Abca4* deletion in *Psammomys obesus* retina following subretinal injection. initially analysis of *Abca4* deletion was performed on the entire retinal tissue, by PCR amplification about 300nt upstream and downstream of exon 5 targeted for deletion. However, considering the small area of retina effectively transduced, cell sorting via FACS was chosen to isolate GFP+ cells and specifically investigate them.

This allowed us to verify that out of the total number of retinal cells, GFP+ cells represent about 12% of the cell population, and based on an estimate of PR representing ~40% total cells this implies around 25% of PR were actually transduced. Following DNA extraction and amplification of a 700nt region surrounding exon 5, it was possible to identify the population deleted. A band of ~700bp represents the non-deleted population, while in the same lane a second band of approximately 500bp represents the deleted population. The presence of two bands is probably due to the fact that the deletion did not occur in all cells among the GFP+ population, in addition to the fact that post sorting was not performed on the isolated sample, which would have resulted in more cleanly purified cells. Sanger sequencing of the band isolated from the gel of about 500bp confirmed the editing by CRISPR-Cas9. Observing the chromatogram, mixed peaks are seen which reflect the heterogeneity of the amplicon sequences. This is explained precisely by the NHEJ mechanisms which subsequently anneal DNA double strands generating indels.

Abca4 expression was analyzed and quantified in the whole retinal tissue as protein and mRNA, and significantly decreased expression was confirmed in the CRISPR-Cas9 compared to the control sample.

This validation enabled us to proceed to observations of the phenotype in our animal model *Psammomys obesus Abca4* KO.

Retinas treated with the CRISPR-Cas9 construct were compared to retinas treated only with RNA guides as a control, using non-invasive Optical Coherence Tomography (OCT). Compared to control retinas where all the retinal layers are present, CRISPR-Cas9 treated retinas exhibited extensive loss of outer retinal layers, in some cases loss of the entire retina. This recalls the phenotype of STGD1 with thinning of the retina and loss of the PR layer (Mena et al. 2021).

These observations were also confirmed by transmission electron microscopic analysis where it was possible to visualize the retina and RPE in detail. We focused our attention on regions

close to the damage site , where we observed clear PR degeneration. Although it was not possible to unequivocally distinguish whether the affected PR were rods or cones, dying cells and fragmented OS were positioned at the same level as the cones, and many apparent rod OS were intact. To be sure of the PR identity, it will be necessary to perform immunogold labelling with specific antibodies that selectively mark the PRs. Melanosomes were seen in the RPE of both CRISPR-Cas9 treated and control eyes (Pelkonen et al. 2016), but in addition numerous small rounded inclusions were observed in the CRISPR-Cas9 Abca4 KO eyes. We speculate that these granules originate from the dying PR debris and contain lipofuscin, a hallmark of the STGD1 disease phenotype.

All trans-retinal dimers (atRAL-dimer), a unique atRAL condensation product, was shown to be low in wild-type mice retinas, yet abundant in *Abca4*−/− mice retinas (Li et al. 2016). It has been shown that *Abca4*−/− mice eyes contain more atRAL-dimer-PEthan A2E (Fishkin et al., 2005, Kim et al., 2007), and it has been suggested that atRAL-dimer plays an even more critical role in the pathogenesis of macular degeneration (Kim et al., 2007). For these reasons we decided to quantify one of the main components of lipofuscin, A2E as well as atRal-dimer which are formed inside the PR discs in the phototransduction process, by Ultra High-Performance Liquid Chromatography (UPLC). We compared the eyes of CRISPR-Cas9 treated animals with GFP-injected controls, but there were no differences between the two samples for the amounts of A2E or atRal-dimer. This could be due to the post-injection time chosen to perform the quantification:.electron microscopic analysis was performed 7 months after injection, while UPLC examination was undertaken after 2 months. As we were also unable to detect auto-fluorescence in injected eyes at 2 months post-injection, it indicates that cone malfunction and death may be a primary event, preceding the build-up of lipofuscin by the RPE. Albino Wistar Rats, which have enhanced formation of A2E compared to pigmented animals, contained no detectable alRal-dimers , whereas *Psammomys obesus* eyes contained significant amounts of this toxic bis-retinoid. This data highlights an important characteristic of this animal species and is in line with our hypothesis.

Electroretinography analyses showed that eyes treated with the CRISPR-Cas9 construct exhibited decreased amplitudes in responses to light intensities 0-0.5-1 Log.cd.s/m2 in scotopic conditions compared to controls. Although low intensity light flashes in scotopic conditions provide information on pure rod responses, such stronger flashes evoke mixed rod/cone

responses. This again agrees with the hypothesis that rod function is much less affected than that of cones. We also observed a significant difference in pure cone responses under photopic conditions, with significant decreases in injected CRISPR-Cas9 compered to controls. Decreases also occurred under photopic flicker conditions, an ERG protocol which provides a robust measure of cone function. These ERG data therefore primarily indicate decreased responsesin cones but not rods, further supporting the idea that cones are more vulnerable.

These data are further supported by mRNA quantification of two genes, rhodopsin specifically expressed in rod cells and mid wavelength-sensitive opsin, specifically expressed in MW ("red/green" sensitive) cones. Expression levels of these two mRNAs allowed comparison of the two PR populations in retinas treated with CRISPR-Cas9 compared to controls. We observed significant decreases in mw *opsin* expression in the CRISPR-Cas9 treated retina compared to controls, and also to wild-type unoperated retinas, indicating a decrease in this cone population in the *Abca4* KO retina. On the contrary, expression of *rhodopsin* mRNA showed no differences between CRISPR-Cas9 and control retinas (or compared to the wild-type). These quantitative data were also supported by qualitative immunofluorescence analysis of MW OPSIN and RHODOPSIN proteins. We confirmed the same expression profiles, ie. in retina treated with CRISPR-Cas9 it was possible to observe decreased MW OPSIN expression compared to controls whereas RHODOPSIN immunostaining was equivalent between the two. The laboratory recently demonstrated that cones exhibit several distinct molecular differences from rods: cones contain significantly more *abca4* mRNA and protein; contain much less docosahexaenoic acid (DHA), an important neuroprotective polyunsaturated fatty acid ; much less phosphatidyl-ethanolamine (PE), a major phospholipid; show reduced amounts of A2E but five times greater amounts of atRal-dimer (Verra et al.; 2022). The reduced amounts of PE compared to rods could alter the stoichiometry of the condensation reaction N-RetPE formation, and explain the relative abundance of atRal-dimers compared to that in rods. Perhaps the inability of *Abca4* to transport atRal-dimers leads to build-up or "congestion" within the continuous membrane folds in conesThe highly toxic nature of these atRal-dimers therefore cause damage to the membrane of the cones prior to their removal by RPE phagocytosis. Even so, significant accumulation of such toxic debris by the RPE would also negatively impact survival of these cells too. On the other hand, the higher renewal rates in rod turnover operated by RPE (Bobu et al 2006) and the formation of A2PE and A2E through the "classic" PE pathway would result in less formation of atRal-dimers. These intrinsic differences provide one

potential mechanism by which cones are more vulnerable to mutations in *Abca4* compared to rods.

It has been shown that *Abca4* plays a fundamental role in the visual cycle and therefore the renewal of 11-cis retinal (11-cis RAL). It is known that in the RPE65-/- mouse where (RPE65 is responsible for the conversion of all-trans-retinyl esters to 11-cis-retinol: ref), the retinoid cycle is disrupted, 11-cis retinal is absent and cone pigments mislocalize and cone PR degenerate. In contrast, rhodopsin localizes normally to outer segments and rods are relatively stable (Zhang et al. 2008). 11-cis RAL therefore seems essential for trafficking of cone opsins to the OS, acting as a chaperone. Furthermore, due to the high demand of 11-cis RAL in light, in addition to RPE-65 cones use an additional pathway supporting photoisomerization in the Muller glia. In this latter case, the chromophore that enters cones is in the form of 11-cis ROL and needs to be oxidized to 11-cis RAL (Hildebrand et al. 2009; Tian et al. 2022).

So in the case of *Abca4* mutations and altered functioning of this transporter essential for the renewal of 11-cis RAL, there may be insufficient supply of chromophore to cones. We speculate that this could be another pathway of direct cone damage.

In the currently accepted pathogenic scenario of STGD1, mutations in the *Abca4* gene cause atRal to accumulate within the discs. In this scenario, NRPE reacts with a second atRal molecule to form the dihydropyridinium molecule A2PE, and then within the RPE, phosphate hydrolysis produces A2E, the major component of lipofuscin (Sparrow et al. 2012). Due to the continuous phagocytic mechanism operated by the RPE, these autofluorescent pigments end up in the liposomes of the RPE. Impaired ABCA4 function leads to increased accumulation of these bisretinoids leading to lysosomal dysfunction and primarily RPE degeneration and loss of function, which then triggers secondary PR death.

We hypothesize a different pathogenic sequence which predicts primary degeneration of cones, dueto their intrinsic characteristics distinct from rods. In *Psammomys obesus Abca4* KO, in line with the phenotype of STGD1, we observed that inhibitionof the *Abca4* gene is more toxic for cones compared to rods. The accumulation of toxic material in cones which causes their death will be transferred to the RPE by phagocytosis mechanism and we hypothesize that RPE death is therefore secondary and depends on the number of cones in contact. In the cone-rich human macula, many cones are in contact with the RPE and as seen in many forms of STGD1, RPE degeneration occurs principally in this region. In the periphery where the cone/RPE ratio is much lower, RPE are much less impacted by cone debris and degeneration does not occur, or

is slowed down. Our animal model *Psammomys obesus* is well suited for exploring fully this mechanism, as its retina can be compared to a “giant macula”, many cones are in contact with the RPEas in the human macula, and this explains the severe *Abca4* KO phenotype similar to the more severe forms of STGD1. It further explains why *Abca4* KO mice, with their low cone numbers, do not exhibit marked retinal and RPE degeneration and do not resemble the human disease.

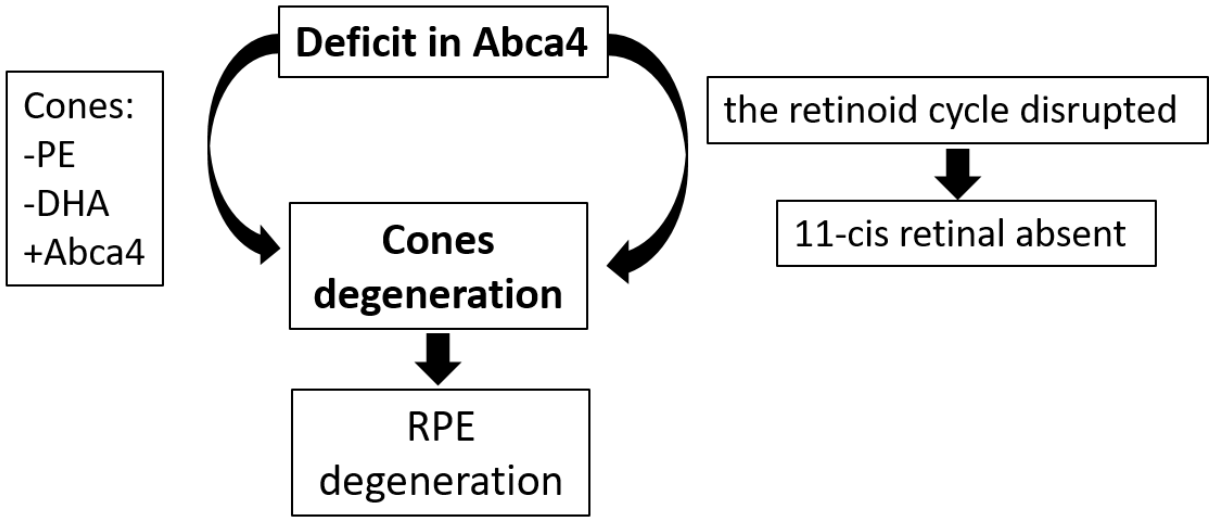

Figure 17 Schematic representation following deficit in *Abca4* gene The mutation in the *Abca4* gene as in Stargardt disease leads to degeneration of the cones due to two hypotheses: 1-intrinsic features of the cones (less PE, less DHA and more *Abca4*) which make them more vulnerable than rods; 2- an alteration of the retinoid cycle that induces absence of 11-cis RAL requires for the trafficking of membrane-associated proteins to cone photoreceptor outer segments and viability of cones too. Both pathways involve degeneration of the cones resulting in degeneration of the RPE by accumulation of toxic material in the phagocytosed outer segments.

GENERAL CONCLUSIONS

General conclusions

The creation of this *Psammomys obesus Abca4* KO model offers the possibility to investigate the effects of modifying the *Abca4* gene. The retina of *Psammomys obesus* represents a sort of magnifying glass of the human macula and this is just the starting point for an animal model that offers many advantages. Our deletion of exon 5 of the *Abca4* gene leads to a "nullozygosity" and to a severe disease phenotype. It would therefore be interesting to create models harbouring specific point mutations related to different human phenotypes. Gene editing and insertion of mutations associated with mild, moderate or severe phenotypes would allow us to better explore the phenotype-genotype relationship of STGD1, which manifests such a broad spectrum of disease progression and features. Our new animal model will also facilitate development of therapeutic approaches for macular degeneration, thus overcoming a major obstacle in the field. The use of cone-rich rodents allows for detailed analysis of structure/function relationships in rod and cone populations.

SUPPLEMENTARY MATERIALS AND METHODS

Supplementary materials and methods

1 Arvicanthis ansorgei in vivo electroporation

1.1 Animals

The initial subretinal injection and *in vivo* electroporation procedures were performed on neonatal animals *Arvicanthis ansorgei* (P0) in accordance with guidelines for animal care.

1.2 Morphology of retina in normal *Arvichantis ansorgei*

To obtain an experimental baseline of our animal model *Arvicanthis ansorgei*, we used immunohistochemistry in normal animals. The eyeballs were harvested from the animals (Male-Female *Arvicanthis Ansorgei*, P30) and directly immerged in PFA 4% for 2h at room temperature. After this fixation, eyeballs were placed in PBS medium and cut along the *ora serrata* to remove the cornea and lens. Then dissected eyeballs were placed in increasing concentrations of sucrose/PBS (10% - 20% - 30%) overnight for cryoprotection. Finally, it was embedded in OCT compound and sectioned by Cryostat (section 10-12µm). *Arvicanthis* retinal sections (10-12µm) were first rinsed with washing buffer (0.1% triton x-100 in PBS) for membrane permeabilization for 5 min at room temperature. Then they were incubated for 1h in blocking buffer (5% BSA in PBS) at room temperature. Primary antibodies were diluted in blocking buffer and incubated overnight at 4°C in the dark. After rinsing the slides with PBS, the secondary antibodies were applied, diluted in the blocking buffer for 2h at room temperature. After rinsing the slides with PBS several times, DAPI was applied, diluted in PBS, for 2 min at room temperature in the dark. Finally slides were rinsed with PBS before applying mounting medium.

Table 1: list of antibodies used for immunostaining

Antigen	Host	Dilution
PRIMARY ANTIBODY		
S-Opsin	Rabbit	1:500
M-Opsin	Rabbit	1:500

Pan arrestin	Rabbit	1:500
Rhodopsin (Rho4D2)	Mouse	1:500
Glial Fibrillary Acidic Protein (GFAP)	Rabbit	1:500
ABCA4	Rabbit	1:100
Rom-1D5	Mouse	1:500
Protein kinase C-α	Rabbit	1:500
SECONDARY ANTIBODY		
Goat anti-mouse Alexa568	Goat	1:1000
Goat anti-rabbit Alexa 568	Goat	1:1000

1.3 Design of CRISPR-CAS9 cassette

The *Abca4* gene has been sequenced in *Arvicanthis* (unpublished data, collaboration with Drs. J. Kaplan and J-M. Rozet), and we possess the whole genome and retinal transcriptome data (Liu et al., 2017). Probe design and optimization was performed in collaboration with personnel at the IGBMC/PHENOMIN-ICS (Dr. G. Pavlovic, head of department, and Dr. M-C. Birling, assistant head of department), possessing extensive in-house expertise in CRISPR-Cas9 technology. The *Arvicanthis Abca4* gene was aligned (CLUSTAL 2.1 MULTIPLE SEQUENCE ALIGNMENT) against the mouse and rat genome.

The organization of the gene looks very similar to the two other rodents. Deletion of exon 5 will induce a frame shift and should result in gene deletion. Firstly, the *Arvicanthis* sequence was confirmed by performing PCR analysis of the region of interest (region surrounding exon 5). The guides RNAs were searched for using the CRISPOR web site (http://crispor.tefor.net/crispor.py). 4 guide RNAs (2 targeting both sites of exon 5) were

synthesized and tested *in vitro* (on the PCR fragment containing the target sequence and in the presence of the Cas9 protein).

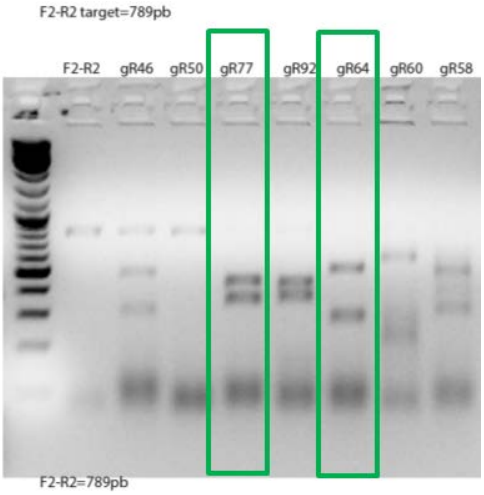

Figure 18 PCR analysis of the exon 5 (F2-R2 target region, 789pb) in the presence of the Cas9 protein and different guide RNAs. Wells containing different gRNAs (gR46-gR50-gR77-gR92-gR64-gR60-gR58) were prepared, gRNA 64 and gRNA 77 were then selected, from which two distinct and clean bands were obtained.

One guide on each extremity (5' and 3' of exon 5) was selected, and then cloned into a plasmid containing Cas9 fused with mCherry under a chicken β-actin promoter cBH (ubiquitous promoter), and 2 tracrRNA sequences preceded by a U6 promoter. As a control plasmid two irrelevant guide RNAs were cloned into a similar plasmid (expressing mCherry fused to Cas9).

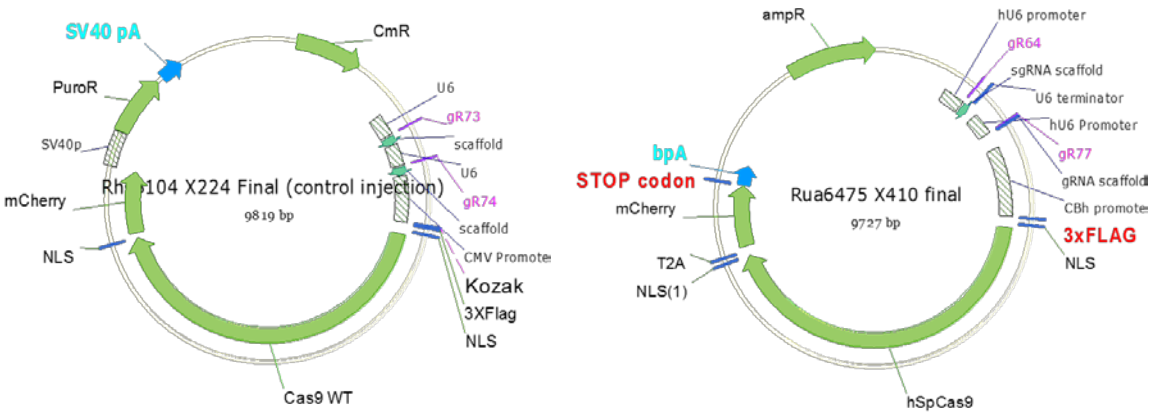

Figure 19 Rua6475 (plasmid for deletion of exon5, 9727pb) and Rho104 (plasmid control, 9819pb).
Left panel, plasmid for delection of exon5 with Cas9 fused to a fluorescence protein T2A-mCherry under the CBh promoter and gRNA77 and gRNA64 (for delection of exon 5 of *Abca4* gene) under the hU6 promoter.
Right panel, plasmid control with Cas9 fused to a fluorescence protein T2A-mCherry under the CBh promoter and two irrelevant guide RNAs (gR73 and gR74) under the hU6 promoter.

1.4 Subretinal injection of newborn *Arvicanthis ansorgei* (p0)

As previously described *(Matsuda and Cepko 2004)* newborn *Arvicanthis ansorgei* (n=5) were anesthetized on ice for several minutes. Only the right eye was injected, the eyelid was cleaned with 70% ethanol. Carefully the edge of the forming eyelid was cut using the tip of a sharp 26-gauge needle and then the eyeball was exposed by pulling down the skin. A small incision was made in the sclera near the cornea using the tip of a sharp 30-gauge needle. An injection needle (Hamilton syringe, 33 gauge blunt end) was inserted into the eyeball through the incision until resistance was felt, and slowly the DNA solution (plamid control Rho104, 1µl) containing a dye (Fast green 1%) was injected into the subretinal space.

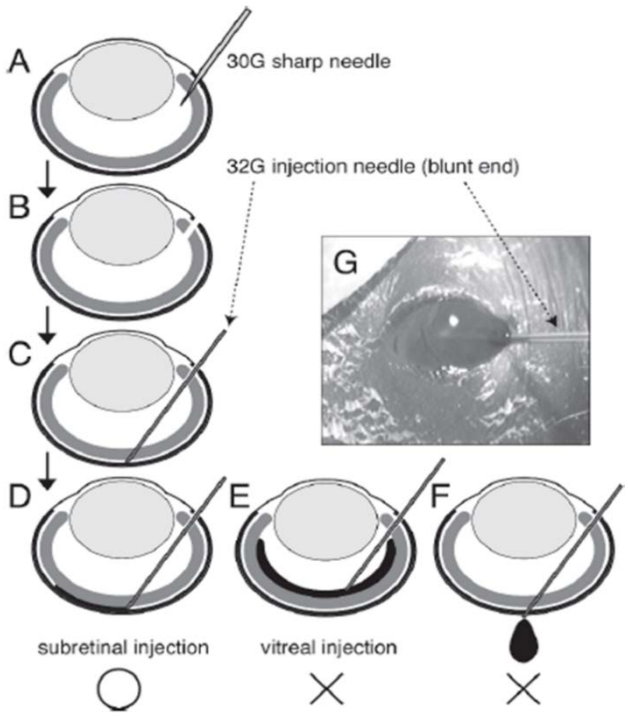

Figure 20 Procedure of Subretinal Injection

Procedure for subretinal injection—illustration. (**A**–**D**) Schematic drawing of the subretinal injection procedure. See text for detailed description the procedure. (**E**, **F**) Examples of bad injection. (**G**) Injection needle can be seen through the lens if the eyelid is opened before injection. From *Matsuda, T., C.L. Cepko, 2008.*

1.5 *In vivo* Electroporation

For *In Vivo* transfection of the retina by electroporation, a square pulse electroporator ECM830 (BTX) was used and the tweezer-type electrodes were lubricated with SignaGel (to increase the contact between the pup and the electrodes). Then the tweezer-type electrodes were placed around the head of the pup, and slightly squeezed. The positive electrode, marked by a plastic screw was at the DNA-injected side (we transfect DNA from the subretinal space into the retina). Five square pulses of 50-ms duration and 100V intensity with one-second intervals between pulses were applied using a pulse generator. The five operated pups were warmed until they recovered, and then returned to the adoptive Wistar mother.

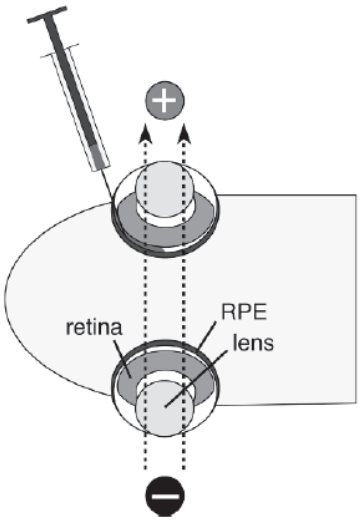

Figure 21 Strategy for *in vivo* electroporation

Electroporation from the scleral (retinal pigment epithelium) side of the retina. .Modified from *Matsuda, T., C.L. Cepko, 2008.*

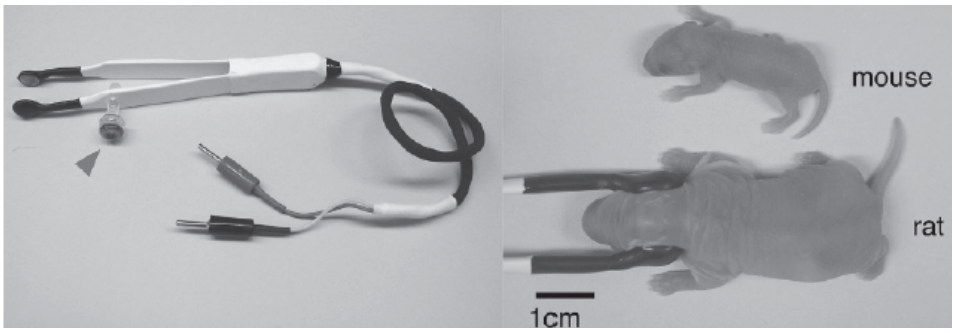

Figure 22 Electrodes and procedure for *in vivo* electroporation.

Electrodes and procedure for in vivo electroporation. Tweezer-type electrodes are placed to hold the head of newborn (P0) *Arvicanthis ansorgei*. *Arrowhead* indicates the plus side of the electrodes. From *Matsuda, T., C.L. Cepko, 2008.*

1.6 Tissue preparation

Animals were sacrificed at post-natal day 14 (P14) (time needed to wait for transcription and synthesis of plasmid marker mCherry) (ref.), five injected and electroporated right eyes were rapidly enucleated and prepared for retinal section to assess mCherry distribution (*Bakondi, B. et al. 2016*). The eyeballs were harvested from the animals (Male-Female Arvicanthis Ansorgei, P14) and directly immersed in PFA 4% for 2h at room temperature. After this fixation, eyeballs were placed in PBS medium and cut along the *ora serrata* to remove the cornea and lens. Then dissected eyeballs were placed in increasing concentrations of sucrose/PBS (10% - 20% - 30%) overnight for cryoprotection. Finally, they were embedded in OCT compound and sectioned by Cryostat (section 10-12µm). The images were captured on a fluorescence microscope (*Leica EL6000).*

2 *In utero* electroporation mouse retina

2.1 Animals

E12.5 embryos from C57BL6J pregnant mice (2-4 months old) were electroporated *in utero* in accordance with guidelines for animal care.

2.2 Injection CAG-GFP vector in retina mouse

A pregnant mouse at embryos stage E12.5 is anesthetized by gas (isoflurane) and then an incision is made in the abdominal wall to gain access to the uterine horns containing the embryos. The uterine horns are exposed on the outside of the animal so that the embryos can be manipulated. The plasmid CAG-GFP 1µl+ 0.1%Fast Green is introduced into the eye of the embryos using a borosilicate microcapillare. The embryos eye are electroporated using a pair of tweezers-like electrodes to drive the constructs into the RPCs. Five square pulses of 50-ms duration and 80V intensity with one-second intervals between pulses were applied using a pulse generator. Once all the embryos have been manipulated, the uterine horns are replaced within the abdomen of the pregnant mouse and the incision is closed.

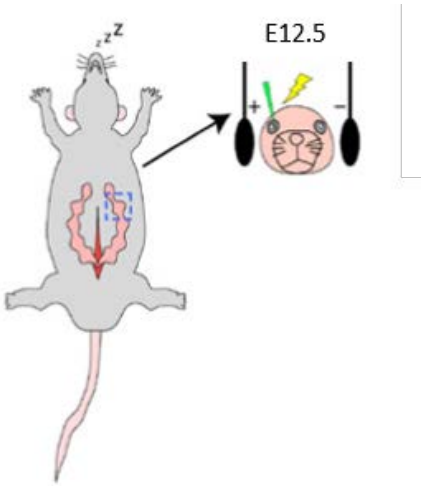

Figure 23 Electrodes and procedure for *in utero* electroporation. The uterine horns are removed from the mother. The DNA solution is injected into the embryo's retina. Through electroporation the DNA is brought into the RPCs. The embryonic hull is placed back in the mother and allowed to survive for 2 days (E14.5)**.** Modified from (Petros, Rebsam, and Mason 2009).

2.3 Tissue preparation

Embryos were collect 48h post in utero electroporation at stage E14.5 was prepared for section to assess GFP distribution The embryo's heads were harvested from the animals (embryos stage E14.5) and directly immersed in PFA 4% for 2h at room temperature. After this fixation, they were placed in increasing concentrations of sucrose/PBS (10% - 20% - 30%) overnight for cryoprotection. Finally, they were embedded in OCT compound and sectioned by Cryostat (section 10-12µm). The images were captured on a fluorescence microscope (*Leica EL6000).*

3 Psammomys *obesus in vivo* AAVs –delivering CRISPR-Cas9 strategy

3.1 Animals

The subretinal injection of two AAVs-delivering strategy CRISPR-Cas9 procedure was performed on P14-P17 animals *Psammomys obesus* (P14-P17) in accordance with guidelines for animal care.

3.2 Searching the *Abca4* gene in *Psammomys obesus*

The entire genome of *Psammomys obesus* has been sequenced *(Hargreaves et al. 2017)*, but not annotated. To trace the sequence of Abca4 in *Psammomys obesus* in order to target a part of the gene through the sgRNA guides of the CRISPR-Cas9 system, the mouse Abca4 gene (intron 4-5, exon 5, intron 5-6) was aligned against *Psammomys obesus* whole genome with an identity of 81%. After obtaining the sequence, two primers were designed to amplify >300pb both side of exon 5 of Abca4 in *Psammomys obesus* to obtain by PCR PFU an amplicon of 792pb. The DNA was than purified (Zymoclean ^{tm} Gel DNA Recovery Kit) and sequenced by Sanger sequencing.

Gene	Specie	Forward	Reverse	Reference
Abca4	Psammomys obesus	GTTCCTTACCCTTCACTCTCTTG	CACGATTGCTCTGCTTCCT	IDT
		CTTCTGTAGTTCCTTACCCTTCAC	GGTAGGTTCAGCTTCACGATT	IDT

Table 2 Two pairs of primers sequence used for *Abca4* gene amplification. IDT: primers designed using *the Integrated DNA Technologies tools*.

RNA guides for the CRISPR-Cas9 strategy were designed and optimization was performed in collaboration with personnel at the IGBMC/PHENOMIN-ICS (Dr. G. Pavlovic, head of department, and Dr. M-C. Birling, assistant head of department), possessing extensive in-house expertise in CRISPR-Cas9 technology. The *Abca4* gene sequence previously obtained was aligned against the *Rattus norvegicus* (identity 94%) and *Mus musculus* (identity 92%) Abca4 gene sequence.

Deletion of exon 5 was again the strategy to obtain a frame shift and consequently a gene deletion. The guides RNAs were searched for using the CRISPOR web site (http://crispor.tefor.net/crispor.py). 2 guide RNAs were selected, the 5' gR58 guide and the 3'

gR80 guide both should cut close to the splice acceptor or donor sites of exon 5 to increase the cut efficiency. The guides were synthesized and tested *in vitro* (on the PCR fragment containing the target sequence and in the presence of the Cas9 protein).

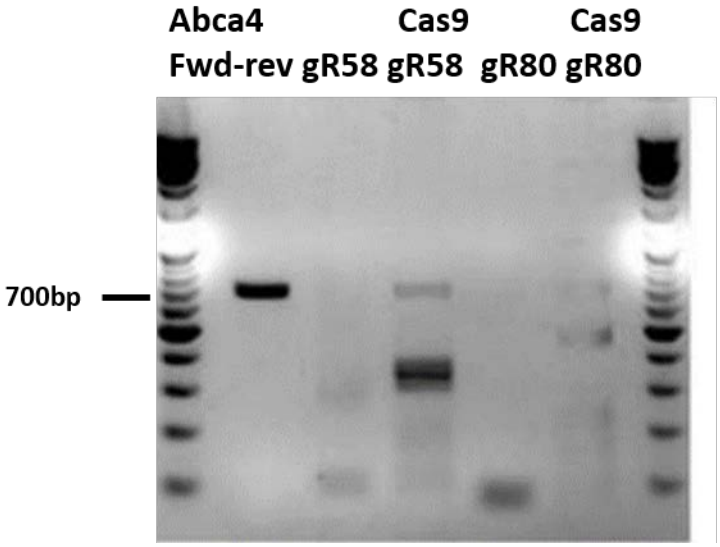

Figure 24 PCR analysis of gRNA58 and the gRNA80.
Abca4 Fwd-rev target region of 707bp in the presence of the Cas9 protein and guide RNA58 and guide RNA80 show different bands resulting from the cut. Wells containing two gRNAs 58 and 80 without Cas9 not show band.

AMPLICON 707BP

PRIMER FORWARD
CTTCTGTAGTTCCTTACCCTTCACTCTCTTGAAAGCCCCTGTCTTAGTCCAACCCTAAAAA
GCACCTGAGATCTCACCCACCCCAGGTTAACATCCCCCACCTTCTATGCCTTTCCACTGTA
TTGTGCCAGGTTCTTTAGCTGTAAGTGGTATGACTGGATGGGTGGCAGATACTGGCAGCAG
CCTTAACCTCCAAGAGTTCCCAAGGAAACCAAGAACACAGCTCTCTTGTAAGAGTCAAGTA
GAAATATTTCCAGTCAATTCTAGCTGCTTTTCTTATTTTCGACTCATCTCCCTTCAACATC
SgRNA58 **EXON5**
CTGTTCTTTCTTTCACTCATGTGCAGGAAGAGGATTACAAATCCGAGACATCCTAAGAGAT
GAAGAGACAATGACTCTATTTCTCAAGAAAAACATTGGCCTGTCTGACTCAGTTGCCCATC
TTCTGGTCAGCTCCCAAGTTCGTGTGGAACAGGTAAGTGAGGCCTGTTAAGAGGAGGAAAA
SgRNA80
AGCACTGAGCCTGAGAGAGACAAGGGTGATTCTGTTTCTTTTCCCTTCTGCGTCTATATTC
AGAATCCATGACTCATGCTCCATATTCAGGGACACACCTGGGGGTTACTGAGCCAACGAGA
ACCCCATCACAGCAGTCTGAAGCAGCACTGGCACTCATAAGACTTCCCAGGTTTTGAAACT
TGAAGGAAGCAGAGCAATCGTGAAGCTGAACCTACC
PRIMER REVERSE

Figure 25 CRISPR-Cas9 target region of 707bp.
Representative diagram of the *Abca4 Psammomys obesus* target sequence. Forward and reverse primers to amplify a region around the exon5 (blue); 5'-TTTCACTCATGTGCAGGAAG- 3' and 5'-AGGTAAGTGAGGCCTGTTAAG-3'(yellow) guides RNA to target the very close to donor and acceptor sites of splicing, in red Protospacer Adjacent Motif (PAM) sequence. Exon 5 in green.

Two plasmids were prepared, the pAAV-CMVep-HA-SpCas9 plasmid and the pAAV-U6-gR58-U6-gR80-CAG-eGFP plasmid for the AAVs production.

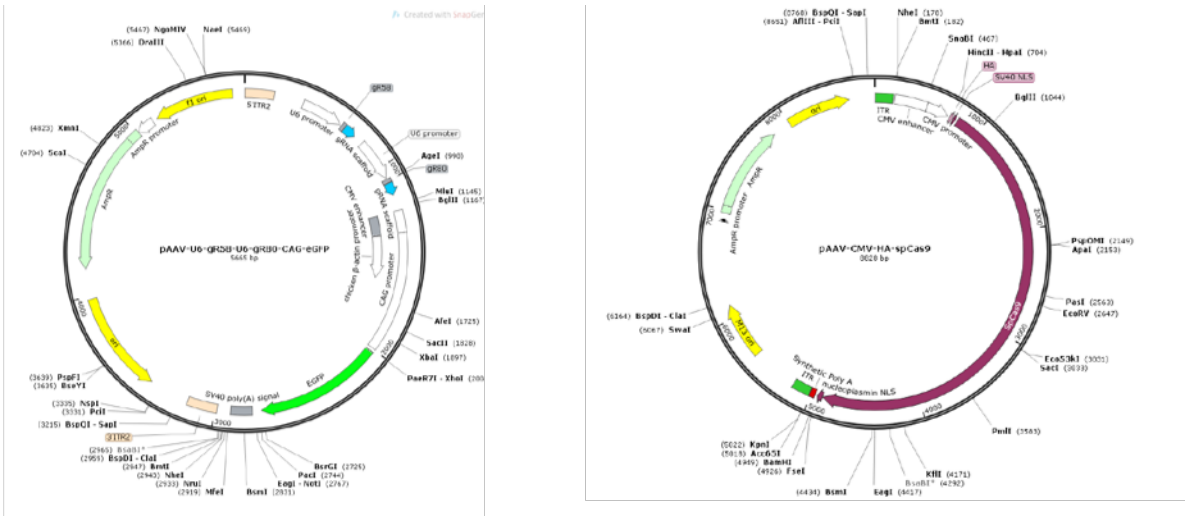

Figure 26 pAAV-CMVep-HA-SpCas9 plasmid and pAAV-U6-gR58-U6-gR80-CAG-eGFP.

Right panel, plasmid delivering Cas9 fused to an HA tag at its N-terminal end, dowstream the CMV promoter and a small synthetic polyA sequence Left panel, plasmid delivering two guide RNAs R58 (TTTCACTCATGTGCAGGAAG) and R80 (GGTAAGTGAGGCCTGTTAAG), under the control of U6 promoter. The pAAV already containing a CAG-eGFP cassette.

RÉSUMÉ

Résumé

Depuis Novembre 2019, je réalise ma thèse sous la direction du Dr David Hicks au sein de l'Institut des Neurosciences Cellulaires et Intégratives (INCI – UPR CNRS 3212). Dans cette unité, je fais partie de l'équipe « Lumière, vision et cerveau », dirigée par les Drs Marie-Paule Felder-Schmittbuhl et Frank Pfrieger. L'objectif de ce projet de thèse expérimental est de tester la vulnérabilité des cônes dans un nouveau modèle animal de la maculopathie héréditaire dite « Maladie de Stargardt de type 1» (STGD1), pathologie provoquant une malvoyance sévère chez l'humain. L'approche finalement choisie concerne le gène Abca4, transporteur localisé spécifiquement sur la membrane discale dans le segment externe (SE) des photorécepteurs (PR) et muté dans la STGD1, qui sera délété chez le rongeur diurne *Psammomys obesus* par inhibition directe de sa transcription après injection sous-rétinienne d'un vecteur viral AAV-CRISPR-Cas9. *Psammomys obesus* est une espèce dans laquelle les cônes sont représentés en nombre important (~40% contre <3% chez les souris), dont la rétine ressemble à la macula humaine et en facilite l'analyse structurelle, fonctionnelle et biochimique.

La décision d'utiliser cette approche expérimentale a été prise suite aux tentatives initiales employant d'autres méthodologies. Nous avons d'abord injecté et électroporé un plasmide CRISPR-CAS9-mCherry dans l'espace sous-rétinien [entre l'épithélium pigmentaire rétinien (EPR) et les PR] chez *Arvicanthis ansorgei*, un autre rongeur diurne semblable à *Psammomys*, au jour post-natal P0. 14 jours après l''injection nous avons visualisé le plasmide par l'expression de mCherry, marqueur fluorescent (Ex λ 587nm - Em λ 610nm). Bien que l'électroporation ait fonctionné, nous avons observé l'expression de mCherry uniquement dans les bâtonnets, alors qu'il était crucial de transfecter les deux populations de PR. L'absence d'expression du plasmide dans les cônes était probablement due à leur différenciation embryonnaire (E12-E13) par rapport à la différenciation plus tardive des bâtonnets (P0). Nous avons donc décidé d'électroporer le plasmide pendant le stade embryonnaire E12-E13. Afin de développer cette nouvelle stratégie, nous avons mis au point la technique d'électroporation de la rétine *in utero* chez les souris C57BL/6J et nous avons injecté avec un micro-capillaire en borosilicate dans l'œil des embryons au stade embryonnaire E13, 1µl de plasmide pCAG-GFP (marqueur fluorescent, Ex λ 395nm et 475 nm - Em λ 505 nm). Nous avons observé l'expression de la GFP dans >50% des cellules progénitrices de la rétine. Malheureusement les embryons électroporés *in utero* n'ont pas survécu jusqu'à la naissance. En raison du faible taux de viabilité et des difficultés de manipuler les embryons (faible nombre d'embryons par mère, difficulté à dater le stade embryonnaire), nous avons exploré une nouvelle stratégie qui nous permettait de

résoudre ces problèmes. Il s'agissait d'utiliser un Adeno Associated Virus AAV en tant que vecteur pour introduire le système CRISPR-CAS9 spécifiquement dans les PR. Un AAV a l'avantage de cibler même des cellules post-mitotiques, nous permettant d'utiliser des *Arvicanthis ansorgei* même à une semaine après la naissance (P7-P8 ; P=jour postnatal). Choisir un sérotype AAV optimal pour la transfection rétinienne (AAV2/8), nous permettra d'avoir un *Abca4*$^{-/-}$ *Arvicanthis ansorgei in vivo* grâce à la technologie d'édition du génome par CRISPR-Cas9. Pour poursuivre cette nouvelle stratégie, nous avons mis au point une injection virale chez *Arvicanthis ansorgei*. Nous avons injecté avec une seringue Hamilton (33G) 1µl d'un vecteur AAV CMV-pGFP (promoteur cytomégalovirus et GFP) dans l'espace sous-rétinien (entre l'EPR et les PR) au jour post-natal P20. La GFP nous a permis de vérifier, 7 jours après l'injection (P28), si l'AAV était correctement entré dans les PR, ce qui s'avérait être le cas : expression de la GFP dans de nombreux cônes et bâtonnets mais pas dans les autres cellules.

En collaboration avec l'IGBMC, nous avons dessiné des cassettes d'expression de la SpCas9 et des ARN guides (sgRNA) délivrés par deux vecteurs AAV séparés. Dans un vecteur AAV, le *Streptoccocus pyogenes* Cas9 (SpCas9) est placée entre un promoteur CMV et la GFP. Dans l'autre, le promoteur U6 est utilisé pour conduire l'expression des sgRNA. Un marqueur de fluorescence est inclus dans le vecteur sgRNA pour suivre la transduction des cellules. Cependant, nous avons décidé de changer de modèle animal, en raison de la faible disponibilité des *Arvicanthis ansorgei*. Nous avons alors utilisé une autre espèce de rongeur diurne, *Psammomys obesus*, qui présente les mêmes avantages pour ce projet (nombre élevé de cônes, nombreuses données déjà acquises sur la structure et la physiologie de la rétine, génome séquencé) et une reproduction plus fiable, même si les portées restent limitées en nombre (~4 petits).

La première partie du projet expérimental prévoit la mise au point technique de l'injection sous-rétinienne dans *Psammomys obesus* d'une d'un vecteur AAV exprimant CRISPR-CAS9-gARN ciblant *Abca4*. En collaboration avec les plateformes de transgenèse (Dr. M-C. Birling) et de virologie (Dr. P. Koeberle) de l'IGBMC, nous avons utilisé la carte génomique de la souris pour designer deux guides ARN qui provoqueraient la délétion de l'exon 5 du gène *Abca4*, et donc l'absence du transporteur dans les photorécepteurs de *Psammomys obesus*. Nous avons identifié la fenêtre temporelle adéquate pour réaliser les injections chez *Psammomys* : avant que la protéine endogène n'atteigne son maximum d'expression. Les rétines ont été étudiées par immunofluorescence, par western blot et par qPCR à différents âges post-nataux. Nous

avons fait fabriquer un anticorps anti-ABCA4 spécifique de la séquence de *Psammomys*. Les marquages montrent une expression très faible de P15 à P20, une augmentation graduelle ensuite jusqu'aux niveaux les plus élevés à 11 mois. Nous avons donc choisi l'intervalle P15-P20, immédiatement après le sevrage, pour réaliser les injections. Pour valider la technique chirurgicale et confirmer la transduction des PR *in vivo*, des constructions AAV-GFP ont été injectées dans l'espace sous-rétinien et 7 jours plus tard les animaux ont été euthanasiés. Des rétines entières montées à plat et des coupes transversales d'yeux ont montré une expression de GFP exclusivement dans de nombreux bâtonnets et cônes, mais leur absence totale des autres types cellulaires rétiniens.

Pour confirmer la délétion du gène *Abca4* chez *Psammomys obesus* suite à l'injection sous-rétinienne des AAVs CRISPR-CAS9, nous avons utilisé le Fluorescence-activated Cell Sorting (FACS) afin d'isoler notre population cellulaire GFP+ de la rétine 30 jours après injection. Après extraction de l'ADN par les cellules GFP+, nous avons amplifié par PCR une région de 700bp (bp=paires de bases) autour de l'exon 5 de *l'Abca4* ; en cas d'édition génétique par CRISPR-CAS9 (et donc délétion de l'exon 5) nous attendions un produit de ~500bp. Effectivement nous avons observé la présence d'un amplicon autour de 500bp que nous avons purifié et séquencé. Les résultats ont montré que l'exon5 a été correctement excisé. Nous avons ensuite analysé le niveau d'expression de la protéine ABCA4 par immunofluorescence en comparant des rétines injectées et des rétines injectées contrôles (AAV-sgRNAs seul) et nous avons observé une diminution de l'expression de l'ABCA4 dans la rétine injectée CRISPR-CAS9. Des analyses par qPCR ont confirmé cette diminution, deux mois (PI60) après l'injection (PI = post-injection) : nous avons observé que le niveau d'expression du gène *Abca4* est significativement réduite dans les rétines injectées CRISPR-CAS9 comparées aux rétines contrôles injectées avec les guides seuls ou aux rétines contrôles non injectées. Nous n'observons pas de différences d'expression d'*Abca4* entre les deux groups contrôles.

La troisième partie du projet portait sur l'analyse fonctionnelle et structurale de la rétine de *Psammomys obesus* suite à l'invalidation d'*Abca4* (animaux intitulés Abca4 ko). Nous avons suivi les animaux après 30, 60, 90 et jusqu'à 210 jours post-injection. D'abord des électrorétinogrammes (ERG) en condition scotopique, photopique et flicker ont été réalisés pour comparer l'œil gauche (injecté avec les AAVs CRISPR-CAS9) et l'œil droit (non injecté). Après 90 jours post injection nous avons remarqué une diminution de la réponse scotopique, photopique et flicker dans la rétine CRISPR-CAS9, par rapport à la rétine contrôle. Nous avons remarqué la même tendance après 210 jours post-injection avec une diminution de la réponse

statistiquement significative en condition photopique entre la rétine contrôle et la rétine CRISPR-CAS9, ce qui suggère une perte de la fonctionnalité essentiellement des cônes dans notre modèle Abca4 ko. Après 210 jours post-injection, nous avons analysé la morphologie et la structure de la rétine par tomographie à cohérence optique (OCT) et par analyse de l'autofluorescence du fond d'œil (FAF pour fundus autofluorescence) pour visualiser l'accumulation dans les cellules de l'EPR de lipofuscine, qui possède des caractéristiques fluorescentes (Ex λ 470nm et 500nm- Em λ 550nm et 600nm). Nous avons observé par OCT une atrophie massive de la rétine CRISPR-CAS9 par rapport à la rétine contrôle non injectée et une dégénérescence des différentes couches de la rétine, mais surtout de la couche des PR. Nous avons constaté une accumulation de débris fluorescents tout autour de la lésion par FAF de la rétine CRISPR-CAS9. Par microscopie électronique, en collaboration avec la plateforme de microscopie de l'INCI, nous avons examiné la structure de la rétine (PI210) à proximité de la lésion, où nous avons détecté une accumulation dans l'EPR de petits granules ronds qui ressemblent à des granules de lipofuscine et qui ne sont pas présents dans les contrôles. En comparant les yeux contrôles et injectés CRISPR-CAS9, nous pouvons constater une dégénérescence très claire des PR. Pour exclure que la dégénérescence soit due aux artefacts mécaniques (injection sous-rétinienne elle-même) et non à la délétion du gène *Abca4*, nous avons injecté les deux yeux, l'oeil gauche avec les deux vecteurs CRISPR-CAS9 et l'œil droit avec le vecteur guides seul en tant que contrôle. En comparant les deux yeux par ERG et OCT deux mois (PI60) après injection, nous avons pu confirmer les résultats décrit ci-dessus. Une diminution de la fonctionnalité une dégénérescence en cours dans la rétine CRISPR-CAS9 par rapport au contrôle injecté avec les guides a été confirmée. En quantifiant par qPCR deux mois (PI60) après injection l'expression des gènes de la rhodopsine (spécifique aux bâtonnets) et de la « MW opsine » (spécifique des cônes) dans les rétines contrôles injectées avec les guides, les contrôles non injectés et les rétines CRISPR-CAS9, nous avons observé que le niveau d'expression de la rhodopsine ne change pas entre les 3 groupes alors que le niveau d'expression de la MW opsine est significativement réduit dans les rétines injectées CRISPR-CAS9 par rapport aux deux autres. Nous avons analysé le niveau d'expression de la protéine Rhodopsine, exprimée dans les bâtonnets et de la protéine MW opsine exprimés dans les cônes par immunofluorescence en comparant l'expression injectée par CRISPR-Cas9 comparé à l'expression dans une rétine en section contrôle injectée juste avec les guides (AAV-sgRNAs) et nous avons observé une diminution de l'expression de l'Opsin M dans la rétine injecté CRISPR-Abca4 comparé à la rétine contrôle mais au même temps, nous n'avons observé aucune différence d'expression de la Rhodopsine entre le deux rétines.

En conclusion, nous avons généré, grâce à l'édition du génome par la technologie CRISPR-Cas9 chez le modèle diurne *Psammomys obesus* une invalidation du gène *Abca4* capable de reproduire le phénotype de la maladie de Stargardt observé chez l'humain. En effet, nous avons observé une diminution de la réponse des cônes mais pas des bâtonnets par électrorétinographie, une atrophie de la rétine et une dégénérescence cellulaire dès 60 jours après l'injection. L'ensemble de ces résultats suggère donc une vulnérabilité accrue des cônes par rapport aux bâtonnets suite à la délétion du gène *Abca4*, ce qui confirme notre hypothèse.

Université de Strasbourg

École Doctorale des Sciences de la Vie et de la Santé STRASBOURG

Fabiana SASSONE

Utilisation de CRISPR-Cas9 chez *Psammomys obesus* pour examiner la vulnérabilité des cônes aux mutations du gène *Abca4* impliqué dans la maladie de Stargardt.

Résumé La maladie de Stargardt 1 (STGD1) est une maladie autosomique récessive. Le gène dans lequel les mutations sont responsables a été identifié, Abca4, codant pour un membre de la super famille des cassettes de liaison à l'ATP, exprimé spécifiquement dans la rétine. L'objectif de ce projet est de comparer la vulnérabilité des photorécepteurs en bâtonnets et cônes à la perte d'Abca4 par une stratégie CRISPR-CAS9 utilisant un rongeur diurne. Le modèle animal, *Psammomys obesus*, est une espèce diurne riche en cônes dans laquelle les cônes sont représentés en grand nombre (~ 30-40% de photorécepteurs totaux), ressemblant plus étroitement à la macula humaine et permettant des détails structurels, fonctionnels et analyses biochimiques. Nous avons effectué des injections sous-rétiniennes de constructions Adeno-Associated Virus (AAV)-CRISPR-Cas9 chez *Psammomys obesus*, pour obtenir un Abca4 - KO. Une fois ayant confirmé la perte d'Abca4, pour analyser les conséquences fonctionnelles et morphologiques nous avons réalisé des analyses non invasives (électrorétinographie, tomographie par cohérence optique, imagerie du fond d'œil). Les yeux traités présentent une dégénérescence rétinienne étendue et rapide 2 mois après l'injection, comme le montre l'OCT, et l'enregistrement ERG a montré une baisse significative des réponses lumineuses photopiques (cônes). En conclusion, les rongeurs riches en cônes offrent un scénario unique pour explorer les changements moléculaires et cellulaires survenant dans les maculopathies humaines telles que STGD1, et devrait fournir un moyen précieux d'évaluer les stratégies thérapeutiques potentielles.

Mots clés : Rétine, photorécepteurs, maladie de Stargardt, gène Abca4, Crispr-Cas9, AAV, *Psammomys obesus.*

Summary Loss of central vision constitutes the major underlying reason for visual handicap in western industrialized nations. Stargardt's Disease 1 (STGD1) is an autosomal recessive disease of early onset and severe visual handicap, representing the most frequent inherited macular degeneration. The gene in which mutations are responsible for STGD1 has been identified, Abca4, coding for a member of the ATP binding cassette super family, expressed specifically in retina. The aim of this project is to compare the vulnerability of rod and cone photoreceptors to Abca4 loss by a CRISPR-Cas9 strategy using a diurnal rodent. The animal model, Fat Sand Rat *Psammomys obesus*, is a diurnal cone-rich species in which cone photoreceptors are represented in large numbers (~30-40% total photoreceptors), more closely resembling the human macula, and allowing detailed structural, functional and biochemical analyses. We performed subretinal injections of Adeno-Associated Virus (AAV)-CRISPR-Cas9 constructs in *Psammomys obesus*, to obtain an Abca4 - KO. After confirming the loss of Abca4; to analyse the functional and morphological consequences to Abca4 loss we performed non-invasive imaging (Electroretinography, Optical coherence tomography, Fundus imaging). CRISPR-Cas9-Abca4 -/- treated eyes exhibit extensive and rapid retinal degeneration by 2 months post-injection, as seen by OCT, and ERG recording showed significant declines in photopic (cone) light responses.In conclusion, cone-rich rodents offer a unique scenario to explore molecular and cellular changes occurring in human maculopathies like STGD1, and should provide a valuable means to appraise potential therapeutic strategies.

Keywords: Retina, photoreceptors, Stargardt's disease, Abca4 gene, Crispr-Cas9, AAV, *Psammomys obesus.*

REFERENCES

References

Allikmets, R., N. Singh, H. Sun, N. F. Shroyer, A. Hutchinson, A. Chidambaram, B. Gerrard, L. Baird, D. Stauffer, A. Peiffer, A. Rattner, P. Smallwood, Y. Li, K. L. Anderson, R. A. Lewis, J. Nathans, M. Leppert, M. Dean, and J. R. Lupski. 1997. 'A photoreceptor cell-specific ATP-binding transporter gene (ABCR) is mutated in recessive Stargardt macular dystrophy', *Nat Genet*, 15: 236-46.

Bakondi, B., W. Lv, B. Lu, M. K. Jones, Y. Tsai, K. J. Kim, R. Levy, A. A. Akhtar, J. J. Breunig, C. N. Svendsen, and S. Wang. 2016. 'In Vivo CRISPR/Cas9 Gene Editing Corrects Retinal Dystrophy in the S334ter-3 Rat Model of Autosomal Dominant Retinitis Pigmentosa', *Mol Ther*, 24: 556-63.

Bascom, R. A., S. Manara, L. Collins, R. S. Molday, V. I. Kalnins, and R. R. McInnes. 1992. 'Cloning of the cDNA for a novel photoreceptor membrane protein (rom-1) identifies a disk rim protein family implicated in human retinopathies', *Neuron*, 8: 1171-84.

Bobu, C., C. M. Craft, M. Masson-Pevet, and D. Hicks. 2006. 'Photoreceptor organization and rhythmic phagocytosis in the nile rat Arvicanthis ansorgei: a novel diurnal rodent model for the study of cone pathophysiology', *Invest Ophthalmol Vis Sci*, 47: 3109-18.

Bobu, C., M. Lahmam, P. Vuillez, A. Ouarour, and D. Hicks. 2008. 'Photoreceptor organisation and phenotypic characterization in retinas of two diurnal rodent species: potential use as experimental animal models for human vision research', *Vision Res*, 48: 424-32.

Bobu, C., C. Sandu, V. Laurent, M. P. Felder-Schmittbuhl, and D. Hicks. 2013. 'Prolonged light exposure induces widespread phase shifting in the circadian clock and visual pigment gene expression of the Arvicanthis ansorgei retina', *Mol Vis*, 19: 1060-73.

Boudard, D. L., N. Acar, L. Bretillon, and D. Hicks. 2011. 'Retinas of the diurnal rodent Arvicanthis ansorgei are highly resistant to experimentally induced stress and degeneration', *Invest Ophthalmol Vis Sci*, 52: 8686-700.

Boudard, D. L., N. Tanimoto, G. Huber, S. C. Beck, M. W. Seeliger, and D. Hicks. 2010. 'Cone loss is delayed relative to rod loss during induced

retinal degeneration in the diurnal cone-rich rodent Arvicanthis ansorgei', *Neuroscience*, 169: 1815-30.

Bringmann, A., S. Syrbe, K. Görner, J. Kacza, M. Francke, P. Wiedemann, and A. Reichenbach. 2018. 'The primate fovea: Structure, function and development', *Prog Retin Eye Res*, 66: 49-84.

Caldelas, I., V. J. Poirel, B. Sicard, P. Pévet, and E. Challet. 2003. 'Circadian profile and photic regulation of clock genes in the suprachiasmatic nucleus of a diurnal mammal Arvicanthis ansorgei', *Neuroscience*, 116: 583-91.

Carroll, D. 2011. 'Genome engineering with zinc-finger nucleases', *Genetics*, 188: 773-82.

Carter-Dawson, L. D., and M. M. LaVail. 1979. 'Rods and cones in the mouse retina. I. Structural analysis using light and electron microscopy', *J Comp Neurol*, 188: 245-62.

Cervia, L. D., C. C. Chang, L. Wang, M. Mao, and F. Yuan. 2018. 'Enhancing Electrotransfection Efficiency through Improvement in Nuclear Entry of Plasmid DNA', *Mol Ther Nucleic Acids*, 11: 263-71.

Charbel Issa, P., A. R. Barnard, M. S. Singh, E. Carter, Z. Jiang, R. A. Radu, U. Schraermeyer, and R. E. MacLaren. 2013. 'Fundus autofluorescence in the Abca4(-/-) mouse model of Stargardt disease--correlation with accumulation of A2E, retinal function, and histology', *Invest Ophthalmol Vis Sci*, 54: 5602-12.

Cheng, H., H. Khanna, E. C. Oh, D. Hicks, K. P. Mitton, and A. Swaroop. 2004. 'Photoreceptor-specific nuclear receptor NR2E3 functions as a transcriptional activator in rod photoreceptors', *Hum Mol Genet*, 13: 1563-75.

Choi, C. C., and R. C. Ford. 2021. 'ATP binding cassette importers in eukaryotic organisms', *Biol Rev Camb Philos Soc*, 96: 1318-30.

Conley, S. M., X. Cai, R. Makkia, Y. Wu, J. R. Sparrow, and M. I. Naash. 2012. 'Increased cone sensitivity to ABCA4 deficiency provides insight into macular vision loss in Stargardt's dystrophy', *Biochim Biophys Acta*, 1822: 1169-79.

Cremers, F. P. M., W. Lee, R. W. J. Collin, and R. Allikmets. 2020. 'Clinical spectrum, genetic complexity and therapeutic approaches for retinal disease caused by ABCA4 mutations', *Prog Retin Eye Res*, 79: 100861.

Daghsni, M., and I. Aldiri. 2021. 'Building a Mammalian Retina: An Eye on Chromatin Structure', *Front Genet*, 12: 775205.

Dellaa, A., A. Polosa, S. Mbarek, I. Hammoum, R. Messaoud, S. Amara, R. Azaiz, R. Charfeddine, M. Dogui, M. Khairallah, P. Lachapelle, and R. Ben Chaouacha-Chekir. 2017. 'Characterizing the Retinal Function of Psammomys obesus: A Diurnal Rodent Model to Study Human Retinal Function', *Curr Eye Res*, 42: 79-87.

Eng, L. F. 1985. 'Glial fibrillary acidic protein (GFAP): the major protein of glial intermediate filaments in differentiated astrocytes', *J Neuroimmunol*, 8: 203-14.

Fakin, A., A. G. Robson, K. Fujinami, A. T. Moore, M. Michaelides, J. Pei-Wen Chiang, E. Holder G, and A. R. Webster. 2016. 'Phenotype and Progression of Retinal Degeneration Associated With Nullizigosity of ABCA4', *Invest Ophthalmol Vis Sci*, 57: 4668-78.

Fares Taie, L. 2012. 'Bases moléculaires et physiopathologiques des affections héréditaires ophtalmologiques : Travaux de création d’un rongeur diurne transgénique modèle de la maladie de Stargardt : Identification d’un nouveau gène d’anophtalmie/microphtalmie'.

Fujinami, K., N. Lois, A. E. Davidson, D. S. Mackay, C. R. Hogg, E. M. Stone, K. Tsunoda, K. Tsubota, C. Bunce, A. G. Robson, A. T. Moore, A. R. Webster, G. E. Holder, and M. Michaelides. 2013. 'A longitudinal study of stargardt disease: clinical and electrophysiologic assessment, progression, and genotype correlations', *Am J Ophthalmol*, 155: 1075-88.e13.

Gianesini, C., D. Clesse, G. Tosini, D. Hicks, and V. Laurent. 2015. 'Unique Regulation of the Melatonin Synthetic Pathway in the Retina of Diurnal Female Arvicanthis ansorgei (Rodentia)', *Endocrinology*, 156: 3292-308.

Gray, S. J., S. B. Foti, J. W. Schwartz, L. Bachaboina, B. Taylor-Blake, J. Coleman, M. D. Ehlers, M. J. Zylka, T. J. McCown, and R. J. Samulski. 2011. 'Optimizing promoters for recombinant adeno-associated virus-mediated gene expression in the peripheral and central nervous system using self-complementary vectors', *Hum Gene Ther*, 22: 1143-53.

Gurevich, V. V., S. M. Hanson, X. Song, S. A. Vishnivetskiy, and E. V. Gurevich. 2011. 'The functional cycle of visual arrestins in photoreceptor cells', *Prog Retin Eye Res*, 30: 405-30.

Hargreaves, A. D., L. Zhou, J. Christensen, F. Marlétaz, S. Liu, F. Li, P. G. Jansen, E. Spiga, M. T. Hansen, S. V. H. Pedersen, S. Biswas, K. Serikawa, B. A. Fox, W. R. Taylor, J. F. Mulley, G. Zhang, R. S. Heller, and P. W. H. Holland. 2017. 'Genome sequence of a diabetes-prone rodent reveals a mutation hotspot around the ParaHox gene cluster', *Proc Natl Acad Sci U S A*, 114: 7677-82.

Hauswirth, W. W. 2014. 'Retinal gene therapy using adeno-associated viral vectors: multiple applications for a small virus', *Hum Gene Ther*, 25: 671-8.

Heavner, W., and L. Pevny. 2012. 'Eye development and retinogenesis', *Cold Spring Harb Perspect Biol*, 4.

Hildebrand, P. W., P. Scheerer, J. H. Park, H. W. Choe, R. Piechnick, O. P. Ernst, K. P. Hofmann, and M. Heck. 2009. 'A ligand channel through the G protein coupled receptor opsin', *PLoS One*, 4: e4382.

Hussey, K. A., S. E. Hadyniak, and R. J. Johnston, Jr. 2022. 'Patterning and Development of Photoreceptors in the Human Retina', *Front Cell Dev Biol*, 10: 878350.

Hutmacher, F. 2019. 'Why Is There So Much More Research on Vision Than on Any Other Sensory Modality?', *Front Psychol*, 10: 2246.

Jaenisch, R., and B. Mintz. 1974. 'Simian virus 40 DNA sequences in DNA of healthy adult mice derived from preimplantation blastocysts injected with viral DNA', *Proc Natl Acad Sci U S A*, 71: 1250-4.

Kim, E., T. Koo, S. W. Park, D. Kim, K. Kim, H. Y. Cho, D. W. Song, K. J. Lee, M. H. Jung, S. Kim, J. H. Kim, J. H. Kim, and J. S. Kim. 2017. 'In vivo genome editing with a small Cas9 orthologue derived from Campylobacter jejuni', *Nat Commun*, 8: 14500.

Kim, H., and J. S. Kim. 2014. 'A guide to genome engineering with programmable nucleases', *Nat Rev Genet*, 15: 321-34.

Klevering, B. J., A. F. Deutman, A. Maugeri, F. P. Cremers, and C. B. Hoyng. 2005. 'The spectrum of retinal phenotypes caused by mutations in the ABCA4 gene', *Graefes Arch Clin Exp Ophthalmol*, 243: 90-100.

Klevering, B. J., S. Yzer, K. Rohrschneider, M. Zonneveld, R. Allikmets, L. I. van den Born, A. Maugeri, C. B. Hoyng, and F. P. Cremers. 2004. 'Microarray-based mutation analysis of the ABCA4 (ABCR) gene in autosomal recessive cone-rod dystrophy and retinitis pigmentosa', *Eur J Hum Genet*, 12: 1024-32.

Konieczka, K., A. J. Flammer, M. Todorova, P. Meyer, and J. Flammer. 2012. 'Retinitis pigmentosa and ocular blood flow', *Epma j*, 3: 17.

Lamb, T. D. 2016. 'Why rods and cones?', *Eye (Lond)*, 30: 179-85.

Li, J., Y. Zhang, X. Cai, Q. Xia, J. Chen, Y. Liao, Z. Liu, and Y. Wu. 2016. 'All-trans-retinal dimer formation alleviates the cytotoxicity of all-trans-retinal in human retinal pigment epithelial cells', *Toxicology*, 371: 41-48.

Liu, C., L. Zhang, H. Liu, and K. Cheng. 2017. 'Delivery strategies of the CRISPR-Cas9 gene-editing system for therapeutic applications', *J Control Release*, 266: 17-26.

Lois, N., G. E. Holder, C. Bunce, F. W. Fitzke, and A. C. Bird. 2001. 'Phenotypic subtypes of Stargardt macular dystrophy-fundus flavimaculatus', *Arch Ophthalmol*, 119: 359-69.

Mak, A. N., P. Bradley, A. J. Bogdanove, and B. L. Stoddard. 2013. 'TAL effectors: function, structure, engineering and applications', *Curr Opin Struct Biol*, 23: 93-9.

Matsuda, T., and C. L. Cepko. 2004. 'Electroporation and RNA interference in the rodent retina in vivo and in vitro', *Proc Natl Acad Sci U S A*, 101: 16-22. 2008. 'Analysis of gene function in the retina', *Methods Mol Biol*, 423: 259-78.

Mena, M. D., A. A. Moresco, S. H. Vidal, D. Aguilar-Cortes, M. G. Obregon, A. C. Fandiño, J. M. Sendoya, A. S. Llera, and O. L. Podhajcer. 2021. 'Clinical and Genetic Spectrum of Stargardt Disease in Argentinean Patients', *Front Genet*, 12: 646058.

Mendoza, J., S. Gourmelen, S. Dumont, D. Sage-Ciocca, P. Pévet, and E. Challet. 2012. 'Setting the main circadian clock of a diurnal mammal by hypocaloric feeding', *J Physiol*, 590: 3155-68.

Molday, L. L., D. Wahl, M. V. Sarunic, and R. S. Molday. 2018. 'Localization and functional characterization of the p.Asn965Ser (N965S) ABCA4 variant in mice reveal pathogenic mechanisms underlying Stargardt macular degeneration', *Hum Mol Genet*, 27: 295-306.

Molday, R. S. 2007. 'ATP-binding cassette transporter ABCA4: molecular properties and role in vision and macular degeneration', *J Bioenerg Biomembr*, 39: 507-17.

Molday, R. S., F. A. Garces, J. F. Scortecci, and L. L. Molday. 2022. 'Structure and function of ABCA4 and its role in the visual cycle and Stargardt macular degeneration', *Prog Retin Eye Res*, 89: 101036.

Molday, R. S., and O. L. Moritz. 2015. 'Photoreceptors at a glance', *J Cell Sci*, 128: 4039-45.

Morrow, E. M., M. J. Belliveau, and C. L. Cepko. 1998. 'Two phases of rod photoreceptor differentiation during rat retinal development', *J Neurosci*, 18: 3738-48.

Mussolino, C., M. della Corte, S. Rossi, F. Viola, U. Di Vicino, E. Marrocco, S. Neglia, M. Doria, F. Testa, R. Giovannoni, M. Crasta, M. Giunti, E. Villani, M. Lavitrano, M. L. Bacci, R. Ratiglia, F. Simonelli, A. Auricchio, and E. M. Surace. 2011. 'AAV-mediated photoreceptor transduction of the pig cone-enriched retina', *Gene Ther*, 18: 637-45.

Mustafi, D., A. H. Engel, and K. Palczewski. 2009. 'Structure of cone photoreceptors', *Prog Retin Eye Res*, 28: 289-302.

Nadal-Nicolás, F. M., V. P. Kunze, J. M. Ball, B. T. Peng, A. Krishnan, G. Zhou, L. Dong, and W. Li. 2020. 'True S-cones are concentrated in the ventral mouse retina and wired for color detection in the upper visual field', *Elife*, 9.

Naso, M. F., B. Tomkowicz, W. L. Perry, 3rd, and W. R. Strohl. 2017. 'Adeno-Associated Virus (AAV) as a Vector for Gene Therapy', *BioDrugs*, 31: 317-34.

Ong, T., M. E. Pennesi, D. G. Birch, B. L. Lam, and S. H. Tsang. 2019. 'Adeno-Associated Viral Gene Therapy for Inherited Retinal Disease', *Pharm Res*, 36: 34.

Osborne, N. N., N. J. Broyden, N. L. Barnett, and N. J. Morris. 1991. 'Protein kinase C (alpha and beta) immunoreactivity in rabbit and rat retina: effect of phorbol esters and transmitter agonists on immunoreactivity and the translocation of the enzyme from cytosolic to membrane compartments', *J Neurochem*, 57: 594-604.

Park, P. S. 2014. 'Constitutively active rhodopsin and retinal disease', *Adv Pharmacol*, 70: 1-36.

Pelkonen, L., M. Reinisalo, E. Morin-Picardat, H. Kidron, and A. Urtti. 2016. 'Isolation of Intact and Functional Melanosomes from the Retinal Pigment Epithelium', *PLoS One*, 11: e0160352.

Perkins, B. D., and J. M. Fadool. 2010. 'Photoreceptor structure and development analyses using GFP transgenes', *Methods Cell Biol*, 100: 205-18.

Petros, T. J., A. Rebsam, and C. A. Mason. 2009. 'In utero and ex vivo electroporation for gene expression in mouse retinal ganglion cells', *J Vis Exp*.

Ran, F. A., L. Cong, W. X. Yan, D. A. Scott, J. S. Gootenberg, A. J. Kriz, B. Zetsche, O. Shalem, X. Wu, K. S. Makarova, E. V. Koonin, P. A. Sharp, and F. Zhang. 2015. 'In vivo genome editing using Staphylococcus aureus Cas9', *Nature*, 520: 186-91.

Robbins, P. D., and S. C. Ghivizzani. 1998. 'Viral vectors for gene therapy', *Pharmacol Ther*, 80: 35-47.

Roorda, A., A. B. Metha, P. Lennie, and D. R. Williams. 2001. 'Packing arrangement of the three cone classes in primate retina', *Vision Res*, 41: 1291-306.

Rozet, J. M., S. Gerber, D. Ducroq, C. Hamel, J. L. Dufier, and J. Kaplan. 2005. '[Hereditary macular dystrophies]', *J Fr Ophtalmol*, 28: 113-24.

Saïdi, T., S. Mbarek, R. B. Chaouacha-Chekir, and D. Hicks. 2011. 'Diurnal rodents as animal models of human central vision: characterisation of the retina of the sand rat Psammomys obsesus', *Graefes Arch Clin Exp Ophthalmol*, 249: 1029-37.

Schmidt-Nielsen, K., H. B. Haines, and D. B. Hackel. 1964. 'DIABETES MELLITUS IN THE SAND RAT INDUCED BY STANDARD LABORATORY DIETS', *Science*, 143: 689-90.

Sharma, A., A. Ghosh, E. T. Hansen, J. M. Newman, and R. R. Mohan. 2010. 'Transduction efficiency of AAV 2/6, 2/8 and 2/9 vectors for delivering genes in human corneal fibroblasts', *Brain Res Bull*, 81: 273-8.

Shu, X., N. C. Shaner, C. A. Yarbrough, R. Y. Tsien, and S. J. Remington. 2006. 'Novel chromophores and buried charges control color in mFruits', *Biochemistry*, 45: 9639-47.

Sparrow, J. R., Y. Wu, T. Nagasaki, K. D. Yoon, K. Yamamoto, and J. Zhou. 2010. 'Fundus autofluorescence and the bisretinoids of retina', *Photochem Photobiol Sci*, 9: 1480-9.

Sun, H., and J. Nathans. 2001. 'Mechanistic studies of ABCR, the ABC transporter in photoreceptor outer segments responsible for autosomal recessive Stargardt disease', *J Bioenerg Biomembr*, 33: 523-30.

Szél, A., P. Röhlich, A. R. Caffé, and T. van Veen. 1996. 'Distribution of cone photoreceptors in the mammalian retina', *Microsc Res Tech*, 35: 445-62.

Tanna, P., R. W. Strauss, K. Fujinami, and M. Michaelides. 2017. 'Stargardt disease: clinical features, molecular genetics, animal models and therapeutic options', *Br J Ophthalmol*, 101: 25-30.

Tian, H., K. M. Gunnison, M. A. Kazmi, T. P. Sakmar, and T. Huber. 2022. 'FRET sensors reveal the retinal entry pathway in the G protein-coupled receptor rhodopsin', *iScience*, 25: 104060.

Verra, D. M., B. S. Sajdak, D. K. Merriman, and D. Hicks. 2020. 'Diurnal rodents as pertinent animal models of human retinal physiology and pathology', *Prog Retin Eye Res*, 74: 100776.

Verra, D. M., P. Spinnhirny, C. Sandu, S. Grégoire, N. Acar, O. Berdeaux, L. Brétillon, J. R. Sparrow, and D. Hicks. 2022. 'Intrinsic differences in rod and cone membrane composition: implications for cone degeneration', *Graefes Arch Clin Exp Ophthalmol*, 260: 3131-48.

Wang, J. S., and V. J. Kefalov. 2011. 'The cone-specific visual cycle', *Prog Retin Eye Res*, 30: 115-28.

Weng, J., N. L. Mata, S. M. Azarian, R. T. Tzekov, D. G. Birch, and G. H. Travis. 1999. 'Insights into the function of Rim protein in photoreceptors and etiology of Stargardt's disease from the phenotype in abcr knockout mice', *Cell*, 98: 13-23.

Whitehead, A. J., J. A. Mares, and R. P. Danis. 2006. 'Macular pigment: a review of current knowledge', *Arch Ophthalmol*, 124: 1038-45.

Wu, L., T. Nagasaki, and J. R. Sparrow. 2010. 'Photoreceptor cell degeneration in Abcr (-/-) mice', *Adv Exp Med Biol*, 664: 533-9.

Wu, Z., H. Yang, and P. Colosi. 2010. 'Effect of genome size on AAV vector packaging', *Mol Ther*, 18: 80-6.

Yamashiro, K., Y. Ikegaya, and N. Matsumoto. 2022. 'In Utero Electroporation for Manipulation of Specific Neuronal Populations', *Membranes (Basel)*, 12.

Yang, S., J. Zhou, and D. Li. 2021. 'Functions and Diseases of the Retinal Pigment Epithelium', *Front Pharmacol*, 12: 727870.

Yu, W., S. Mookherjee, V. Chaitankar, S. Hiriyanna, J. W. Kim, M. Brooks, Y. Ataeijannati, X. Sun, L. Dong, T. Li, A. Swaroop, and Z. Wu. 2017. 'Nrl knockdown by AAV-delivered CRISPR/Cas9 prevents retinal degeneration in mice', *Nat Commun*, 8: 14716.

Yu, W., and Z. Wu. 2021. 'Ocular delivery of CRISPR/Cas genome editing components for treatment of eye diseases', *Adv Drug Deliv Rev*, 168: 181-95.

Zhang, H., J. Fan, S. Li, S. Karan, B. Rohrer, K. Palczewski, J. M. Frederick, R. K. Crouch, and W. Baehr. 2008. 'Trafficking of membrane-associated proteins to cone photoreceptor outer segments requires the chromophore 11-cis-retinal', *J Neurosci*, 28: 4008-14.

Zhang, N., Y. Tsybovsky, A. V. Kolesnikov, M. Rozanowska, M. Swider, S. B. Schwartz, E. M. Stone, G. Palczewska, A. Maeda, V. J. Kefalov, S. G. Jacobson, A. V. Cideciyan, and K. Palczewski. 2015. 'Protein misfolding and the pathogenesis of ABCA4-associated retinal degenerations', *Hum Mol Genet*, 24: 3220-37.

Zhang, T., L. Zhu, M. C. Madigan, W. Liu, W. Shen, S. Cherepanoff, F. Zhou, S. Zeng, J. Du, and M. C. Gillies. 2019. 'Human macular Müller cells rely more on serine biosynthesis to combat oxidative stress than those from the periphery', *Elife*, 8.